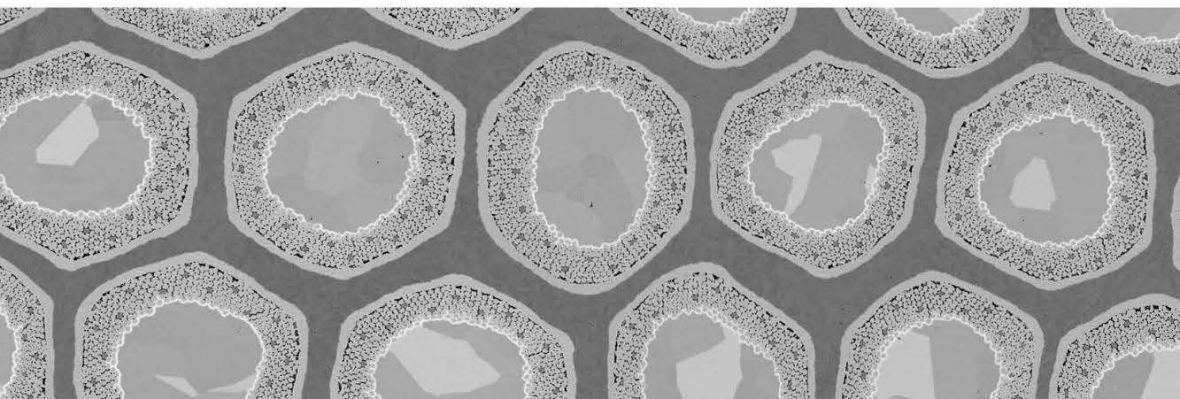# A NEW UNDERSTANDING OF THE HEAT TREATMENT OF NB-SN WIRES

Charlie Sanabria

A new understanding of the heat treatment of Nb-Sn superconducting wires

FLORIDA STATE UNIVERSITY

THE GRADUATE SCHOOL

A NEW UNDERSTANDING OF THE HEAT TREATMENT OF NB-SN

SUPERCONDUCTING WIRES

BY CHARLIE SANABRIA

A Dissertation submitted to the
Materials Science and Engineering
in partial fulfillment of the
requirements for the degree of
Doctor of Philosophy

2017

Charlie Sanabria defended this dissertation on April 11, 2017.

The members of the supervisor committee were:

David Larbalestier
Professor Directing Dissertation

Vincent Salters
University Representative

William Oates
Committee Member

Michael Shatruk
Committee Member

Irinel Chiorescu
Committee Member

Chiara Tarantini
Committee Member

Peter Lee
Committee Member

The Graduate School has verified and approved the above-named committee members, and certifies that the dissertation has been approved in accordance with university requirements.

Para Mario y Genith

Acknowledgments

There is no such thing as a personal accomplishment. Every action we take, and every goal we set in our lives, is utterly impossible to achieve on our own. In my case, if I were to think about my career as a house, I could go around such house assigning names to every brick, every beam, every tile, and every detail of every corner of it, with the names of everyone who has lend me a hand and those who have had an impact on its construction. These names will forever remain there, and they all have contributed in one way or another to this beautiful house that I have built so far.

At the base, for obvious reasons, you may find the names of those whom without the house would not even be standing today: my family and friends. In my family the term "extended" (although extensive) is not in the slightest way extended or distant. We are as close as we can be, and it is the most solid ground I can imagine building this house on. I will not dare to add any names here because I would inevitably forget one of you and never forgive myself for it. I love you all.

The frames of this house have the names of my colleagues. The most important beams have David Larbalestier and Peter Lee written on them, but the rest of the structure has the names of all of those friendly faces I come across each day when I come into the Applied Superconductivity Center. You have truly been a second family to me, and you are directly responsible for the sturdiness of this house. Thank you for making it stormproof.

The roof; has in fact been built by the numerous colleagues that make up the magnet community—across national laboratories, industry, and universities. I would like to thank the entire ITER "dream team" who patiently listened to a younger more credulous version of myself, and very often stopped me on my tracks towards a dead end. Arnaud Devred, Matt Jewell, and Ian Pong, thank you for helping my ideas take shape—and become useful in such an important project like ITER. I must say that although very little of my ITER work has actually made it in this document, your influence can be found in every corner of it. To Mike Field and Jeff Parrell, I cannot

be more grateful to you for taking me under your wing and letting me play with your precious technology, your baby.

Some of the above-mentioned names are ASC alumni, and there are many others like Arno Godeke, Lance Cooley and Dave Smathers who have shown interest in my work, and have given me the occasional pat in the back whenever we meet at international conferences. This is my chance to say how much that pat in the back means to me. Thank you.

As a scientist and an educator, I would like to thank (in a very symbolic way because I never met most of them) all the scientists that have come before me and have made an effort to advance, popularize, and embellish the scientific enterprise. From Johannes Kepler, to Michael Faraday, to Carl Sagan (and many others in between), your enthusiasm to show the world how wonderful and mysterious mother nature can be, is a breeze that fills this house with a fresh scent every morning and encourages me to get out of bed and stay as curious as I have always been.

Finally, to my beautiful girlfriend Kayla—whom I cannot live without anymore—thank you for decorating this house with your laughter, your art, your kindness, and love. I have been building this house for years in a very systematic and almost mechanical way—without realizing what it was missing all along: a bit of disorder, a bit of creativity, a bit of silliness… but most importantly a whole lot of love.

Thank you all!

Sincerely,

Cha

Table of Contents

Author's note

From the moment I first sat down to put the last three years of my scientific research into a single document, I knew that it was going to be a serious challenge to keep the readers awake. Copying and pasting scientific papers into disconnected chapters (with an almost robotic tone), was the last thing I wanted to do for my thesis work. Instead, I made it my goal to create an entertaining and educational document for future ASC students to understand that science does not have to be boring. In fact, I think that with the right mentality, a simple PhD research subject can be as fascinating as any cutting edge research.

When Richard Dawkins wrote his first iconic book, The Selfish Gene, he said there were three readers looking over his shoulder for every page he wrote: the expert, the student, and the casual reader. I sat down to write this thesis work with a similar set of readers looking over my shoulder, and although I doubt I will get any casual readers, I think both the expert and the student will appreciate the common thread of enthusiasm and scientific passion that joins all these chapters together.

At times, it felt like I was taking it too far, and that those who have to read this as part of their responsibilities would shake their heads and think *"what a waste of time"*. I apologize in advanced if you are one of these readers. But if at the end of the day, the expert feels grateful for the walk down memory-lane, and the student feels encouraged to tackle their own research with the same enthusiasm that I tackled mine with, I will know that I have accomplished what I have set out to do.

I must beg the reader to be patient about typos and nearly nonsensical sentences that I have failed to clarify given the absence of a proper editor. I know my sentences can be long at times, but if it helps any, imagine I was sitting next to you telling you a story. Because to me, that is exactly what this is: a really cool story.

Chapter 1 - Introduction: Why Study Particle Physics?

——Nothing exists, but atoms and the void——

Democritus

Over the last three years (the time that I have been involved with LHC[a] research), it has been almost impossible to avoid telling friends and family—over dinner or drinks—that I do scientific research related to the LHC. And after a short and simple explanation of what the LHC does, a very common question I get asked is:

> *What is the LHC good for?*

I must admit this is a perfectly valid question; and I am afraid that if I do not answer it from the beginning, my thesis work would lose its entire purpose. However, to answer such question I must visit several historical events and philosophical concepts that span thousands of years—from the birth of science in the Ionian culture over 2,500 years ago, passing through the Enlightenment of the 17th and 18th centuries, and finally the explosion of science that has made the 20th and 21st century a time filled with discovery and wonder.

In this chapter I will explore this amazing journey of human curiosity that has revealed not only the secrets of the strange and capricious atom, but also the deepest mysteries of the universe.

1.1   The 'unable to cut' and its 'corpuscles'

The earliest recorded instance of somebody thinking about the most fundamental building block of matter was made by Democritus, who lived in Abdera, Greece. He was a deep thinker, and one of the most daring of Ionian scientists. Like many Greeks of the time, he spent his days wondering about natural phenomena—and his specialty was the infinitesimally small. He envisioned a slice taken out of a cone (making two cuts parallel to the cone's base) and he noticed that such slice would

---

[a] The Large Hadron Collider

always have a larger area on one of its sides; the side closest to the base of the cone. He assured that this would *always* be the case—no matter how thin the slice was cut—down to a point where the slice would be impossible to cut-out. Democritus coined this incredibly small scale the scale of the *atom*, which means *unable to cut* in Greek. *"Nothing exists"* he used to say *"but atoms and the void"*[1].

However, Democritus' explanation was merely a philosophical concept. It did not have any practical consequence. For centuries, it was agreed that visualizing such scale was not only impossible, but useless. Then, in the 17th century, (without really thinking about the atomic scale) humans got the first glimpse of the wonderful things sub-atomic particles can do. This was facilitated by one of the most important inventions of the time (although often taken for granted): the air-pump. Robert Boyle was the first to fabricate a reliable air-pump[2] in 1682, and he used it to study the effects of a vacuum on pretty much anything he could get his hands on; from burning matches, to wine, and even insects and birds[a].

This vacuum (produced by the air-pump) enabled the conditions for matter to manifest in ways never thought possible under human creation. One of the first persons to witness the wonderful things matter can do under vacuum was Isaac Newton's assistant Francis Hauksbee. In 1705, Hauksbee put a small amount of mercury inside a glass bubble under a vacuum (produced by an air-pump just like that used by Boyle years earlier), and then rotated the glass sphere—as fast as his belt-and-handle apparatus allowed him to. When doing so, he noticed that a purple glow would appear inside the rotating glass whenever his hand was placed near it[3]. Hauksbee later lost interest in these *"fine appearances"* (as he called them) but his invention made him the first person to see the effects of *electricity in vacuum*— bringing us a step closer to asking more fundamental questions of matter.

Aside from being a rather lousy light source, Hauksbee's sphere had a far more interesting application for the time: it was also a source of *static electricity*. This (rather) accidental discovery was something that delayed our atomic curiosity for over a century, and focused all our scientific efforts on plain and simple *electricity*.

Electricity through metals became the hot topic in the scientific community for the next 160 years—and truly magnificent inventions and discoveries followed. A few examples are Alessandro Volta's pile[4] (1800), Michael Faraday's homopolar

---

[a] The last one (birds) landed him on a very macabre painting named "An Experiment on a Bird in the Air-Pump" by Joseph Wright.

motor[5] (1821), Nikola Tesla's[6] synchronous motor (1888), and Heinrich Hertz's discovery of electromagnetic waves[7] (1893). Throughout these years, the scientific community seemed to be constantly struggling to catch up with the ever-expanding demand for electric power and communication. But once the electrical revolution slowed down (at the end of the 19th century), some scientists revisited the curious phenomenon discovered by Hauksbee years earlier.

Armed with more advanced and reliable glass forming techniques (than Hauksbee), as well as better pump systems, William Crookes was one of the dozens of scientists that helped develop the technology of *vacuum tubes*. These tubes, when linked to an electric circuit, produced a similar glow to that seen by Hauksbee in his sphere. Furthermore, Crookes noticed that this glow was responsive to magnetic fields[8]—a seemingly simple and frivolous observation, but one that triggered many questions.

Different names were given to different versions of these tubes (depending on who was fabricating them), but in the end, they came to be known as Cathode Ray Tubes. It was inside this nearly empty space (enabled by Boyle's invention) that humans first started to delve into the atomic world and the first piece of the puzzle was put forth by J. J. Thomson in 1897. Thomson proposed the hypothesis that these rays were made of particles he named *'corpuscles'*. Thomson also noticed that these were apparently *"charged with negative electricity"*, and that *"atoms of the ordinary elements are made up of corpuscles and holes"*[9]. With this, Thomson was the first to identify a sub-atomic particle (later known as the electron) putting Democritus' idea of *that which cannot be cut* back on the map.

A portrait of J. J. Thomson is shown in Figure 1 as well as a sketch of Cathode Ray Tube similar to the one used by William Crookes.

1.2   Radioactivity and X-rays

There is another invention—often taken for granted just like the air-pump— which played a crucial role in our atomic explorations: the photographic film. The term *photography* was coined by John Hershel, who in 1819 discovered that certain acidic solutions of silver salts were sensitive to light[10] and that two-dimensional imprints of a light source could be produced on what later came to be known as photographic film. Although photography was a revolutionary invention in itself, it was used years later (1896) by Henri Becquerel to make other kinds of revolutionary

findings. Becquerel found that certain uranium salts seemed to leave imprints on these photographic films when left in their proximity for a prolonged period of time[11]. The conclusion, naturally, was that certain rays of *invisible light* seemed to be coming out of these uranium salts, leaving a mark on the photographic films. Even more remarkable, was the fact that this "light" had the ability to pass through thin sheets of metal[12]. In 1898 Marie Curie expanded Becquerel's discoveries and coined these special materials as *radioactive*, pointing out that they were a seemingly unlimited energy source.
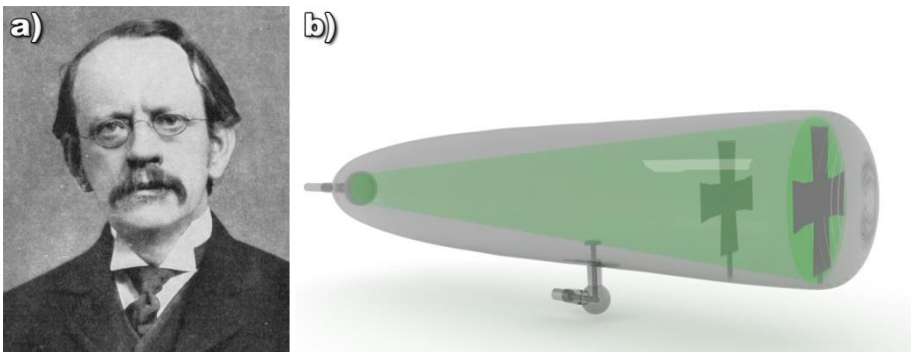
Figure 1 (a) A portrait of J.J. Thomson (image under the Public Domain via via <u>Wikimedia Commons)</u> and (b) a sketch of a Cathode Ray Tube similar to that used by William Crookes.

This was indeed an exciting time for science, and to add more wonder and awe to Curie's radioactivity and Thomson's charged particles, a certain kind of *unknown* rays were accidentally found by Wilhelm Röntgen in 1896 when he was studying Cathode Ray tubes. He enclosed one of these tubes inside a black box to prevent light from escaping, but upon setting up the experiment he noticed that a piece of a barium compound (sitting nearby) lit up with *"with brilliant fluorescence"*[13]. Röntgen concluded that the barium compound was reacting to a special kind of rays coming out of the Cathode Ray Tube, but he was not sure what to call these rays—and therefore he named them with a variable, X.

1.3   The '15-inch shell'

Despite having the suspicion that radioactivity, cathode rays, X-Rays, and perhaps light itself were all somehow linked to the most fundamental particle of matter (the atom), many physicists rejected the atomic theory. These skeptics refused to believe that there was a fundamental building block of matter, and they viewed Boltzmann's equations (which reduced substances to small indivisible

particles[14]) as a mathematical simplification that could not represent our reality. But in 1905 Albert Einstein brushed this skepticism aside when he was studying the movement of pollen in a glass of water[15]. With rather elegant mathematics, Einstein concluded that the vibration of the pollen (in otherwise static water) must be due to the vibrations of small spheres of which the water is made of, namely, atoms (or molecules)—and he accurately calculated their size[a].

Despite Einstein's proposition, the atom still remained a very complicated system with many mysteries. The distinction of particles and rays was still not very clear. Even Lord Ernest Rutherford in his most influential radioactivity papers (before 1911) exchanged the words *particles* and *rays* rather spontaneously[16, 17], and had a hard time determining the similarities and differences between Becquerel's radiation emissions and Röntgen's X-Rays. Nonetheless, having the approximate size of the atom—and knowing that radioactive emissions could be scattered by matter—Ernest Rutherford connected the dots with his famous 'gold foil' experiment when his assistants noticed that the radioactive *α* particles occasionally bounced back from the gold foil[18]. Knowing the incredible energy that the radioactive particles had, Rutherford claimed that *"It was almost as incredible as if you fired a 15-inch shell at a piece of tissue paper and it came back and hit you"*. A portrait of Ernest Rutherford is shown in Figure 2.

Although the experiment was devised in 1909, it took Rutherford and his colleagues two years to understand the significance of this discovery. Given the minute percentage of particles that actually bounced back, they concluded that the atoms were made almost entirely of empty space—with a very dense but incredibly small core which they called the Nucleus. Looking for an analogy of this description, they found one in our solar system—suggesting a hypothesis in which the negatively charged electrons found by J. J. Thomson were orbiting around a positively charged nucleus. Surprisingly, to this day, such description is still the easiest way to describe the atom—and it is still the picture that comes to our minds when we think of the atom (see Figure 3). But, as it will be shown below, this description is not enough to explain the complex and counterintuitive reality of the quantum world.

---

[a] Unfortunately Boltzmann was never shown Einstein's proof and he hung himself in 1906 after a long battle with depression exacerbated by the scientific community's disbelief of his molecular theory.
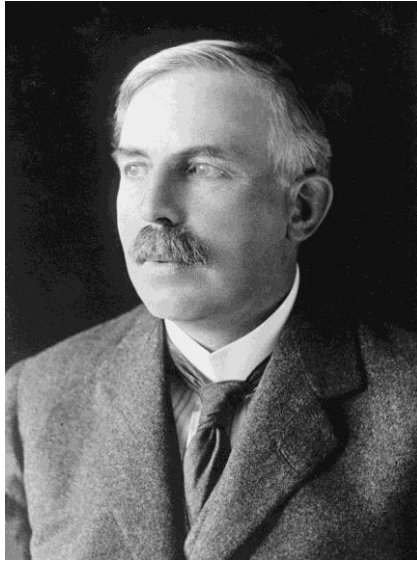
Figure 2 New Zealand chemist and Nobel Prize laureate Ernest Rutherford (1871-1937).
Image in the Public Domain via Library of Congress.
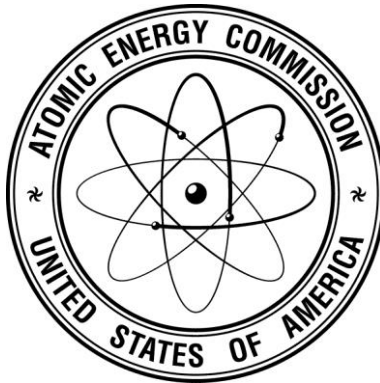
Figure 3 An example of the visualization of the atom made by Rutherford. This picture is widely
accepted despite not being representative of the reality that was later exposed by Niels Bohr.
Image by the Idaho National Laboratory under Creative Commons license CC BY 2.0 via Flickr,

1.4   A revolution on our scientific thinking

The intimate connection between radioactive particle emissions, light rays, and
sub-atomic particles was done by Niels Bohr in 1913—two years after the discovery
of the nucleus by Rutherford—and in doing so, Bohr revolutionized the way we look
at science. In his three-part paper *"On the Constitution of Atoms and Molecules"*[19],
Bohr's contribution to the atomic model placed a series of counterintuitive

arguments[a] that according to him were showing a *"conformity with experiments on a number of different phenomena"* and therefore could be regarded as real. This notion was in fact rejected by many conservative physicists (like Albert Einstein), who up to now had based their discoveries on direct observation—and their conclusions were drawn on parameters that agreed with common intuition.

But conformity with common intuition was definitely not the case of Bohr's quantum world, and his theories were just the beginning of a series of strange sub-atomic particle behaviors that could only be explained through ideas almost impossible to visualize. Among these ideas, sparked by Bohr's pioneering quantum physics, we have the Pauli Exclusion Principle[21] which places even more restrictions on the possible location of the electrons, and Heisenberg's uncertainty principle[22] which makes one unable to know both the position *and* the speed (angular momentum) of an atom at the same time. Such revolutionary concepts baffled scientists and forced them to express their concepts using very abstract mathematics—causing a polarization of ideas among the scientific community.

For most of the conservative scientist these abstract ideas had no place in science, but the argument of whether quantum mechanics was truly the most logical representation of the atom was finally settled in the Solvay conference in 1927. At this conference, each day, Einstein and the conservatives would try to poke a hole in the ideas proposed by Bohr and his colleagues. But at the end of the day, Bohr would always find a solution that made Einstein's arguments invalid. This interpretation of quantum mechanics came to be known as the Copenhagen interpretation, and indeed proved to be one of the most difficult concepts ever suggested by science—which is why the great Richard Feynman used to say *"If you think you understand quantum mechanics, you don't understand quantum mechanics"*.

1.5   Knowing sin

Despite all of this *electronic uncertainty*, the fundamental picture of the nucleus painted by Rutherford still agreed with Bohr's model—and it represented a playground for experimental particle physicist of the early 20th century. At this point

---

[a] Such as the existence of *"stationary states"* in which the electrons would exist (and were forbidden to exist in between), and that light would be emitted when an electron jumped *instantaneously* between these states[20].

we knew atoms were composed of a positively charged nucleus surrounded by negatively charged electrons. We also knew that some special (radioactive) materials spontaneously produced similarly charged particles—having an outstanding velocity. These materials were essentially particle *"machine guns",* and in a way, a stationary nucleus was a particle *"target"*[a].

Rutherford knew there were even more secrets of nature behind radioactivity, and the best way to expose them was by firing these projectiles (α and β radiation) at other atomic nuclei. Therefore, in 1919 he set out to study the collisions between α radiation and some gaseous elements like hydrogen, oxygen, and nitrogen. In his experiment with nitrogen, he noticed that somehow hydrogen was a byproduct[23], despite it not being part of the constituents. A few years later Rutherford and James Chadwick hypothesized that the collisions of nitrogen atoms with α particles were *transforming* the nitrogen atoms into oxygen, leaving a proton (hydrogen) behind[24]. Realizing this, Rutherford was the first person to identify a transmutation of matter; he had become the first real alchemist.

Eventually these collision experiments led Rutherford to think further about his nucleus, and he suggested that the nucleus must be made of protons[b]. He also pointed out that different elements were made of atoms with different amounts of protons in their nuclei—which matched the number of electrons orbiting around. This number was known as the atomic number, but the issue with this idea was that the protons alone could not explain the four-fold increase in atomic weight with increasing atomic number. In other words, an atom of helium (containing two protons) is four times as heavy as an atom of hydrogen (containing one proton). James Chadwick would later show that there were other particles inside the nucleus that could solve the issue, and these particles were electrically neutral, so he named them neutrons[25].

The humble neutron was unlike anything they had seen before. Being electrically neutral it became the *stealth bomber* of the particle world. If accelerated, it could approach the nucleus undetected and undisturbed, and given that all of our findings (up to that point) were done through ballistic collisions, the neutron presented a

---

[a] It is very interesting to see that particle collisions have been (from the beginning) the best way for us to understand matter. The LHC is just a more sophisticated and powerful *particle machine gun*.

[b] A word he borrowed from the Greek 'first'

whole new level of possibilities. In 1939, Otto Hahn was studying collisions of neutrons with radioactive uranium, and noticed that the element barium was coming out of his experiments[26]. This reaction contained an incredible amount of energy as it was splitting the uranium atoms into lighter elements.

Over the next few decades it was understood that this energy was released whenever the *strong nuclear force* was broken—and is by far the highest concentration of potential energy we have ever discovered. This eventually led to the creation of the atom bomb and some of the darkest times in human history—which is a story I do not need to re-tell here. But I would like to point out that Robert Oppenheimer marked the occasion as the moment when *"the physicists had known sin, and this is knowledge which they cannot lose"*.

1.6   Particles of cosmic origins

Parallel to all of these particular revelations of the early 20th century, astrophysicists were beginning to make direct connections between theories of sub-atomic particles and the observation the cosmos. One of the most revealing connections was made by Victor Hess[27], who in 1912 realized the radiation coming from the sky was strangely similar to the radiation coming from Becquerel's uranium salts[a]. Other connections with outer space were the calculations that in 1954 led Fred Hoyle to find that supernovas (and other star explosions) enabled the conditions for atoms to fuse together and form heavy elements that otherwise could not be formed in regular star fusion[29]. But Hoyle was not the only astronomer thinking about atoms and their origins, during the decades preceding Hoyle's finding, the physical[30] and chemical[31] evidence for the Big Bang Theory were found—and even more intimate connections between the universe and particle physics were made.

One of the most incredible findings that linked particle physics directly to cosmic observation, was the discovery of the anti-electron (or the positron)[32] as a particle of anti-matter—made by Carl Anderson in 1932. Such concept of anti-matter had already been suggested by Paul Dirac[33] in 1928 when his famous unification

---

[a] This was hardly the first intimate connection between matter and the heavens. One of the most iconic examples of this was the detection of helium in the Sun before it was found on Earth[28], a discovery that happened 45 years before Victor Hess' suggestion of cosmic radiation.

equation[a] resulted in two equal but opposite solutions—one for matter and one for anti-matter. This outstanding discovery was facilitated by yet another invention that (amid all of this wonder) is often taken for granted: the cloud chamber. The cloud chamber was invented years back in 1904 by Charles Thomson Rees Wilson, when he was studying cloud formations in controlled environments of supersaturated water vapor[34]. These cloud chambers enabled physicists to observe the traces left behind by charged particles as they moved through the saturated air and caused condensation. A background magnetic field placed on a cloud chamber allowed Anderson to notice that cosmic rays contained a particle of similar mass to the electron but with an opposite charge, hence the positron. Figure 4 shows a photograph of the first positron ever observed.
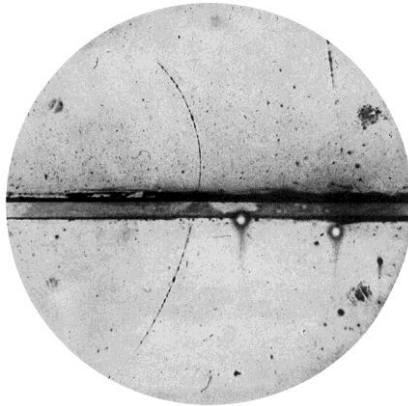
Figure 4 Cloud chamber photograph of the first positron ever observed
Image in the Public Domain via Wikimedia Commons

A collaborator of Anderson's, named Seth Neddermeyer was also studying cosmic rays in 1937, and that year, he found evidence of a particle that behaved very much like an electron, but had an much larger mass[35]. This was later known as the muon, and it raised many questions about the existence of more unstable particles like this one—but we were just getting started. In 1947 the pion[36], the kaon[37] and the lambda baryon were discovered using cloud chambers and magnetic fields as well—proving once again that high energy events (such as cosmic rays and radioactive emissions) were the most effective means to identify and study particles. The most relevant particle findings up to the 1950s are shown in Figure 5.

---

[a] Which reconciles relativity and quantum physics (although at the level of a single electron)
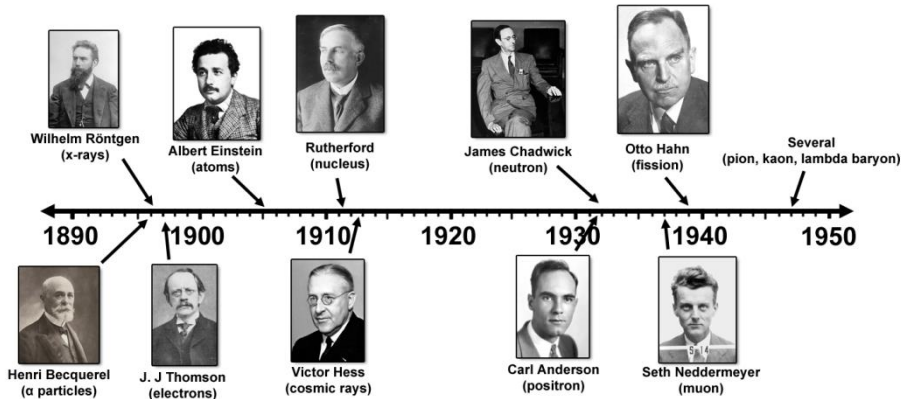
Figure 5 Timeline of the most relevant particle findings up to the 1950s.
Image made with photos in the Public Domain via Wikimedia Commons

1.7   Cyclotrons and synchrotrons

Nonetheless, natural sources of high energy particles (like radioactive materials and cosmic rays) were not our only hope. The cathode ray tube used by J. J Thomson decades earlier is an example of artificially accelerated particles. In fact, as early as 1930, John Cockcroft had already developed a method to accelerate protons[38] which he later used it to split the lithium atom[39]. This was in fact the first particle accelerator ever created with the goal of colliding particles.

Such device used a container filled with hydrogen gas where electric discharges would ionize the gas producing isolated protons. These protons were then attracted by an electric potential in order to isolate them and commence the acceleration[a]. Once the protons were inside the accelerating chamber, an intricate stack of capacitors was activated in sequence—allowing Cockcroft to reach energy levels of about 800keV. A much smaller value than the 2.3 MeV in α particles but at least they were free from β and γ rays[38].

Another clever particle accelerator idea was invented by Ernest Lawrence in the late 1920s, and later patented[40] in 1934. It is called a cyclotron and it uses a small flat circular chamber[b] inside a magnetic field where an electric potential could be alternated from one half of the circular chamber to the other half. A charged particle

---

[a] This method is still the same method used to inject protons into more sophisticated particle colliders like the LHC.

[b] In high vacuum, as all particle accelerators must be.

sitting at the center of this chamber would feel the attraction towards one side (half) of the circle, but because of the constant background magnetic field its trajectory would be deviated tangentially. Then, if the alternating electric field is synchronized adequately, the particle would spin in an outward spiral trajectory—eventually leaving the chamber with a considerable energy. A diagram of a cyclotron is shown in Figure 6.
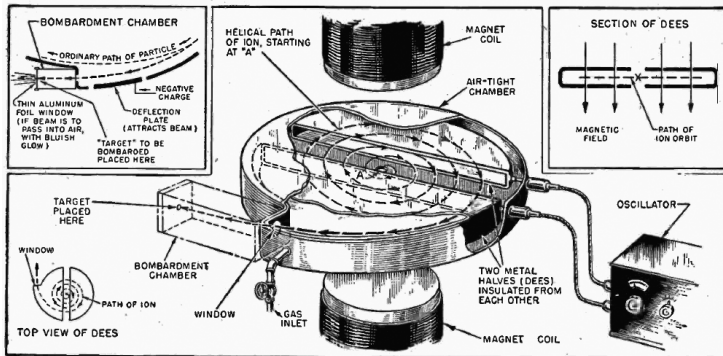
Figure 6 A diagram of a cyclotron showing the vacuum chamber and the two semi-circular plates that induce the electric field, these are called dees. A magnetic field is produced by two coils above and below the cyclotron.
Image in the Public Domain via Wikimedia Commons

Cyclotrons had the advantage of being very compact. The first prototype could fit inside your back pocket; and the largest one ever built was only 152 cm in diameter[41]. The latter, achieved a beam energy of 16 MeV—a milestone in particle physics. However, the *"appreciable variation in angular velocity"*[42] soon proved it obsolete—and instead, a similar idea (but at a much larger scale) succeeded the cyclotron.

In combination with the principle of the synchronous motor[6] (hence its name), the synchrotron uses a doughnut shaped vacuum chamber with a varying magnetic field engineered to match (*i.e.* to be synchronized with) the angular velocity of the particles. It was proposed by Edwin McMillan[42] in 1945 but his idea required a complex synchronization of the linear acceleration from the electric field and the centripetal acceleration of the magnetic field *at the same time*. This was solved rather simplistically the following year by Horace Richard Crane who proposed having a couple of semicircular sections solely responsible for the *centripetal acceleration* and a couple of straight sections solely responsible for the *linear acceleration*. Crane adequately called this "The Racetrack"[43], characterized by its

two "straight sections" and its two (later called) "arcs"[a]. A sketch of Crane's *racetrack* is shown in Figure 7.
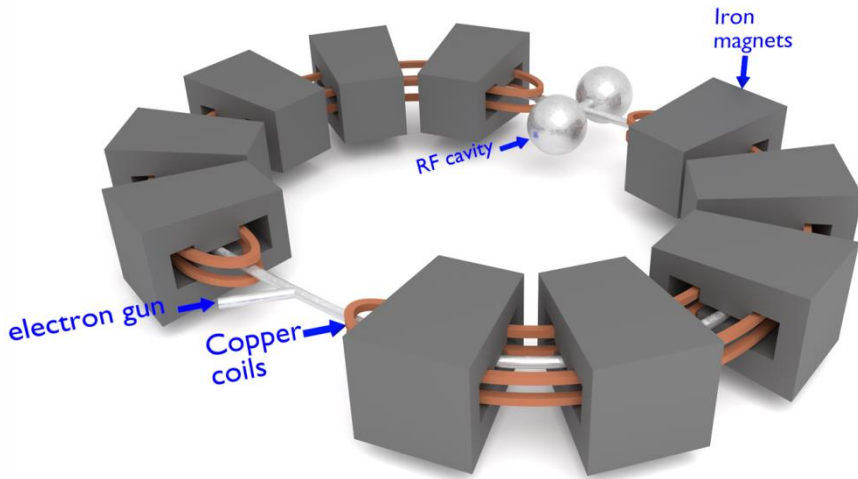
Figure 7 A sketch of the "racetrack" concept. A scale is not given since this was never built.

In 1948 William Brobeck[44] saw the potential of this technology, pointing out that *"The maximum obtainable energy…appears to be limited only by engineering capabilities"*, an affirmation that seems to be true even to this day. Brobeck also made a remarkable prediction when he said that similar machines would be built in the future without *"departing from the techniques used on machines at present in operation"*[b].

If you have been paying attention to the timeline, between 1930 and 1950, these artificial particle accelerators had been invented and engineered in silence—without any significant discoveries for many years. Meanwhile, scientists studying cosmic rays were basking in the limelight (or should I say cosmic light) using simple cloud chambers and magnets[32, 35–37]. This would soon change.

---

[a] Notice the straight sections have RF cavities on them while the arcs have magnets. RF cavities are devices of linear acceleration while magnetic coils are devices for centripetal acceleration.

[b] Once again he was right: the LHC and its planned successors are (and will be) based on these techniques.

1.8   Ramping up the energy

The first large scale synchrotron for particle physics was named the "Bevatron", and was capable of accelerating particles to 6 billion eV (or 6 GeV)[a] around a ring of approximately 153 meters in circumference. Built at the Lawrence Berkeley National Laboratory (LBNL), the Bevatron used four straight sections[b] and therefore four quarter-circular arcs filled with large iron magnets and copper coils weighing over 10,000 tons.

This multi-million dollar and ambitious project[c] had many challenges. Including trouble with the magnet power supply, and a small fire which required a three-month long repair[46]. Nonetheless it was a very promising prospect, after all—if the anti-electron was found—theory suggested that there must exist an anti-proton. This was in fact the main driver for the Bevatron project: the search for the anti-proton through collisions of a proton beam (accelerated by the Bevatron) against a copper target. In the end, neither the theory nor the engineering disappoint, the anti-proton was found[47] in 1956 by Owen Chamberlain's team. This discovery confirmed Dirac's anti-matter for the second time, and showed that we did not just have to rely on natural sources of high energy particles to make revolutionary findings. A sketch of the Bevatron is shown in Figure 8.

The Bevatron did not have a collimating system[d], and therefore had a massive aperture (4 feet wide). But once the synchrotron concept was proved, methods of collimating the beam were developed at the Brookhaven National Laboratory (BNL), in order to make more precise synchrotrons. The method was called strong-focusing, proposed by Ernest Courant, and it had the advantage of being suitable for both synchrotrons and linear accelerators alike[48]. This method suggested using a magnet/coil configuration which produces a 4-pole magnetic gradient capable of flattening the beam of charged particles. Using two of these magnets in series but rotated 90° along their common axis would effectively condense the beam to a single point. These were eventually called quadrupole magnets as opposed to the dipole magnets used to bend the beam along the arcs of a synchrotron. A pair of

---

[a] The average energy of primary cosmic ray particles is 10 GeV[45]

[b] Instead of two straight sections as proposed in the Racetrack idea

[c] It was suspected (at the time) that each GeV would cost between one to two million dollars[45].

[d] Beam concentration system

quadrupole magnets is shown in Figure 9 depicting the effects that each magnet has on the beam.
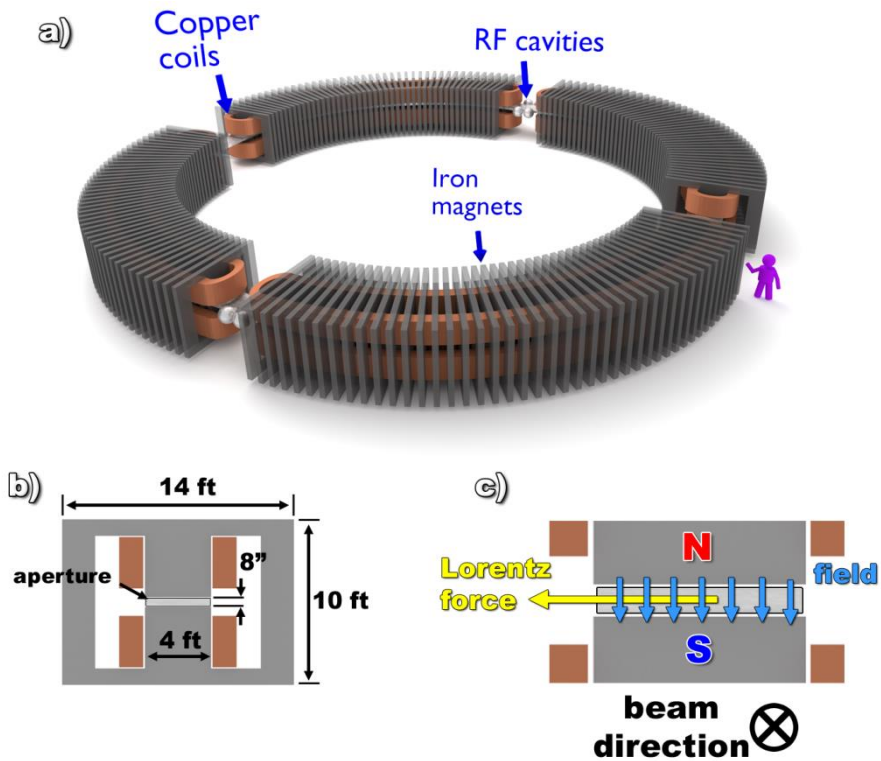
Figure 8 (a) A sketch of the Bevatron with (b) a cross section of its dipole (bending) magnets and (c) a close-up of the aperture showing the direction of the Lorentz force keeping the charged particles in the ring.

This collimation method (introduced in 1952) was the last piece of the puzzle regarding the main components of modern particle accelerators, which are:

1. A vacuum tube for the particles to move through.
2. A varying electric field (produced by RF Cavities) whose frequency matches that of the particle's velocity.
3. In the case of synchrotrons, a magnetic field (produced by dipole magnets) which induces a centripetal acceleration to keep the charged particles inside the ring.
4. And a complex magnetic field (produced by a pair of quadrupole magnets) that concentrates the particle beam.

These are still the main components used in *all* the successors of the Bevatron. Including the 28 GeV Proton Synchrotron at CERN (1959), the 33 GeV Alternating Gradient Synchrotron at BNL (1960), the 50 GeV linear accelerator of the Stanford Linear Accelerator Center (1962), and many others. These accelerators, in combination with a better version of the cloud chamber (called the bubble chamber[a]), would later prove extremely effective at finding new particles. The findings were in fact so common and overwhelming, that the collection of these new particles was famously coined the "particle zoo". The most relevant events in particle acceleration between 1930 and 1970 are shown in the timeline of Figure 10.
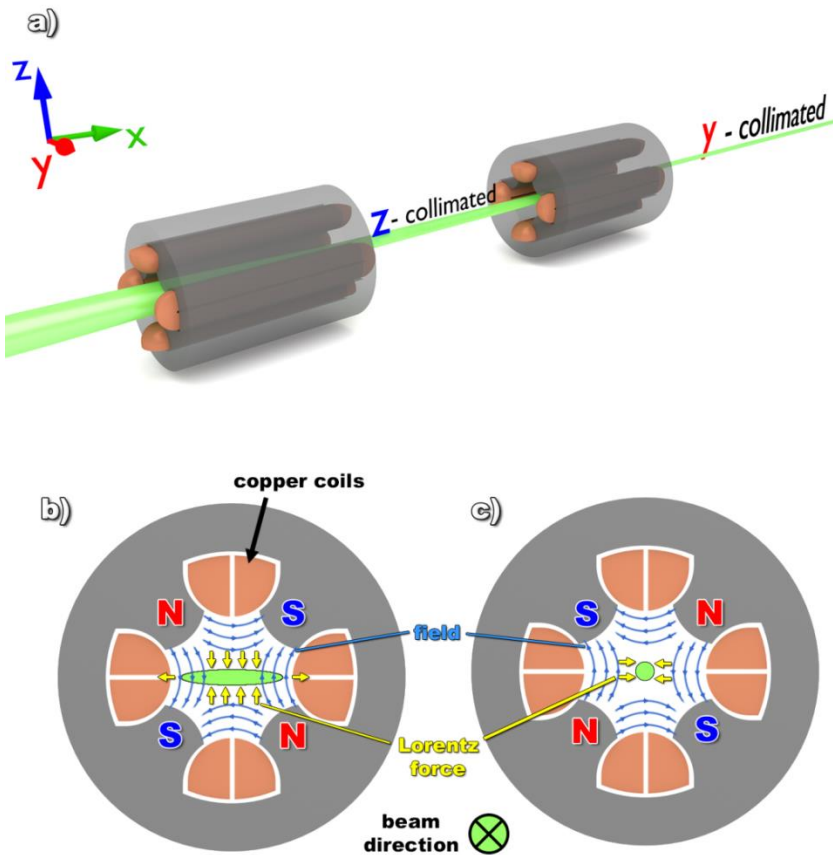
Figure 9 A sketch of a pair of quadrupole magnets placed in series but rotated 90° along their common axis showing their collimating effect. Cross sections of the two magnets and the beam morphologies after their influence are shown in (b) and (c).

---

[a] Invented by Donald Glaser[49] in 1952
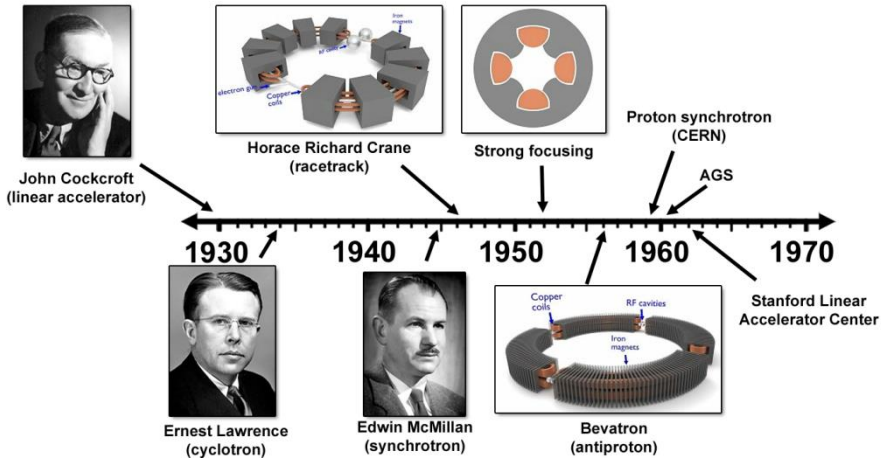
Figure 10 The most relevant events in particle acceleration advances until 1970.
Image made with some photos in the Public Domain via Wikimedia Commons

1.9   The standard model

In reality, any *high energy* scenario can lead to the detection of sub-atomic particles—which is why particle physics is often referred to as High Energy Physics. A nuclear reactor for example is a source of high energy radiation, and in 1956 the Savannah River Plant in the United States was used to detect a particle that had been predicted by the theory nearly twenty years earlier: the neutrino[50]. In reality the neutrino itself had not been observed, instead a very distinctive sequence of events predicted by the theory which were essentially 'footprints' of neutrinos. This became the most common way of identifying other elusive new particles—instead of detecting them, physicist would infer their presence—a connection that would be impossible to make without a proper understanding of the theory that had been formulated in parallel with all these amazing discoveries.

Understanding this particle zoo proved to be a monumental challenge, and in the 1960s theoretical physicists were having serious trouble classifying the particle zoo. Fortunately Murray Gell-Mann[51] came to the rescue when he introduced the concept of quarks which were later found by Elliot Bloom at the Stanford Linear Accelerator Center when his group was colliding high energy electrons with protons inside a bubble chamber[52]. Over the next couple of decades, this quark concept organized the particle zoo, showing that most particles (even those found later) were made of different arrangements of quarks. Furthermore, there were other fundamental particles called leptons, and a few bosons. This theoretical model is now known

today as the standard model, and it has been proven time and again inside particle accelerators. Today, thanks to this *ping-pong* match between theory and experiments, we have reached a pretty good understanding of what the atom (and therefore the universe) is made of. The different particles of the standard model are shown in Figure 11.
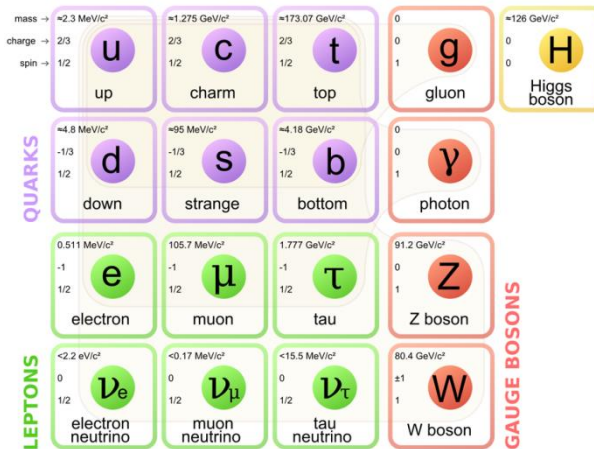
Figure 11 The model of elementary particles showing the three main groups of particles, quarks, leptons and bosons. Image under the Public Domain via Wikimedia Commons

1.10   To answer your question…

Over the last 120 years, high energy particle events have supplied us with the means to revolutionize our understanding of the world around us. From Rutherford's discovery of the nucleus, passing through the deep (and energetic) connection between stars and atoms, then the unveiling of the particle zoo, and lately the discovery of the Higgs Boson[a]. All of these are outstanding examples of the adventurous human spirit and the power of science—and all of these happened in a very small fraction of our existence.

Throughout this whole adventure, our curiosity has pushed human capability and has fueled some of our most daring hypotheses about the origin of the universe and its constituents. It has also spawned collaborations that go across borders and cultural barriers united by one common goal. And although at times it has exposed some of the most dangerous aspects of our own immaturity, it has also helped us grow and understand who we are, where we come from, and how far we are willing

---

[a] Made by CERN's LHC[53]

to go to unveil the secrets of nature. Additionally, we have made significant technological advances that have had a significant impact in our lives. Whether they are as simple as a vacuum system, or as complex as a nuclear reactor, these have been some of the unforeseen outcomes of our endless search for that which cannot be cut.

But the journey is not over. There are still many mysteries to be solved inside this intricate structure. For example, we have not been able to reconcile gravity with particle physics, and we still do not know what dark matter is made of—or what dark energy is. We are still searching for those answers. And even to this day, high energy events—such as those found both in particle accelerators and in celestial bodies—are our best bet for unveiling more mysteries of matter. So, to answer the question posed at the beginning, *"Why study particle physics?"*

I am afraid I must answer it with another question…

Why stop now?

Chapter 2 - Superconductivity in Particle Acceleration

——Superconductivity is a magic potion, an elixir to rejuvenate old accelerators——

Robert R. Wilson

As we have seen throughout this historical journey, higher energy means a higher probability of finding new particles upon collision. However, in the case of a synchrotron, this also means a need for higher magnetic fields in order to keep the beam inside the ring—or a larger ring (when increasing the magnetic field is not an option). For example, the Alternating Gradient Synchrotron (AGS) of BNL, was capable of producing a beam energy of 33 GeV (five times higher than the pioneering Bevatron), but because of its larger circumference, it required a lower magnetic field[a].

But whether it is *stronger magnets* or *more magnets* inside a bigger tunnel, their manufacturing represents a major construction cost for particle accelerators. Additionally, when made of copper and iron, the operation cost of these magnets is quite demanding[55]. To solve this dilemma, particle physicists focused their attention on *superconducting* magnets.

2.1   Superconducting magnet requirements

By the late 1960s superconductivity was already a well understood phenomena, and commercial Nb-Ti wires were already being widely used for research magnet manufacturing[56]. Nonetheless, building 774 7-meter long dipole magnets—with a high precision field that could be ramped from 0 T to 4.5 T in tens of seconds—was not an easy task. But in 1979 the US Department of Energy authorized the Fermi National Laboratory (FERMILAB) in Illinois, USA to build the first particle accelerator reaching 1 TeV, and the first to use superconducting magnets. Its name:

---

[a] The Bevatron magnets reached 0.98 T in a circumference of 153 m[45] while the AGS magnets reached 0.18 T in a circumference of 402 m[54].

the Tevatron[55].

2. 1. 1   *Challenges of superconductivity*

Although it is the logical thing to use, superconductivity is not an easy beast to tame. In order for a superconducting material to stay superconductive it must meet three conditions, or else its superconductivity is lost and any remaining flow of electrical current may result in a significant temperature spike—possibly damaging the magnet. These three conditions are:

1. A temperature lower than a certain "critical temperature", or T_c.
2. A magnetic field lower than a certain "upper critical field", or B_{c2}.
3. and, a flow of electrical current lower than a certain "critical current", or I_c.

These critical properties vary depending on the superconducting material, and they have been optimized throughout the years (within the natural limits of each material) reaching outstanding values in modern superconductors[57]. I do not want to go into the details and the physics behind superconductivity; I am more interested in the practical aspects of it—and the engineering ingenuity that has made them useful for particle accelerators.

The first issue that comes to mind is the necessity to keep these materials cold. Operating the Tevatron and any particle collider based on superconducting magnets requires every magnet to be inside its own cryostat, and each cryostat to be connected to a refrigeration system capable of keeping the magnets at liquid helium temperatures. The Tevatron magnets for example, require an operation temperature of 4.5 K in order to reach their peak field of 4.5 T without loss of superconductivity[55], while the LHC magnets are currently inside 400,000 liters of superfluid helium at 1.9 K[58] in order to push the operation field to 8 T[59].

2. 1. 2   *Rutherford cables*

Aside from the low temperature demands, magnet engineers had to deal with all the challenges that arise when an electrical current is moving through a magnetic field. Electrons in motion (either through metals or vacuum) produce an electric field that in turn responds to any background magnetic field[a]. This interaction affects the current flow and often produces current losses as well as local heating. This issue

---

[a] Including the one they create as a result of their movement, aka self-field

is also present in normal copper wires, and was partially solved decades earlier by engineers and physicist alike (including Lord Kelvin himself) during the industrial revolution after the failure of the transatlantic telegraph cable. The solution consisted on a simple geometrical alteration to the cables transporting the electric current: twisting. For superconducting cables this principle works the same way, and therefore a twisted cable was developed[60] in 1973 at the Rutherford laboratory in Oxfordshire, United Kingdom.

This cable was later known as the Rutherford-type cable (or just Rutherford cable). It is composed of a few dozen superconducting round wires transposed (or twisted) and flattened into a tape-like shape as shown in Figure 12.
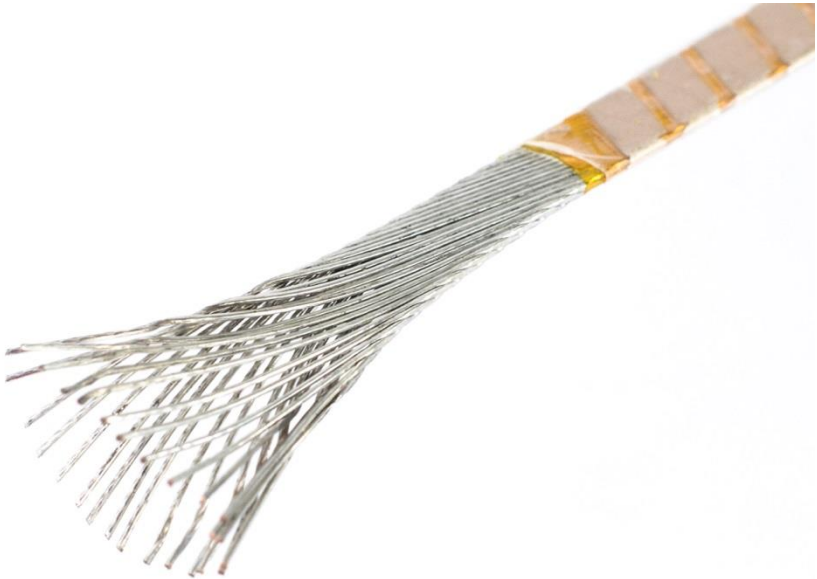
Figure 12 A photograph of a Rutherford cable slightly untwisted to show the transposition.

Rutherford cables also benefit from their compacted high aspect ratio geometry and their improved flexibility (compared to monolithic conductors)[61]. Today these cables are still the main prospect for any foreseeable accelerator-type magnets[62]. Nonetheless, it should be mentioned that that these cables are not perfect. During the Tevatron days, Nb-Ti Rutherford cables often had current values 14% lower than that of the short sample test summation[63], and preventing wire movement inside the magnets was quite challenging[64]. This current degradation was later improved to less than 8% during the optimization of cables for the Superconducting Supercollider

(SSC)[a]—mainly by improving the tooling and shaping of the wires during cabling[61].

2. 1. 3 *Cos-theta magnets*

The compact and well transposed design of Rutherford cables gave magnet engineers the means to create high-homogeneity dipole and quadrupole magnets, increasing the beam control like never before—and enabling smaller beam apertures. In the case of the Tevatron of FERMILAB, the magnets had an aperture diameter of 5 cm[55], compared to the ~7.6-by-16.5 cm elliptical aperture of the AGS at BNL[54], and the massive ~122-by-20 cm rectangular aperture of the Bevatron at LBNL[44]. From this point forward, field homogeneity and magnet compaction became a crucial way of cutting costs and increasing the precision of particle accelerators.

After many concepts were proposed on how to wrap Rutherford cables around to produce a homogeneous field inside a cylindrical volume[66], one of the most effective methods came to be known as the *cosine theta* configuration[67], proposed by S. C. Snowdon of FERMILAB. A cosine theta dipole magnet is essentially made of two elongated *pancake solenoids* that sit above and below the beam aperture. However, there are many geometrical considerations that need to be taken into account in order to make this shape possible. The necessary shape adjustments to transform a six-turn Rutherford pancake solenoid into a cosine theta coil are shown in Figure 13.

What we see in Figure 13(c) is often called a *block* (of a cosine theta magnet), and it is common for its Rutherford cables (tapes) to be aligned so that they all point to the center of the aperture. Now, the block of Figure 13(c) is not a very compact block, and therefore not very efficient for high fields. Ideally, one wants the tapes to be as close to each other as possible, but in order to have these tapes tightly packed—while conforming to the aperture circumference—there must be a "keystone angle" associated with these Rutherford cables. A sketch of a cross section of a simple Rutherford cable made of copper wires is shown in Figure 14, where its most relevant dimensions are shown. As you can see there is a certain deformation induced during cabling which in most cases results in current degradation.

---

[a] The SSC was a 20 TeV particle accelerator project that was cancelled in 1993 by US congress decision. Its funding was given to the Human Genome Project[65]
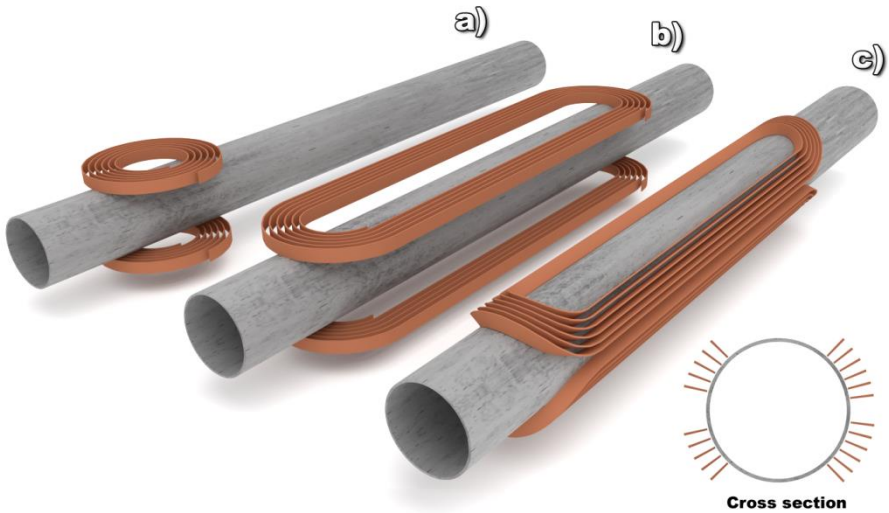
Figure 13 Sketches of (a) two pancake solenoids made of tapes (Rutherford cables) sitting above and below the beam aperture, (b) an equivalent elongated pancake (which is often called a racetrack coil), and (c) a cosine theta "block", which is the result of shaping a racetrack coil around a cylindrical volume. A cross section of this cosine theta coil is also shown.
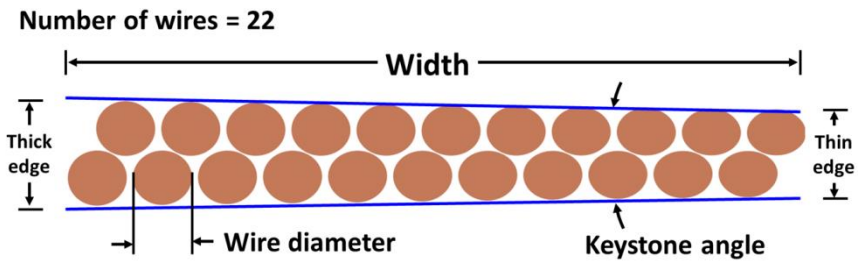
Figure 14 A simple Rutherford cable showing the most relevant dimensions required for a cosine theta block arrangement. All of these parameters can be changed depending on the magnet design.

More blocks are often desired to increase the number of turns and therefore the magnetic field. However, the high aspect ratio of the Rutherford cables allows for a limited number of blocks to be added before the keystone angle becomes insufficient to go around the circumference of the aperture. For this reason, *filler wedges* are added to maintain the integrity of the cosine theta blocks. Additionally, several block *layers* can be added to increase the turns further more. Figure 15 shows a sketch of a cosine theta dipole coil cross section with each coil (top and bottom) having an outer layer of two blocks, and an inner layer of three blocks. A similar design was used for the LHC[68].
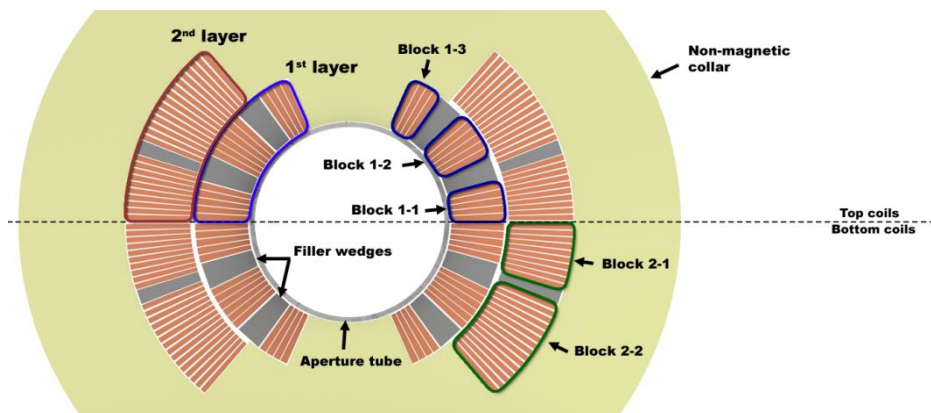
Figure 15 A sketch of a cosine theta dipole coil cross section with each coil (top and bottom) having an outer layer of two blocks and an inner layer of three blocks

All of the above are the main features of a cosine theta coil, a configuration that can be applied to both dipole and quadrupole magnets as well as other beam shaping magnets (that I have not talked about but that were developed during the Tevatron days) such as sextupoles, octapoles and decapoles.

As shown in Figure 15, this assembly of cosine theta coils are placed inside a non-magnetic collar (often made of stainless steel), which are then impregnated with epoxy to keep the coils in place. Finally, they are surrounded by an iron magnet (often called the iron yoke)[a] which provides a very small portion of the field and helps confine the field within the magnet[55]. A sketch cross section of an LHC magnet with its most relevant parts is shown in Figure 16. Notice that the LHC magnets have two apertures. Each aperture has a proton beam running in opposite direction to each other, and they are expected to meet at the collision points in order to produce a head-on collision (essentially doubling the energy). This dual beam concept was introduced for the Tevatron—thanks to the increased beam control— and proved very effective given the new particles found through it[69].

2.2   *Superconducting wires*

As you can see, the magnets inside a particle collider are very complex machines—with the ultimate goal of producing a homogeneous magnetic field over a very small cylindrical volume. However, there is one component which I have not

---

[a] If you recall, these iron yokes were also present in the Bevatron, just not inside cryogenic fluids (see Figure 8).

made the proper allusions to (given its vital task): the superconducting wires.
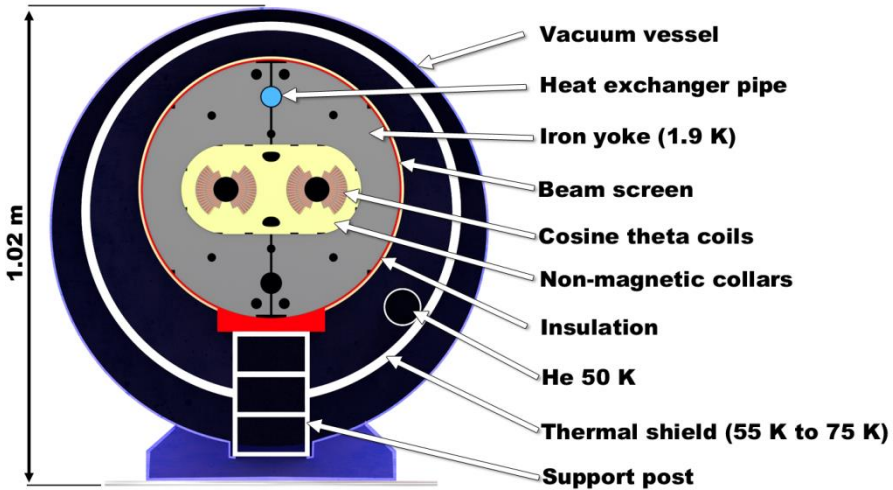
Figure 16 Cross section of an LHC dipole magnet

2. 2. 1   *Wire properties*

One of the most conspicuous features when looking at a cross section of a modern superconducting wire is the fact that it is made of multiple filaments inside a metallic matrix. This matrix is called the copper fraction (as is most often made of copper) with everything else being the non-copper fraction or Non-Cu area[a]. This was a feature introduced in 1965 when it was noticed that wires with a larger Cu-fraction were significantly more stable[b] than wires with a low Cu-fraction[70]. This concept, although found in Nb-Zr wires, applies to all wires, and the stability comes from the fact that any heat produced inside the superconducting filaments is able to travel through this matrix (out) towards the cryogenic bath surrounding the wires.

Often called a cryostabilizer, this matrix is required to be a high-purity metal with a large residual resistivity ratio (RRR) in order to be more efficient at heat conduction. For the LHC, because of the demanding magnet requirements[c], Nb-Ti

---

[a] This term can also be used for superconducting wires made of Bi-2212 where a silver matrix is used—despite the correct term being Non-Ag.

[b] Less prone to losing their superconductive state by transitioning into their normal state

[c] The LHC magnet ramp rate can cause significant flux-jumps (heating) and the particle beam itself can have enough energy to affect the magnets.

wires were fabricated with a rather large Cu:Non-Cu ratio between 1.65 and 1.95—as well as a RRR larger than 150. Another essential benefit of the high purity matrix is its ability to conduct the electric current whenever superconductivity is lost. Otherwise, this electric current would flow through the superconductor in its normal state, posing a threat to the integrity of the magnets because of the high resistance of superconductors in their normal state.

The shape of the filaments is also an important source of magnet stability. This feature was discovered in 1960 on permanent magnets made of parallel iron wires inside a Cu matrix.[71] In these magnets, it was found that the smaller the filaments, the higher the coercivity of the magnets. In the case of superconductors, it was later found[72] that smaller filaments made it easier for the wires to withstand a change in the background magnetic field without producing flux-jumps (which are also sources of heat)[73, 74].

Because of their outstanding ductility, Nb-Ti wires such as those currently in the LHC, can be fabricated with thousands of filaments of a few microns in diameter[75]. Such wires have a considerably low hysteresis loss [a] and a very narrow magnetization curve which result in a higher stability during magnet ramping. Because of this direct relationship between stability and filament size, the filament diameter is therefore a very common specification for superconducting wires—and it is often called the effective filament diameter, or D_{eff}.

Finally, the ability to conduct electricity is (for obvious reasons) the most important figure of merit of a superconducting wire. A superconductor reaches its critical current, I_c, at a point in which some of the current starts flowing through the stabilizing Cu, producing heat and eventually destroying superconductivity. This I_c is measured in amperes (A) and can vary between a few dozen amperes at high fields to a few hundred amperes at low fields depending on the superconductor material and the wire quality. However, because the wire diameter can vary depending on the magnet design (as well as the Non-Cu fraction), this value is often normalized to the equivalent area of superconductor. The normalized value of this critical current is called the *critical current density*, J_c measured in amperes per millimeter squared (A/mm^2). Figure 17 shows the two relevant areas for a generic example of a superconducting wire. J_c is equal to I_c over the Non-Cu area.

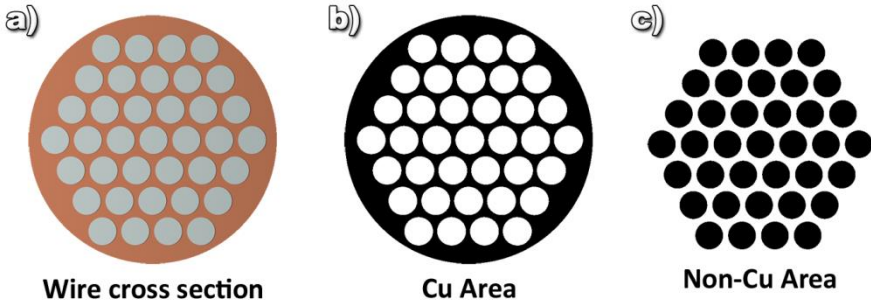[a] Hysteresis loss is also often referred to as AC loss

Figure 17 (a) A sketch of a generic superconductor wire showing the two relevant areas, (a) Cu area and (b) Non-Cu. The J_c is normalized over the Non-Cu area.

Now, because the critical current of all superconductors is a function of the temperature and the background magnetic field, it is very common to report a single number at a standard temperature and field value for wire benchmarking purposes. For convenience (unless otherwise stated) I will report J_c values for the rest of this thesis work at 4.2 K and 12 T—which has been a very common criterion for Nb_3Sn over the last few decades.

2. 2. 2   *Wire fabrication*

Most superconducting wires are fabricated using similar techniques. They all start with a single rod of the filament-material which is placed inside a tube of the matrix-material—and reduced in size through a series of extrusions, stacking operations, and wire drawing processes. In the case of Nb-Ti, its fabrication is relatively straight forward thanks to the ductility of Nb-Ti, and the starting "monofilament" is a rod of bulk Nb-Ti surrounded by a Cu tube (or jacket). Figure 18 shows the different fabrication steps of a Nb-Ti wire which are essentially repetitive steps of reduction and stacking—with intermediate steps of shaping and Cu-cladding. It should be mentioned that MRI-type Nb-Ti wires do not require this many filaments.

Extrusion is preferred whenever the ratio between the length and the diameter is low (*i.e.* large diameter), such as the first reduction of a monofilament or the first reduction after a stacking operation. Hot extrusion is also particularly beneficial to increase the Cu bonding between monofilaments and sub-bundles after each stacking operation. Additionally, extrusion often allows for very large reduction steps which are obviously beneficial to cut fabrication time. Cold-drawing on the other hand, is necessary at later reduction steps (when extrusion is not viable

because of a large length to diameter ratio). Drawing is also the preferred method for shaping the rods into hexagons. The result, as shown in Figure 18(c) is a wire of a few kilometers in length, a diameter of less than one millimeter, and a cross section made of multiple sub-bundles of stacked filaments. In wire manufacturing terms the final wire piece is called a billet, and since breakages during drawing are rather common, each billet could result in two or more wire pieces of a few kilometers in length.[a]

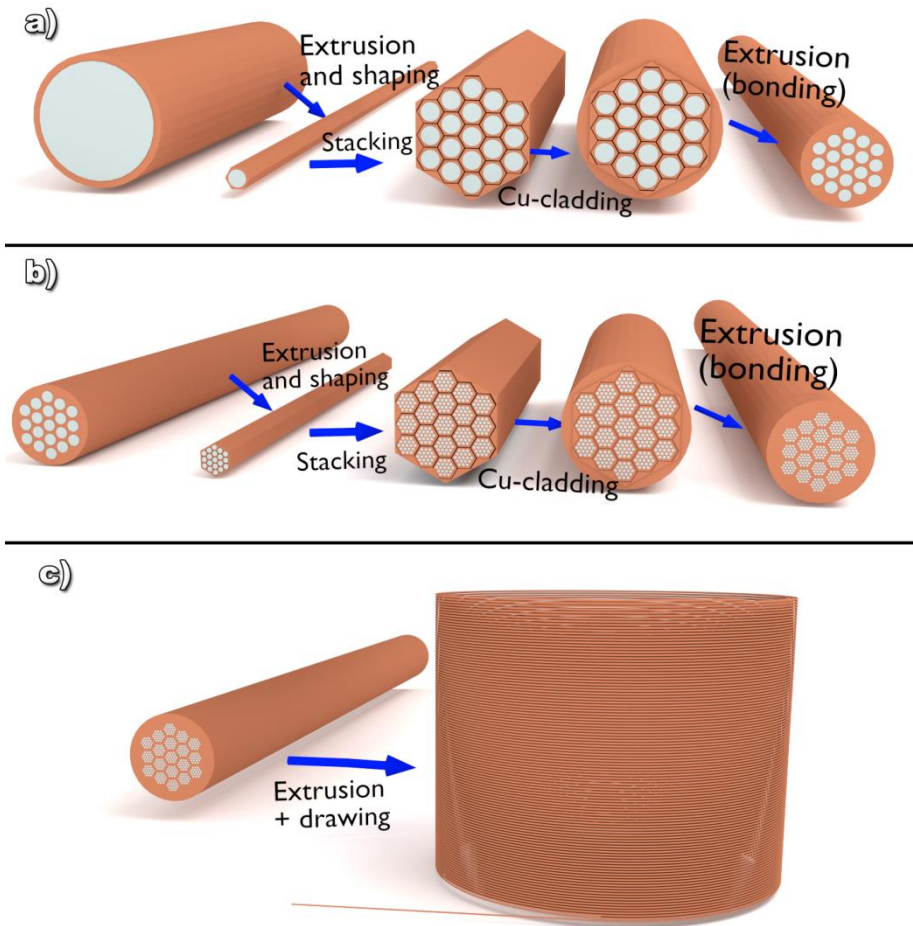Figure 18 The different fabrication steps of a Nb-Ti wire. (a) A Cu-clad Nb-Ti monofilament which is reduced, shaped, stacked, and bonded. (b) a Cu-clad sub-bundle of monofilaments which is reduced, shaped, stacked, and bonded. (c) a "final stack" which is reduced to an "as-drawn" wire.

---

[a] Is worth adding that before the last die pass the wires are twisted—this increases the electromagnetic stability.

2.3   The role of Nb₃Sn in magnet technology

Using Nb-Ti wires, the LHC currently produces a proton beam center-of-mass energy of 14 TeV. This historic record is achieved thanks to superconducting magnets running at a peak field of 8 T, which is (unfortunately) the practical limit of Nb-Ti dipole magnets[59]. So, if our goal for the future is to produce higher energy collisions we will most likely need dipole magnets made with superconducting wires capable of reaching higher fields.

The next wire technology in line, because of its cost and fabricability, is Nb₃Sn. However, there are many challenges when making magnets out of Nb₃Sn wires. The high strain sensitivity[76] of this intermetallic compound often lends itself to significant performance degradation during magnet operation[77]. Additionally, the fact that it is mainly a wind-and-react technology[a] increases the probability of impurities diffusing into the high-purity Cu—essentially *"poisoning"* it and affecting the RRR of the wire. Nonetheless, the advantages of using Nb₃Sn are far beyond Nb-Ti capabilities since the upper critical field of Nb₃Sn is ~29.5 T[78] compared to ~14.5 T for Nb-Ti[79].

Today, Nb₃Sn wires are commonly used to fabricate NMR magnets and other research magnets that require fields beyond the capabilities of Nb-Ti[80]. It is also the primary workhorse of the ITER experimental fusion reactor magnet system currently being built in the south of France[81]. However, there is not a single particle collider working with Nb₃Sn magnets to this day—despite the fact that our attempts to raise its standards go back as far as the year 2000[82] and many test-magnets have been built since.

The history and advancement of Nb₃Sn will be covered in the next chapter. For now, I would like to focus on the current state of this technology and the specifications required for the upcoming LHC upgrades or any future particle collider.

---

[a] Wind-and-react means that the wires are fabricated using ductile components, and the cables (as well as the magnets in their entirety) are assembled before the superconducting material inside the wires is formed through high temperature solid state reaction—or put more simply: a heat treatment.

2. 3. 1   State-of-the-art

Today there are four main Nb_3Sn wire types (or wire technologies) actively used in superconductor magnet manufacturing:

1. Bronze-process wires
2. Low-hysteresis Internal-Tin wires
3. High-J_c Internal-Tin wires
4. and High-J_c Powder-in-Tube wires

Over the last couple of decades, these four technologies have been used to make NMR magnets[80], fusion magnets[83], and even experimental dipole magnets[84]. It must be mentioned that each one of these magnet technologies requires slightly different wire properties depending on their operation demands. The ITER magnet system for example, because of the pulsed nature of its central solenoid, requires low-hysteresis loss wires—and therefore wires with a small D_{eff} such as Bronze-process[81]. NMR magnets, on the other hand, operate at peak-field permanently and are ramped up slowly—therefore a small D_{eff} (to mitigate flux-jumps) is not a main concern. Instead, NMR magnets are commonly fabricated using the so-called high-J_c wires[85] which often have a D_{eff} larger than 50 µm (compared to the 3-6 µm required by ITER).

Unfortunately, dipole magnets for particle colliders require the best of both of these worlds: a high-J_c and a low-hysteresis loss which are currently pushing the capabilities of the state-of-the-art Nb_3Sn wires.

All of the wire types mentioned above have slightly different components and architectures—with different means to deliver the Sn to an array of Nb filaments. But in the end, their ultimate goal is precisely that: using high melting temperature (>670°C) Sn-rich phases to diffuse Sn into Nb and form Nb_3Sn superconducting filaments. Now, being a wind-and-react technology, Nb_3Sn wires must be fabricated using ductile components: namely Sn, Nb, Cu, bronze, and/or powders of Sn-rich phases. Below I will describe the fabrication methods and the final electromagnetic properties of each one of these technologies.

2. 3. 1 (a) Bronze-Process method

Bronze-Process wires are fabricated very similarly to Nb-Ti wires. However, instead of using Nb-Ti filaments, they use pure Nb filaments or Nb-Ta, and instead of using a Cu matrix, they use and α-bronze (Cu-Sn solid-solution) matrix—often

alloyed with Ti[a]. The only issue with using a metallic solution as the matrix material is that the RRR is severely compromised[88], even after most of the Sn has left the matrix and has reacted to form Nb_3Sn. To counteract for this loss of RRR, a sheath (or jacket) of high-purity Cu is put around these wires—with a diffusion barrier in between in order to prevent poisoning of the Cu during the reaction.

Another issue of using an α-bronze matrix is the tendency of this material to work-harden during drawing steps (because of the notable deformation it undergoes). This work-hardening can therefore induce wire breaking, and for this reason, Bronze-Process wires require annealing steps between die passes (drawing steps) in order to recrystallize the bronze matrix to restore its ductility. A sketch of the stacking steps of a Bronze-Process wire is shown in Figure 19.
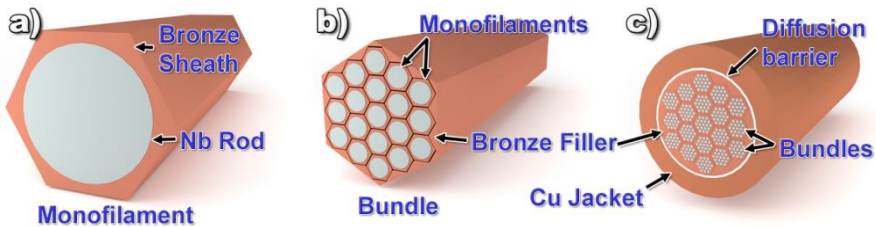
Figure 19 A sketch of the stacking steps of a Bronze-Process wire. (a) A monofilament made of a Bronze-clad Nb rod. (b) A group of monofilaments stacked into what is called a bundle (or sub-bundle). (c) These bundles are then stacked, and a diffusion barrier of either Nb, Ta, or both is added—as well as a Cu jacket to form the final wire. During drawing of the wire, annealing is necessary between steps in order to avoid work hardening of the bronze.

Modern Bronze-Process wires[89, 90] can reach J_c values as high as ~900 A/mm^2 at 12 T and 4.2 K (optimized for ITER use), but it should be mentioned that the Non-Cu area in this case includes the solid-solution matrix and the diffusion barrier also. In other words, *only* the high-purity Cu counts as the Cu-fraction; the rest of the wire (regardless of what it is made of), *is* part of the Non-Cu. Such restriction causes the J_c normalization to produce a much lower value because of the larger area—and therefore wire engineers are often inclined to minimize the real estate area taken by components which are neither the superconducting filaments nor the high-purity cryostabilizer.

Bronze-Process wires are the Nb_3Sn technology which allows for the lowest

---

[a] Ti is used[86] to increase the high field properties of Nb_3Sn, but in Bronze-Process it also enables the α-bronze to support a higher Sn content without producing intermetallic precipitation in the solid solution[87]

hysteresis loss[a], reaching values as low as ~200 mJ/cm^3 for a ±3 T cycle as a result of the thousands of well separated filaments with diameters between 1 to 4 µm (depending on the wire design).

2. 3. 1 (b) Single-barrier Internal-Tin

Internal-Tin[b] is the main focus of this thesis work, but as you will see in the next chapter, this wire type can have different versions within this same subdivision. One of these is the single-barrier Internal-Tin—which was also significantly driven by the ITER project[91]. It consists of circular (or ring-like) arrays of Nb filaments inside a Cu matrix with a Sn core inside of each one of these rings—often called sub-elements. These wires can produce slightly larger J_c values than Bronze-Process wires (~1000 A/mm^2 at 12 T and 4.2 K) but this comes at a cost of a slightly larger D$_{eff}$ and therefore a higher hysteresis loss (~900 mJ/cm^3 for a ±3 T). A sketch of the stacking steps of a single-barrier Internal-Tin wire is shown in Figure 20.
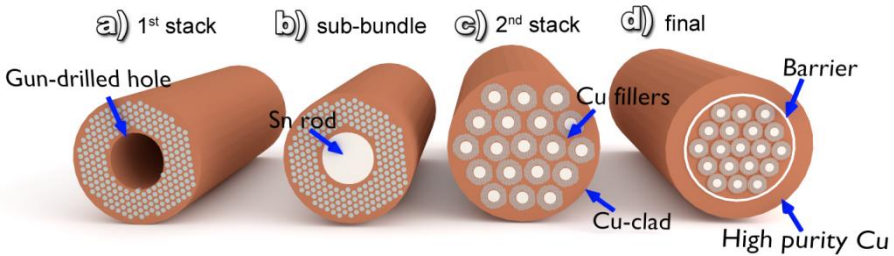
Figure 20 Sketch of the stacking steps of a single-barrier Internal-Tin wire. (a) The first stacking sequence made of a ring-like array of a Nb filaments inside a Cu matrix with a gun-drilled hole in the center. (b) The first stack after a Sn rod is inserted; this configuration is called a sub-element. (c) A stacked array of sub-elements. (d) A wire cross section after the diffusion barrier and the stabilization Cu have been added.

2. 3. 1 (c) High J_c Internal-Tin

High J_c Internal-Tin wires are nowadays being fabricated solely by Oxford Superconducting Technology (Bruker-OST since early 2017) and their particular product is denominated Restacked-Rod Process (RRP®). These wires consist of similar sub-elements like those used in single-barrier Internal-Tin except that each

---

[a] We should keep in mind that the Nb-Ti wires are far superior regarding hysteresis losses (lower loss value) because of the small filaments achieved thanks to the great ductility of Nb-Ti.

[b] I have decided to use the word Tin (instead of Sn) for this unique case when talking about wire types since it is very common to refer to Internal-Tin using its acronym IT.

sub-element has its own diffusion barrier—which is why this wire type is often called distributed-barrier Internal-Tin.

Aside from having a barrier of their own, the sub-elements in a distributed-barrier Internal-Tin wire have a much lower Cu content (than their single-barrier counterparts) between the Nb filaments—causing them to be in close proximity with each other. This Nb filament proximity, combined with the significant expansion of Nb in the Nb_3Sn reaction, produces bonding of the filaments and in many cases a monolithic ring of Nb_3Sn. As expected, the bonding of the filaments results on an increased D_{eff}—which in fact matches very closely the size of the sub-element[92].

This wire approach has produced the highest J_c ever achieved[93] in a Nb_3Sn wire (~3000 A/mm^2), but unfortunately in a massive 85 µm D_{eff}—and therefore not very practical for dipole magnets and much less pulsed magnet applications[a]. We will explore RRP® in much more detail in later chapters, but for now, it is worth mentioning that the best combination of high J_c and small D_{eff} reached by an RRP® billet batch (in average) is roughly 2,900 A/mm^2 and 55 µm[b]. The stacking steps of an RRP® wire are shown in Figure 21.

2. 3. 1 (d) Powder-in-tube

Powder-in-Tube is another wire technology that can be regarded as "high-J_c", and in fact it has been considered for particle collider magnets as well[84]. This technology uses powdered $NbSn_2$ (another Nb-Sn compound) inside a Nb tube with a small Cu sheath between the inner tube walls and the powder[95]. These are then stacked to form a wire that can reach ~2,700 A/mm^2 with a D_{eff} between 30 µm and 50 µm[96]. A sketch of a cross section of a PIT wire is shown in Figure 22.

As they stand today, the different (approximate) J_c values and D_{eff} of these four technologies are shown in Table 1, it is worth mentioning that the Cu-fraction can shift these normalized values up or down depending on the required cryostability.

---

[a] This 3000 A/mm^2 record is an average value, some billets have been reported[94] as high as 3300 A/mm^2

[b] At such large D_{eff}, the hysteresis loss values (in mJ/cm^3) get to be much larger than the previously mentioned values and are therefore not measured for benchmarking purposes. Instead the D_{eff} is the easiest way to compare these wires regarding their hysteretic properties.
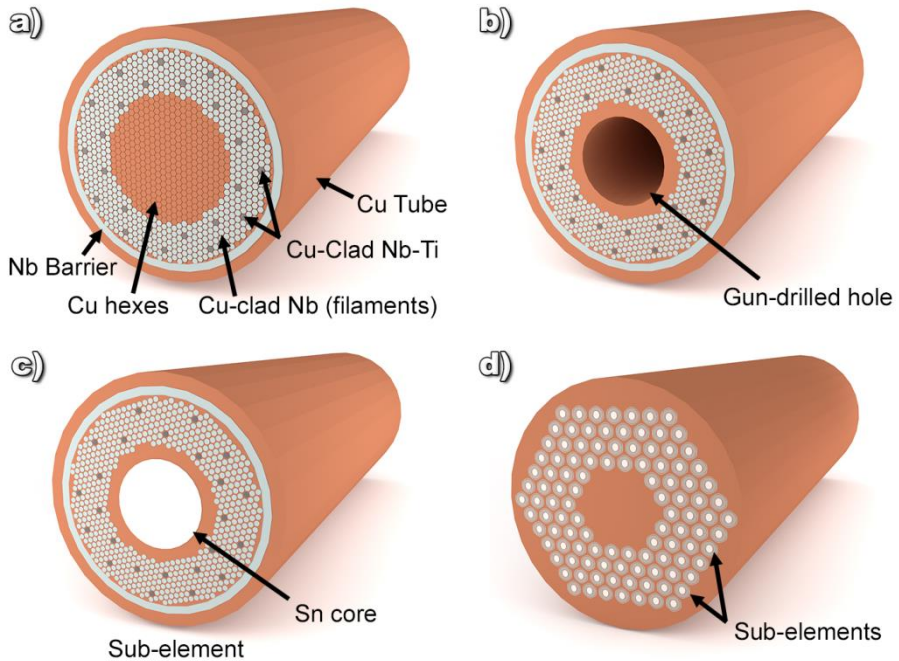
Figure 21 (a) A sketch of stacked Cu hexes and Cu-clad Nb rods-in-hex surrounded by a Nb tube and a Cu tube. Notice a few Cu-clad Nb-Ti rods are used for doping purposes. (b) A sketch of the previous stack after extrusion to bond the components, and after gun-drilling the center in order to insert a Sn rod. (c) The sub-element complete once the Sn rod was inserted and the components bonded via cold-drawing. (d) A sketch of a fully processed RRP® wire after the sub-elements have been restacked and a Cu jacket added
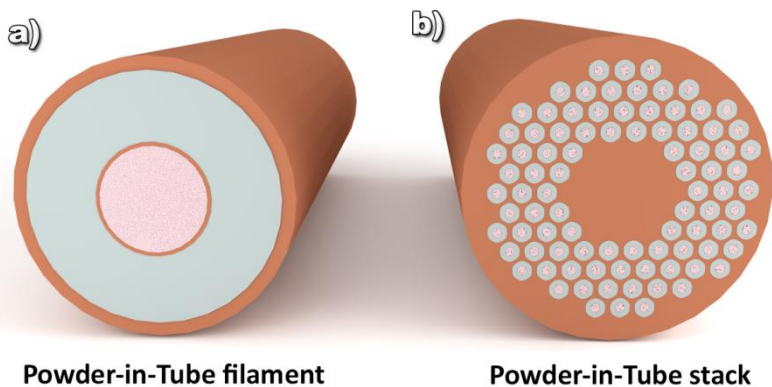
Figure 22 A sketch of (a) a single Powder-in-Tube filament and (b) a final stack of a Powder-in-tube wire after the Cu jacket was added and the filaments fully bonded.

Table 1 Critical current density of the most commonly used Nb_3Sn wire technologies.

Wire type	J_c (A/mm^2)	D_{eff} (µm)
Bronze-Process	~900	2-4
Internal-Tin	~1000	3-6
PIT	~2700	30-50
RRP®	~2900	40-70

2. 3. 2   *Nb₃Sn for the LHC*

Upgrading the present capabilities of the LHC is the most logical path to towards further understanding of the standard model and beyond. The first step in CERN's approach towards higher energy collisions is replacing a few of the key quadrupole and dipole magnets of the present collider in order to increase the beam concentration and therefore the luminosity[97] (number of collision events). This is expected to be achieved using a few dozen (shorter) 11 T dipole magnets to make room for more collimators[84], and some large-bore quadrupole magnets at the interaction regions[98], all made with Nb_3Sn wires. The project is called the High-Luminosity LHC which will be the first time a particle accelerator relies on Nb_3Sn magnets.

After many adjustments of magnet design and wire specifications, the RRP® wire design proposed for Hi-Lumi LHC quadrupole magnets must have a diameter of 0.85 mm, containing 108 discrete sub-elements and a Cu fraction of no less than 52.4%[99]. This wire should be capable of transporting over 600 A of electricity in a background magnetic field of 12 T and a temperature of 4.22 K. It has also been established that the dipole magnets will use a very similar wire design[84]. We can boil down the requirements for both magnet types as wires with a J_c of ~2500 A/mm^2 and a D_{eff} of 50 µm, as well as a RRR of over 150—a target that is currently possible with both RRP® and PIT wires.

However, looking further into the future, CERN and its numerous collaborators around the world have put forth a concept for an ambitious 100 TeV collider[100] requiring over 5000 Nb_3Sn superconducting magnets along its 100 km tunnel[a]. The project is called the Future Circular Collider (FCC), and it will require[102] magnetic fields in the range of 16 T. One of the biggest challenges for such magnet system is the fabrication of hundreds of tons of (cost-effective and high-quality) Nb_3Sn wires. For this reason, several national laboratories around the world as well as industry

---

[a] Compared to the 14 TeV center-of-mass energy, and 27 km circumference of the LHC[101]

vendors have been collaborating for decades to make this project viable.

As far as wire specification requirements go, the demanding FCC magnet goals make it more convenient to report the benchmarking wire J_c at 16 T instead of 12 T J_c as it has been done for decades. Thus, the FCC requires wires with more than 1500 A/mm^2 at 16 T[84] which can be translated (roughly) to 3000 A/mm^2 at 12 T[103].

If you recall, this is the current Nb$_3$Sn record J_c achieved[93] by an RRP® wire, therefore it does not seem like an impossibility. However the most important challenge will be reducing the D$_{eff}$ to less than 20 µm while still maintaining a RRR of 150[84]. Other FCC wire specifications are shown in Table 2.

Table 2 Specifications of the Nb$_3$Sn "dream wire" expected for the FCC[84].

Wire diameter	(mm)	0.5 to 1
Non-Cu J_c (16 T, 4.2 K)	(A/mm^2)	≥1500
D$_{eff}$	(µm)	≤20
RRR	(--)	≥150
Length	(km)	≥5

2.4   Conclusion

The Large Hadron Collider is the result of over three decades of international scientific collaboration[104]. Driven solely by human curiosity, we have built a particle accelerator that can recreate instances similar to those produced at the birth of the universe—and has enabled us to test some of the most daring theories about matter[53]. Superconductivity is one of the technologies that has made this ambitious experiment (the LHC) a reality, but unfortunately it has also been its most important limitation[59]. In order to unveil more secrets of the sub-atomic world, we are determined to increase the collision energy of the LHC, but to do so we must move beyond Nb-Ti and improve Nb$_3$Sn wire technology to unprecedented demands. This thesis work is an attempt to improve the properties of RRP® wires—with the ultimate goal of meeting the FCC demands—while at the same time exploring metallography and microscopy techniques which can be applied to other wire technologies.

Chapter 3 - History of Internal-Tin Wires

> —*The duty of the man who investigates the writings of scientists–if learning the truth is his goal–is to make himself an enemy of all that he reads...and attack it from every side. He should also suspect of himself, as he performs this critical examination, to avoid falling into either prejudice or careless thinking—*

> *Alhazen*

The first few decades of the Nb_3Sn technology can be better understood when paralleled with Nb-Ti—because when we do this, it is inevitable to ask the following question:

> *What the hell took Nb_3Sn so long?*

Superconductivity in Nb_3Sn was discovered[105] in 1954, that is, seven years *before* the discovery of Nb-Ti. And as you can see in the timeline of Figure 23, it took seventeen years for the first *experimental* Nb_3Sn multifilamentary wire[106] to be developed—as opposed to the twenty-month period between the discovery of Nb-Ti[107] and its first experimental multifilament wire[108]. Furthermore, the first *commercial* Nb_3Sn wire[109] came eight years after the first commercial Nb-Ti wire[56]. So what happened?

Both technologies grew up together, and both benefited from various electromagnetic discoveries[110] such as twisting[72], having multiple filaments[71], and using Cu as a cryostabilizer[70]. But Nb_3Sn seems to have had a much longer incubation time[a], despite its substantially superior superconducting properties—and our ever-growing hunger for higher fields.

To add to this delay, the first multifilamentary Nb_3Sn wire was made by what could be called the '*easy way*' of making Nb_3Sn wires: the Bronze-Process method[106, 111], using Nb filaments inside a matrix of workable α-bronze phase[112].

---

[a] The time period between its discovery and its commercialized product

Once fully processed, this bronze/Nb composite is heat treated in order to form Nb_3Sn by reacting the Sn in the α-bronze matrix with the Nb filaments. In the early days of Nb_3Sn, this method was the most feasible despite requiring very time consuming annealing steps[a], and it is still widely used today[80]. However, the main drawback of the Bronze-Process is its limited current carrying capabilities due to the low solubility of Sn in Cu—even with the so-called super-bronze[87], which can have up to 18.5 wt% Sn (10.8 at% Sn) as opposed to the binary solubility limit of 15.8 wt% Sn (9.1 at% Sn)[113].
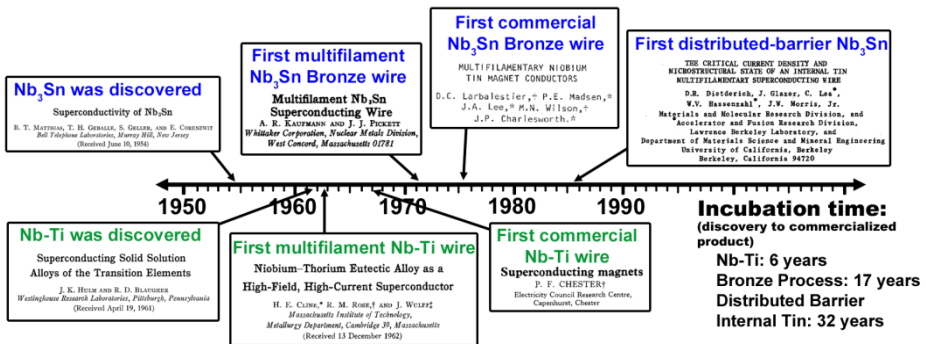

Figure 23 Timeline of the most relevant events in the early history of Nb_3Sn and Nb-Ti.

It was not until three decades after the discovery of Nb_3Sn, that the first wires[114] resembling today's most viable candidates[62] for the LHC came to be. These wires are called distributed-barrier Internal-Tin, and are the result of the Internal-Tin method[115] fabricated as discrete sub-elements—each with its own diffusion barrier. Recall Figure 21(d) on page 36.

In this chapter I will go over the entire history of Nb_3Sn wires (focusing mostly on Internal-Tin). As you will see, this technology took a very long path to its current state-of-the-art, filled with detours that later proved inferior[116] as well as promising research initiatives that moved on to other technologies[117]. Nonetheless distributed-barrier Internal-Tin wires are still the most viable candidates for a Nb_3Sn-based particle collider.

---

[a] To avoid work hardening of the bronze

3.1   Strenuous beginnings

As evidenced in the scientific literature, the Nb-Sn system took several years to be adequately understood. To begin with, the first phase diagram produced in 1959 (four years after the discovery of Nb_3Sn)[118], failed to identify two of the most easily formed phases in the system[a]. Three years later[119], these phases were detected, but mislabeled as Nb_3Sn_2 and Nb_2Sn_3. That same year (1962), one of these mislabeled phases was reported in the second phase diagram attempt[120], as well as two other imaginary phases: Nb_4Sn and Nb_2Sn. It was not until after sixteen years from the discovery of Nb_3Sn that a proper Nb-Sn phase diagram was formulated (in 1970)[121]—with its three distinctive, and unique intermetallic phases: Nb_3Sn, Nb_6Sn_5, and $NbSn_2$. The most important of these three is (of course) the practical superconducting phase Nb_3Sn, while the other two are not as practical and are rather problematic[122]—although still superconducting at lower temperatures[123]. Figure 24 shows the latest phase diagram of the Nb-Sn system[b].

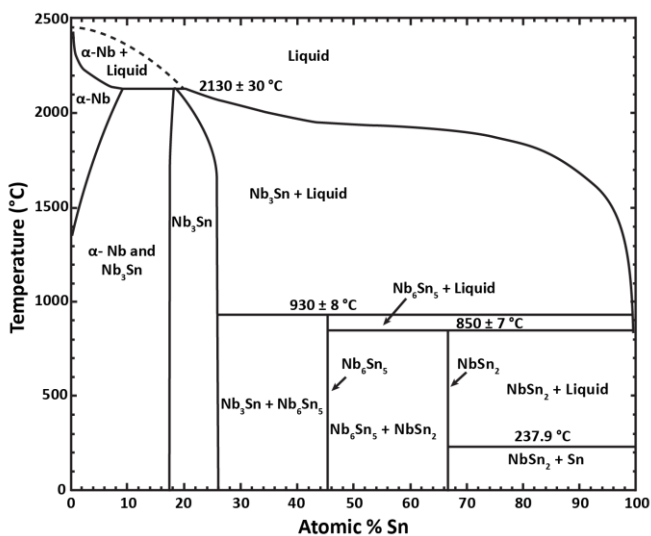Figure 24 Phase diagram of the Nb-Sn system

It should be mentioned at this point that Nb_3Sn is often called by the name of its crystal structure, a body centered cubic lattice with two Nb atoms on each face as

---

[a] $NbSn_2$ and Nb_6Sn_5

[b] Notice that Nb_3Sn has a rather wide composition. This lends itself to non-stoichiometric formations of lower Sn content which often produce lower quality wires.

seen in Figure 25. It is very common to exchange the term Nb_3Sn and the term A15 back and forth without any particular consistency.
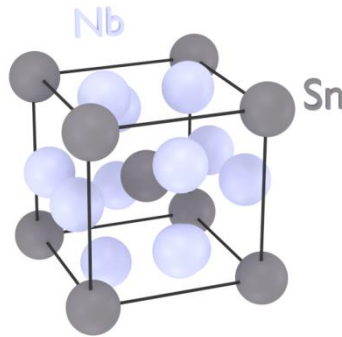

Figure 25 The A15 crystal structure of the Nb_3Sn superconducting intermetallic compound.

The scientific literature also evidences that, while the material scientists were bashing their heads against the wall trying to understand this complex thermodynamic system, the engineers were not necessarily sitting around twirling their thumbs waiting for the science to be understood. Even nine years before the Nb-Sn phase diagram was established, engineers at Bell Labs were readily mixing Nb and Sn powders inside Nb tubes and annealing (or heat treating) them at very high temperatures[a], producing a wire with very promising practical applications[124]. These properties caught the attention of General Electric who two years later managed to produce 88 A/mm^2 at 12 T on a short sample[b], and made a small solenoid reaching 2.38 T[125].

Despite the complicated system and the difficulty of making such wires, it was very clear that a new game in high-field superconductivity had begun. Figure 26 shows the relevant events mentioned in section 3.1.

3.2   The bronze detour

The efforts to understand the Nb-Sn phase diagram and to produce a successful Nb_3Sn wire using pure Sn came to a hold with the discovery of the Bronze-Process method in 1971[106]. By this time, the benefits of a twisted multifilament composite

---

[a] One case going as high as 1800°C to sinter the powders and then melting at 2400°C to form Nb_3Sn upon cooldown.

[b] Although still reporting imaginary phases

were already known[71], therefore the multifilament feasibility of this method gained much attention[112]. Another important benefit of the Bronze-Process method was the fact that the presence of Cu seems to lower the Nb_3Sn formation temperature from well above 1000°C to a much more accessible ~700°C[111]. It is worth recalling the fabrication process of a Bronze-Process wire at this point; see Figure 19 on page 33.
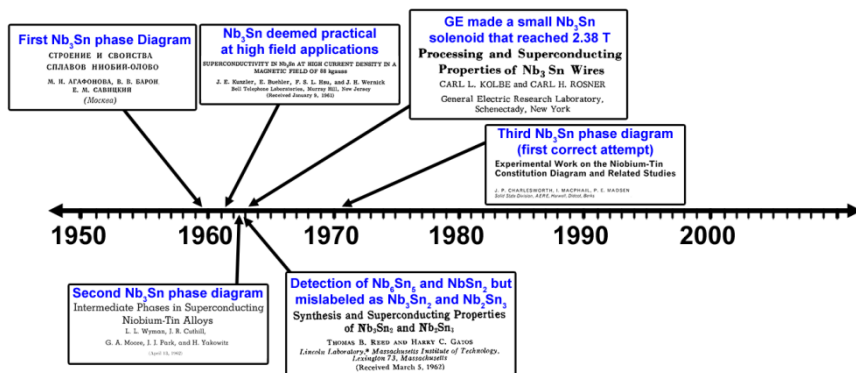

Figure 26 A timeline of relevant events mentioned in section 3.1.

I do not want to digress too much into the evolution of the Bronze-Process method, but it is worth mentioning that its rise, facilitated several advancements of Nb_3Sn wire fabrication, such as the use diffusion barriers[109], and the use of Ti as a doping agent[86, 126]. Additionally, the Bronze-Process industry helped fund several research initiatives towards our understanding of the Internal-Tin method[116, 127]. So despite having a glass ceiling (foreseen even in its early days[109]), the Bronze-Process method was essential for the understanding of the Nb_3Sn technology as a whole— and today these wires are widely used in the NMR industry as well as in research laboratory magnets[80]. These wires also represent a significant fraction (if not the majority) of the Nb_3Sn conductors in the ITER magnets[83].

The obvious way to overcome the low Sn content of α-bronze was to use high-Sn alloys (or even pure Sn) as the Sn source. However this presented many challenges for wire manufacturers for two reasons: (1) any wire containing pure Sn cannot be hot-extruded without melting the Sn[128] and (2) most Sn-Cu phases (see Figure 27) or Sn-Nb phases (see Figure 24) are very brittle, and cannot be drawn into wires[128, 129] unless they are used as powders[95]. So, it is of no surprise that the Bronze-Process method remained the leading Nb_3Sn technology for many years—and it is very competitive even to this day given its scalability and its low cost.
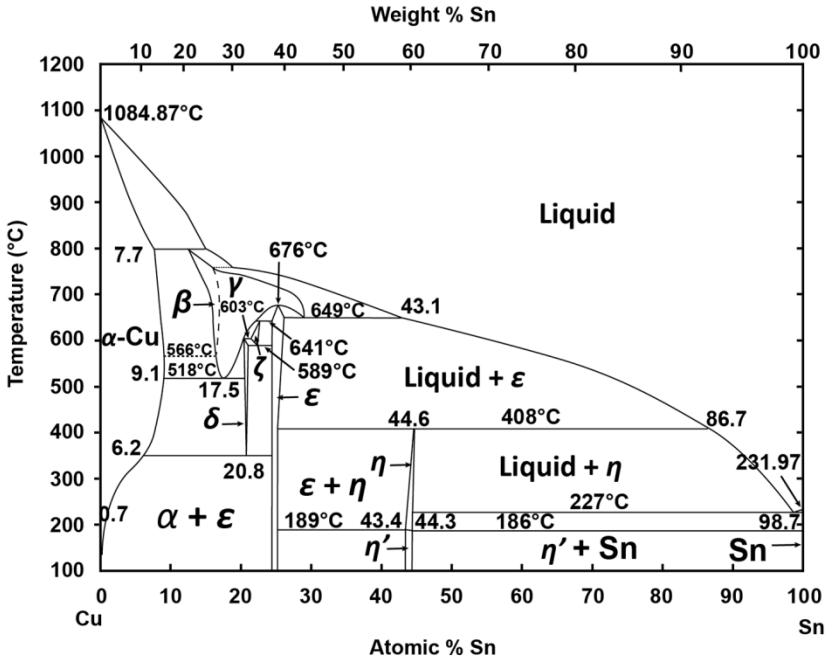
Figure 27 The Cu-Sn phase diagram. This phase diagram will be very relevant for the rest of this chapter and in chapters to come.

3.3 The Modified Jelly Roll detour

The Modified Jelly Roll (MJR) method was a wire fabrication method proposed, patented, and commercialized by Teledyne Industries, Inc.[130]. It was first patented to form Bronze-Process composites in 1981[131], then patented with a diffusion barrier (still bronze) in 1983[132], and finally patented to form distributed-barrier Internal-Tin wires in 1990[133]. The method uses an expanded sheet of niobium, and a solid sheet of Cu (or bronze) rolled several times around a Sn (or a bronze) core. This multilayered *"jelly-roll"* is then surrounded with a diffusion barrier and a stabilizing Cu jacket. Figure 28 shows the fabrication method of an Internal-Tin MJR element. The MJR-*Bronze* element uses the same steps, except that the Cu sheets (and the core) are made of α-bronze. Another difference of the MJR-*Bronze* element is that the barrier is preferably made of Ta since a Nb diffusion barrier would form a surrounding ring of Nb_3Sn which would increase the hysteresis losses of the wires. It should also be mentioned that although these expanded sheets do not appear to form a filament-like array when rolled at this size (Figure 28), they do form very long and discrete filaments when drawn to final size. The drawing process elongates these

diamond shapes so much, that their intersections are miles apart at final size[134], so a single MJR-Bronze element is essentially a multifilament wire.
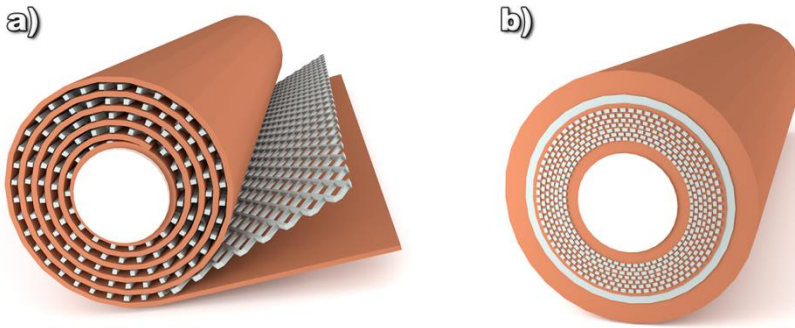

Figure 28 The fabrication steps of an Internal-Tin MJR element showing (a) the wrapping process and (b) the final product after the Nb barrier and Cu jacket are added and cold-drawn to bond the components.

A few years after the method was first patented, Teledyne shifted their efforts towards an MJR distributed-barrier Internal-Tin wire, that is, a restacked version of the MJR element in Figure 28. However, this posed two challenges: the first challenge was that restacking would require Nb barriers, since Ta diffusion barriers often produced wire breakages[132]. The use of Nb as a barrier also meant the MJR elements would form a Nb_3Sn layer on the inside of the barriers, making the D_{eff} as big as the MJR element. The second challenge was that, as mentioned before, using Sn cores makes the final composite unable to be extruded, and it can only be cold-drawn, which produces poor Cu-Cu bonding when stacking[135]. Nonetheless the stacked MJR (Internal-Tin) multifilament quickly became feasible[136] and was patented by 1990[133].

The method definitely seemed promising, and Teledyne quickly explored many aspects of the wire including Mg as an alternate dopant[133], and V or Ta as alternate diffusion barriers[130]—although with little success on either attempt. The main challenge for MJR in the 1990s, was the high hysteresis loss due to the fact that the D_{eff} is roughly as big as the MJR element[130]. Teledyne managed to reduce this hysteresis loss slightly with the use of Mg[133] as well as by altering the heat treatment schedule[136], but ultimately the most obvious way to decrease hysteresis loss was to stack more MJR elements in the same wire to reduce their size, and therefore reduce D_{eff}.

This was not achieved until 1997 when Oxford Superconducting Technologies

(Bruker-OST since early 2017) acquired the MJR patent, hired some of Teledyne's employees[137], and managed to produce a 91-stack MJR wire[a].

Between 1997 and 2001, OST was experimenting with various wire fabrication methods, including Bronze-Process, Powder-in-Tube, distributed-barrier Internal-Tin, single-barrier Internal-Tin, as well as MJR[116]. All these wire methods were significantly improved during this time, but as far as MJR goes, OST managed to tune certain wire properties through the alteration of the metal ratios in the MJR element. For example, it appears that having excess Cu lowers D_{eff} significantly[b]; an effect that is owed to the fact that the Nb_3Sn mass is sufficiently separated by Cu phases in order to inhibit magnetization currents. However, this comes with a sacrifice in J_c since the excess Cu represents an important non-superconducting fraction of the real estate in the non-Cu package. MJR wires fabricated with excess Cu are often called medium-J_c or low-J_c material, and, as it will be discussed in a later chapter, a similar effect is seen in RRP® wires with the same name given to these low-hysteresis options.

OST also improved the critical current density of their "high-J_c"[c] MJR material by 25%[116] compared to the MJR of the Teledyne days[130]. But despite all the advantages of MJR such as being able to make small test billets[137] and the ability to fine-tune J_c and D_{eff}, MJR was ultimately overtaken by distributed-barrier Internal-Tin[116] in 2001. And since then, OST focused most of its R&D on distributed-barrier Internal-Tin—later patented as RRP®[138]. MJR has not been commercialized since 2001. Figure 29 shows the relevant events mentioned in sections 3.2 and 3.3

3.4   Other detours

Before going further into the history and development of Internal-Tin, I would like to pay tribute to the inventive wire engineers who managed to come up with other ingenious methods that unfortunately did not become feasible wires. As it will be shown below, one of these methods in particular (the External-Tin method),

---

[a] One more hexagonal row than the 61-stack produced by Teledyne

[b] This effect was known since the Teledyne days[133] but OST improved it as far as to be considered for ITER use[137].

[c] High-J_c refers to the grade of MJR and Internal-Tin that is optimized for J_c at the expense of some hysteresis loss.

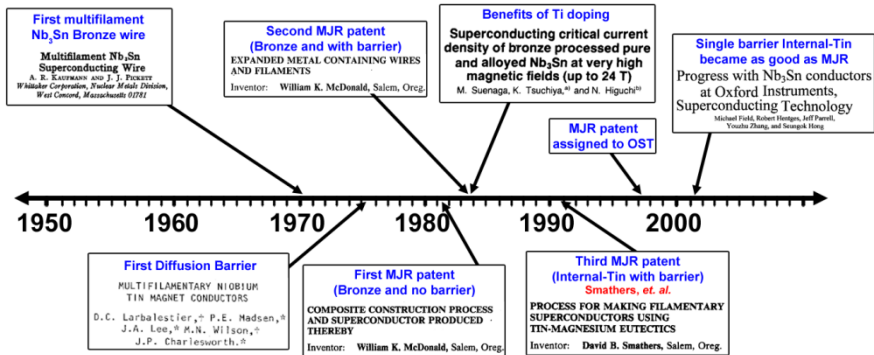significantly influenced the industry, and its effects are still seen today.

Figure 29 Timeline of the relevant events mentioned in sections 3.2 and 3.3.

3. 4. 1   External-Tin method

Taking our timeline aback slightly, one of the early attempts to produce a Nb_3Sn wire without the intricate annealing steps of Bronze-Process, as well as without having to avoid extrusion, was called the External-Tin method, pursued by Cogan *et al.* from the department of materials engineering at the Massachusetts Institute of Technology (MIT)[139]. The process itself was introduced a few years earlier[111, 140], but by the early 1980s, the engineers at MIT were the main drivers of this technology[139]. The method consisted of an array of Nb filaments inside a Cu matrix[a], drawn to final size, and electroplated with Sn. This coated wire was then heat treated at low temperatures to "mix" the Sn with the Cu, and later heat treated at higher temperatures to form the Nb_3Sn

The main issue with this wire fabrication method was the delamination of the Sn source from the wire[142] that occurred during the mixing heat treatment because of the significant volumetric changes produced as the different Cu-Sn intermetallic phases formed[143]. Figure 30 shows sketches of the External-Tin reaction. Notice that the Nb_3Sn reaction does not happen until the wire is taken above 600°C, the rest of the reaction is just an attempt to mix the bronze and consume low melting temperature phases (see Figure 27 for melting temperatures).

By the second half of the 1980s, the reaction complexity, the low RRR, and the

---

[a] With filaments as small as 100 Å in diameter, and some wires having up to 9.8 million filaments[141].

delamination during reaction proved this method ineffective. Nonetheless, I would like for the reader to keep this process in mind, because for the first time, a multi-step heat treatment was suggested[140] in an attempt to homogenize the Cu-Sn phases and avoid porosity[144]. These multi-step heat treatments were later known as "mixing heat treatments". And as it will be seen later in this chapter, the multi-step heat treatment introduced by McInturff and Larbalestier[140] and later improved by Cogan *et al.*[139]—to prevent delamination in External-Tin wires—set the tone for the heat treatments later adopted by the Internal-Tin method[127].
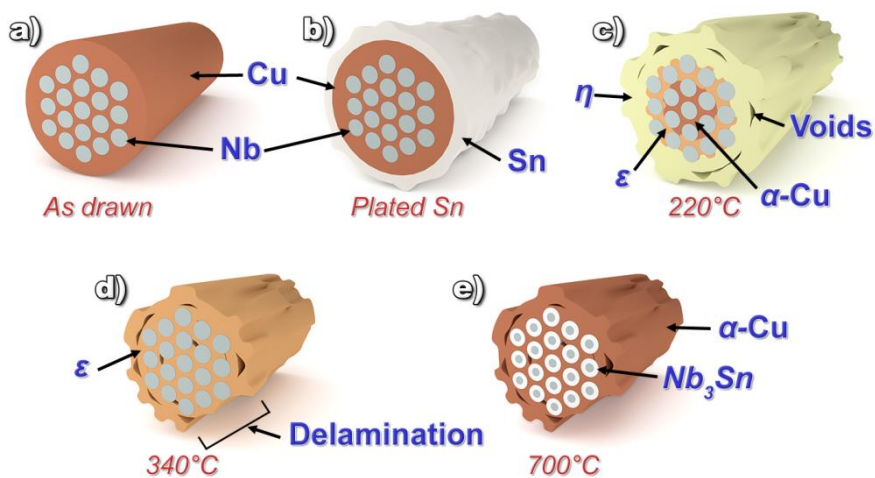

Figure 30 Sketch of the External-Tin process and its reaction. (a) The Cu/Nb composite at final size. (b) Electro-plated Sn layer. (c) Initial isothermal step at 220°C to consume the pure Sn. (d) Second isothermal step at 340°C to consume all η and ideally obtain only ε or α-bronze. (e) Final isothermal step at around 700°C to form the Nb_3Sn—leaving an α-bronze matrix behind.

3. 4. 2   Other early alternatives

There are other interesting alternatives that are worth mentioning for completion. One of them was called the in-situ method[145–147] proposed first in 1973. This method used a ductile alloy prepared by induction-melting Cu and Nb powders. The melt was then water-quenched to form dispersed dendrites of Nb inside a Cu matrix. This ductile metallic mix was drawn to final size—making the Nb dendrites very elongated, but despite being very close they fundamentally disconnected. The as drawn wire was finally electroplated with Sn (or submerged in a Sn bath), to be reacted in a similar manner as External-Tin. This method disappeared from the literature after 1981[128]—two years before the last External-Tin paper.

Another failed wire fabrication method was called the infiltration method[148]

proposed in 1977. The method used a porous piece of Nb, obtained by powder metallurgy techniques, which was "infiltrated" with liquid Sn. Once cooled, it was mechanically reduced to final size and then reacted to form Nb_3Sn. The method had promising properties for the time, but the absence of Cu demanded very high reaction temperatures. The last paper referencing this method was published in 1979[149].

Finally, the last failed wire attempt I want to mention here came from Intermagnetics General Corporation (IGC, nowadays Luvata-Waterbury). It must be mentioned that IGC later became a very successful wire manufacturer—being the first to make a commercialized Internal-Tin wire in 1983[150], and dominating the *distributed-barrie*r Internal-Tin industry until RRP® came along in 2003[151]. However, during their pioneering years, IGC attempted many wire fabrication techniques[152] that seem counterintuitive nowadays. In one of their most ambitious composites, their monofilament was made of a Sn-rich Cu-Sn alloy[a] surrounded by a Cu jacket. They successfully reduced this monofilament through extrusion and drawing, although reporting serval issues (as one would expect in hindsight). IGC never reported any progress on this wire style, most likely due to the countless issues that can arise when stacking and processing such large amounts of brittle Cu-Sn phases. Figure 31 shows the relevant events from section 3.4.
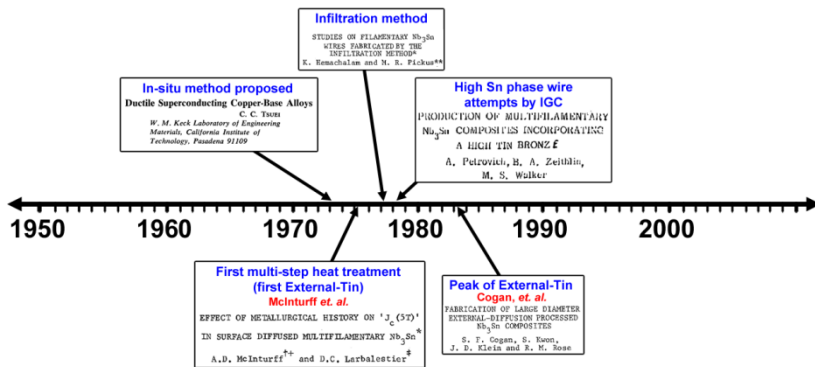

Figure 31 Timeline of the relevant events from section 3.4.

---

[a] 70 % Sn, which would be mostly made of the brittle phase η (see Figure 27).

3.5   *The Internal-Tin method*

Having introduced all these previous technologies, I can now focus on the Internal-Tin method and therefore RRP®. The first Internal-Tin wire was fabricated by Mitsubishi Electrical Company in 1974[115], and it quickly called the attention of the entire superconducting community since it had almost four times the J_c of the Bronze-Process at the time[112]. The method, as previously explained in sections 2. 3. 1 (b) and 2. 3. 1 (c), uses a pure Sn core[a] surrounded by a ring-like array of Nb filaments inside a Cu matrix.

During the early stages of the Nb$_3$Sn wire industry, the main merit of Internal-Tin was the fact that (unlike the Bronze-Process) it did not need annealing steps between reduction steps[128]—albeit with the downside of not being able to be extruded.

Mitsubishi's first wire used only 118 well separated Nb filaments, but ten years later, IGC managed to stack 72,102 Nb filaments around a Sn core with very little Cu spacing between the filaments[150]. They called it "Tin Core Process", a name that never stuck. A sketch of the cross sections of the Mitsubishi wire and the IGC sub-element are seen in Figure 32. As you can see, these are indeed two very different wire designs despite falling under the same category by today's wire nomenclature.
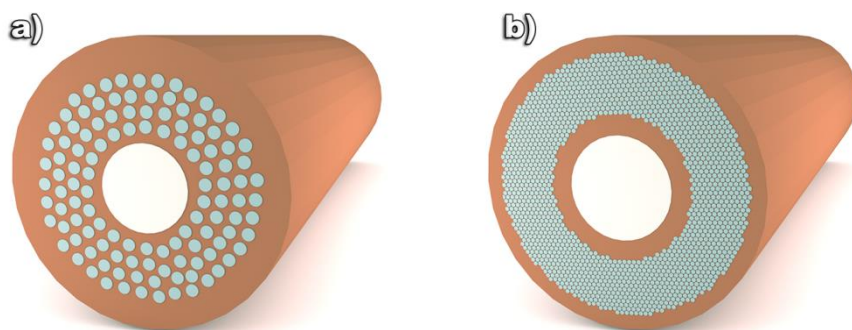

Figure 32 Two sketches illustrating the metal ratios of (a) the first Internal-Tin wire from Mitsubishi and (b) IGC's first Internal-Tin sub-element of a wire known as Tin Core Process.

---

[a] Although nowadays it can include up to 1 wt% Cu[138]

The ability to independently determine the filament size[a] and their spacing[b], gave this process an incredible versatility. Soon IGC came up with the distributed-barrier Internal-Tin[114], and by 1985 they had made significant advances on the performance, the fabricability, the reliability, and the cost effectiveness of both the distributed-barrier and the single-barrier Internal-Tin —to the point where they could justify stopping all work on Bronze-Process[127].

3. 5. 1   *Reaction crossroads*

The main issue with Internal-Tin was that the Sn source was highly concentrated, and Sn gradients during the A15 reaction were suspected[115]. This assumption led wire manufacturers to try and "mix" the Cu-Sn phases before reacting to form Nb_3Sn[c]. Material scientists[d] also supported the idea of mixing, since a kinetic model that would work across all wire types[114] could be extremely useful[e]. In an attempt to improve their knowledge about mixing Cu-Sn phases, IGC engineers looked for guidance from the *mixing experts* (at the time): the MIT engineers working on External-Tin[f]—after all, they deemed their process as *"the art of plating"*[127].

The problem was that the engineers working on External-Tin had stronger reasons to "mix" the phases. For them, the melting of high-Sn phases, the rapid Sn diffusion, and the formation of Kirkendall voids meant delamination and loss of wire integrity—which is not the case *at all* for Internal-Tin. But regardless of the significant differences in the wire types, a mixing heat treatment was readily adopted by IGC.

This alliance of the External-Tin experience and the Internal-Tin immaturity was the beginning of an empirical search for an ideal *stepped* heat treatment under the assumption that Kirkendall voids were detrimental to wire properties, and that a homogeneous bronze mix needed to be obtained (around the Nb filaments) before

---

[a] It is very important to keep in mind that (in Internal-Tin wires) a filament is different from a sub-element (see Figure 21)

[b] In RRP®, this spacing is often called the Cu-channel[92]

[c] The mixing was later shown to be nearly impossible in LHC-type wires[153].

[d] Particularly a group from Brookhaven National Laboratory (BNL)

[e] Such model is still a "holy grail" that has not been found. Most successful kinetic models only work for a reaction through bronze phases[154,155].

[f] Their collaboration is seen in reference [150], having Cogan (from MIT) as a co-author.

the A15 reaction—supposedly to obtain better wire properties. From here on, IGC engineers set out to *"homogenize for several hundred hours at low temperatures"*[150], and (as it will be shown below) most papers regarding mixing were empirical shots in the dark at a very complex kinetic system that even today is not well understood[156]. The utopian situation of a perfect mix is depicted in the sketch of Figure 33 for a wire similar to Mitsubishi's first wire[115], needless to say this would be much more difficult to attain in a wire like IGC's (see Figure 32).
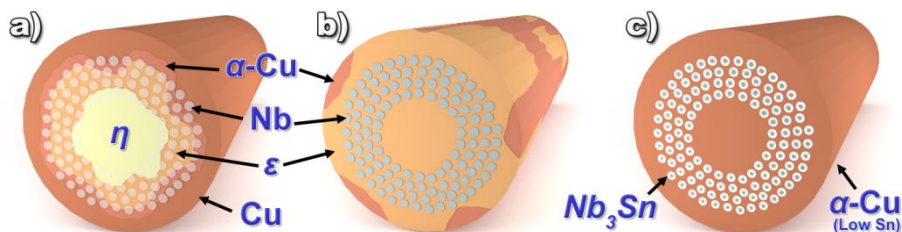

Figure 33 Sketches of what an ideal mixing should look like (ignoring the formation of Kirkendall voids to emphasize just the Cu-Sn mix). (a) Below 227°C, and ideal consumption of Sn and a full transformation to η, ε, and α-Cu (a certain transparency was applied to the filaments to see the Cu-Sn phases more clearly) (b) Below 408°C, an ideal consumption of η and a full transformation to ε or α-Cu and (c) Above 650°C, the final reaction of Nb and Sn facilitated by the ε surrounding the Nb filaments.

3. 5. 2   *Jumping to conclusions*

After the alliance between IGC and MIT in 1983, their eagerness to mix the Cu-Sn phases was very clear[150]. They even introduced a term called the "Bronze-to-Nb Ratio" referring to the ratio between *"the bronze formed after homogenization"* and the Nb[a]. They also claimed (using images of fully reacted wires) that a "*uniform reaction*" is indicative of a *"proper homogenization of the bronze*", yet no Cu-Sn micrographs were ever shown to prove this claim.

The success of the IGC Internal-Tin process encouraged other research groups to improve their *stepped* heat treatment, but several articles in the scientific literature evidence the lack of understanding behind the Internal-Tin reaction. One key paper[157] from BNL attempted to optimize Cogan's heat treatment in IGC wires, and concluded (empirically) that the *"amount of void content does not influence the values of J_c for these wires"*. Another paper[114] from LBNL pointed out that the mixing reaction suggested by IGC (at 200°C for over 100 hours) made no difference in J_c. These two claims seem to contradict the reasons why such stepped heat

---

[a] That is assuming homogenization actually happens, which it does not[153].

treatments were suggested in the first place! Nonetheless, the fear of voids and the affinity to mix the Cu-Sn continued alive and well throughout the 1990s[158].

To make matters worse, once MJR started being manufactured commercially as Internal-Tin in 1990, Teledyne Inc. also embarked their heat treatment R&D under the assumption that *"Large Kirkendall voids are detrimental to the wire"*[131] with very little science behind this claim[a]. Finally by the time OST was ready to acquire the MJR patent (1997, see Figure 29), and develop their own distributed-barrier Internal-Tin, both Teledyne and IGC had settled for a *stepped* heat treatment—still under the assumption that Kirkendall Voids should be avoided and that a proper mixing is to be obtained before A15 reaction. This gave OST no other choice but to search for a heat treatment under similar assumptions given the many years of extensive empirical research done by such expert companies.

3. 5. 3 The mixing reaction evolution

So far I have only introduced the general picture of mixing heat treatments, which is:

> Stepped heat treatments were rooted in External-Tin ideas and
> were tested empirically for years under the assumption that
> avoiding Kirkendall voids and promoting Cu-Sn mixing was
> vital for optimizing the A15 reaction.

However, let us go back to the beginning of the idea of mixing in order to understand why the different mixing reactions were suggested, and hopefully at the end of this section we will have a clearer idea of why there are so many different Internal-Tin heat treatments—and why there are so many contradictions about today's purpose for a mixing heat treatment[156].

3. 5. 3 (a) McInturff and Larbalestier[140], 1975

This is, as far as I could find, the first instance where a stepped heat treatment

---

[a] It must be mentioned that in some instances, the variation of the mixing isothermal steps and their ramp rates *did* affect the wire properties. For example, it was found that a fast ramp rate could decrease the D_{eff}[159], and a smaller amount of voids could reduce the J_c scatter[158] (both effects were seen in single-barrier Internal-Tin wires). However in most cases the conclusions applied only to some Internal-Tin wire designs and not for others—and most papers such as reference [159] contained too many variables to reach a solid conclusion.

was attempted in a Nb_3Sn wire. As I have mentioned before, it was applied to an External-Tin wire in order to avoid melting away and/or physically separating the phases (delamination). The wire was coated through a method called 'thick' tinning, done in a Sn bath (therefore above 227°C, see Figure 27 for the phase diagram). After this thick-tinning, two isothermal mixing steps were applied, one at 400°C which they labeled the "solid-state phase" or the "η-phase" stage—presumably to transform the η phase into the ε phase. And another isothermal mixing step at 550°C said to be a *"Compromise between minimum Nb_3Sn formation and uniform distribution of the Sn"*[140]. Finally, the wires were held above 650°C to produce the Nb_3Sn^a. The heat treatment schedule used by McInturff and Larbalestier[140] is shown in Figure 34.[b]
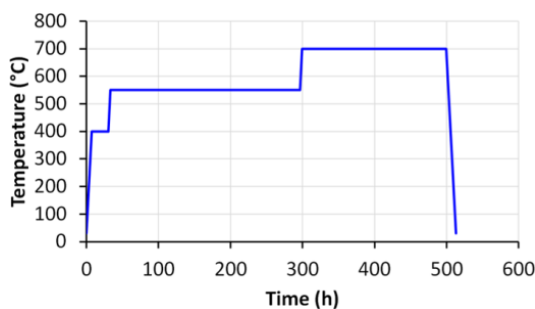

Figure 34 The heat treatment schedule used by *McInturff and Larbalestier*[140]

In their paper, McInturff and Larbalestier[140] concluded that *"the uniformity and similar thickness of the Nb_3Sn layer…is indicative of a uniform Sn distribution"*[140] a conclusion that is rather common in later Internal-Tin papers[150, 160]—and one that was never questioned. But perhaps the most important (and undisputable) result from this paper was that the A15 isothermal step (final reaction) was the most influential on J_c, seeing as *"most of the curves indicate that J_c is still increasing with [A15] heat treatment time"*[140]. The relevant information from this influential paper is summarized in Table 3.

---

[a] This final isothermal step is often referred to as the A15 step, usually between 650°C and 700°C.

[b] All heat treatment schedules for the remainder of this chapter will be shown under the assumption that the ramp rates between isothermal steps are all 50°C/h (since they are often not specified).

Table 3 Lessons learned and relevant information from *McInturff and Larbalestier*[140], 1975

Author and date	*McInturff and Larbalestier*, 1975
Company or research group	Rutherford Lab
Wire type	External-Tin
Mixing isothermal steps used	23 hours at 400°C and 240 hours at 550°C
Reference	(none)
Justification for mixing steps	• 400°C: not mentioned, but most likely to consume η • 550°C: *"compromise between minimum Nb_3Sn formation and uniform distribution of the Sn"*
Conclusion (regarding mixing)	Mixing was successful judging by Nb_3Sn reaction uniformity
Conclusion (regarding J_c)	J_c is mostly determined by the A15 reaction

3. 5. 3 (b) Cogan et al.[139], 1983

At their peak, the External-Tin wires from MIT were undergoing *four* different isothermal mixing steps before the A15 reaction. The first step, at 220°C for 250 hours, was most likely used to dissolve the electroplated Sn into the Cu to form η (although no direct mention of this was made in their papers). The second isothermal step was a relatively short 50-hour mixing at 250°C (which they never justified). The third isothermal step was done at 340°C for 200 hours, right below the formation temperature of the δ phase. This one was implemented in order to *"avoid complications which might occur with the formation of δ phase above 350°C"*[139]. Cogan *et al.* made it very clear that the δ phase was associated with void formation, and that the peak of void formation happened around 450°C[a], therefore the δ phase became a threat to External-Tin wires. The final isothermal mixing step was done at 500°C for 200 hours. There is no justification behind this step either, but it most likely had to do with McInturff and Larbalestier's reasons behind their 550°C isothermal step (homogenization of Sn). However, this temperature (500°C) is also right below the formation temperature of the γ phase (518°C), and perhaps an isothermal step below 518°C was beneficial since any phase transformation results in volumetric changes that may stimulate delamination. The heat treatment schedule used by Cogan *et al.*[139] is shown in Figure 35.

---

[a] Although there were no mixing reactions done at this temperature and no images to back this claim
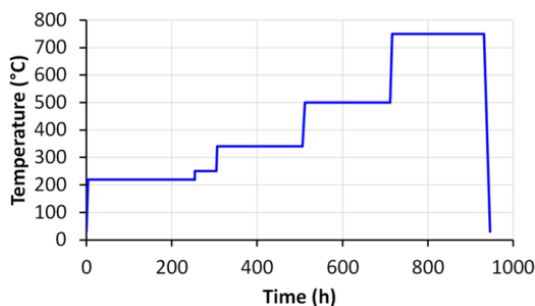
Figure 35 The heat treatment schedule used by Cogan et al.[139]

Papers like these were an important influence on our fear of Kirkendall voids. Claims like: *"Kirkendall porosity will form around 450°C unless sufficient lower temperature annealing takes place"* or *"in order to avoid the porosity it is necessary to anneal for extensive periods of time at intermediate temperatures"*[139] echoed through the scientific literature, and have led to years of searching for an ideal mixing heat treatment (unfortunately) under the erroneous assumption that Kirkendall voids are detrimental for Internal-Tin as well[a].

The amount of attention and effort that this ideal mixing heat treatment was later given, is even more surprising seeing as the conclusion of this paper (an many more papers resulting from similar work) was that J_c is mostly affected by the A15 reaction, instead of the mixing steps—just like McInturff and Larbalestier[140] had found eight years earlier. The relevant information from this influential paper is summarized in Table 4.

3. 5. 3 (c) Schwall et al.[150], 1983

This paper is by the aforementioned alliance between IGC and Cogan from MIT. In this paper, the newly developed single-barrier Internal-Tin wires from IGC (with a significantly reduced Cu-channel) underwent isothermal steps at 200°C for 200 hours, at 375°C for 33 hours, and at 580°C for 218 hours[b]. Given their 200°C isothermal step, we could assume that they followed the notion of dissolving the Sn before it melts, just like External-Tin (although this time at a slightly lower

---

[a] I say erroneous because I still have not found a paper that shows clear evidence of detrimental results from voids being present.

[b] The specifics of this IGC/MIT-engineered heat treatment are not mentioned in this paper, but they were later published by Higuchi et. al.[157]

temperature). Also notice that the 375°C isothermal step is *above* the formation temperature of the δ phase (unlike Cogan's External-Tin paper that same month and year[139]). Perhaps Cogan was ambivalent about the *"complications"* associated with this phase, and in this case he leaned more towards what was later described as a *"more rapid [mixing] rate due to a higher temperature"*[157].

Table 4 Lessons learned and relevant information from Cogan *et al.*[139], 1983

Author and date	Cogan *et al.*[139], 1983
Company or research group	MIT
Wire type	External-Tin
Mixing isothermal steps used	250 hours at 220°C, 50 hours at 250°C, 200 hours at 340°C, and 200 hours at 500°C
Reference	(none)
Justification for mixing steps	220°C: not mentioned, but most likely to consume pure Sn 250°C: not mentioned 340°C: *"avoid complications which might occur with the formation of δ phase above 350°C"* 500°C: no mention, I assume similar effect as in McInturff and Larbalestier, 1975. Also right above γ formation
Conclusion (regarding mixing)	Kirkendall voids are a threat to these wires and seem to be strongly tied to the δ phase.
Conclusion (regarding J_c)	J_c is mostly determined by the A15 reaction

The third isothermal step, at 580°C, is also higher than anything suggested in the past, and they don't necessarily justify a good reason for it other than the fact that *"the ε phase is converted to the δ phase and to the α phase"*[157], hinting a desire for Sn homogeneity (but towards the lower Sn-concentration phases, δ and α). This claim, conflicts with their other conclusion, in which they mention that *"it is advantageous to maintain the highest possible Sn concentration at the Nb interface and hence the fastest growth rate of Nb₃Sn"*[150]. It should also be noted that this third isothermal step is right below the formation temperature of the ζ phase and the decomposition of the δ phase, which could be an indication that they were trying to homogenize things before crossing phase transformation temperatures[a]. The heat treatment schedule used by Schwall *et al.*[150] is shown in Figure 36.

---

[a] One could say that this is an indication that the fear of volumetric changes that haunted External-Tin for years had now creeped into Internal-Tin.
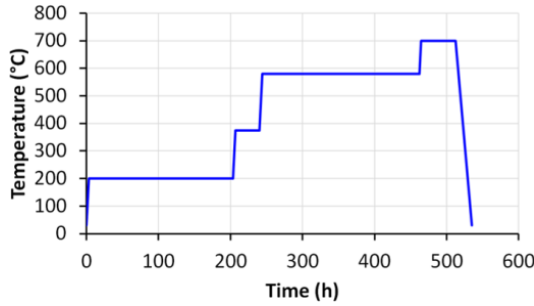
Figure 36 The heat treatment schedule used by Schwall *et al.*[150]

Good engineers that they were, they tried more variables, especially the variation of the A15 reaction. And once again, found that this reaction is far more influential than the mixing steps since *"higher field J_c requires higher temperatures (usually 700°C or higher) to attain better stoichiometry and order"*[150]. The relevant information from this influential paper is summarized in Table 5.

Table 5 Lessons learned and relevant information from Schwall *et al.*[150], 1983

Author and date	Schwall *et al.*[150], 1983
Company or research group	IGC and MIT
Wire type	IGC's single-barrier Internal-Tin
Mixing isothermal steps used	200 hours at 200°C, 33 hours at 375°C, and 218 hours at 580°C
Reference	They don't mention the earlier paper by Cogan *et al.*[139], but it is clear that these reactions are modifications of the MIT work.
Justification for mixing steps	• 200°C: not mentioned, but most likely to consume pure Sn • 375°C: *"a more rapid rate due to a higher temperature"* • 580°C:homogenization of Sn
Conclusion (regarding mixing)	*"It is advantageous to maintain the highest possible Sn concentration at the Nb interface and hence the fastest growth rate of Nb₃Sn"* and *"note uniform reaction indicating proper homogenization of bronze"*
Conclusion (regarding J_c)	J_c is mostly determined by the A15 reaction

3. 5. 3 (d) Higuchi et al.[157], 1984

The BNL group was highly influential in the early days of Internal-Tin, and in this particular paper they compared two heat treatments: One directly taken from

Cogan et al.[139] (for External-Tin) and the other one suggested by IGC[a]. The heat treatments used here were the same as in Cogan et al.[139] and Schwall et al.[150], and they concluded that the J_c difference of these two mixing heat treatments is *"not very great"* and also *"[felt] that the present pre-heat treatment conditions are excessively long and can be reduced without sacrificing the values of J_c"*. The conclusions, as you can see, are not very convincing, except for the one that has been confirmed in almost every paper: Highest J_c was found at highest A15 reaction temperature. The relevant information from this influential paper is summarized in Table 6 and the heat treatment schedules used are those already shown in Figure 35 and Figure 36.

Table 6 Lessons learned and relevant information from Higuchi et. al.[157], 1984

Author and date	Higuchi et. al.[157], 1984
Company or research group	BNL
Wire type	IGC's single-barrier Internal-Tin
Mixing isothermal steps used	• 250 hours at 220°C, 50 hours at 250°C, 200 hours at 340°C, and 200 hours at 500°C • 200 hours at 200°C, 33 hours at 375°C, and 218 hours at 580°C
Reference	Cogan et al.[139] and Schwall et al.[150]
Justification for mixing steps	Same as Cogan et al.[139] and Schwall et al.[150]
Conclusion (regarding mixing)	Heat treatment differences are *"not very great"*, and they think heat treatments are too long.
Conclusion (regarding J_c)	J_c is mostly determined by the A15 reaction

3. 5. 3 (e) Dietderich et al[114] , 1985

This particular paper from LBNL was studying distributed-barrier Internal-Tin IGC wires—which were very similar to the current RRP® wire designs. In fact, they reached conclusions that are very similar to those we are concluding for RRP® today (in this thesis work), such as the fact that the ~200°C step does not affect wire properties, and that during the ~375°C step there is a significant amount of porosity observed in the filament region. It is possible that, had they had better microscopes back then, they would have come to the same conclusions reached in this thesis, given that (at 580°C) they found what *"appear to be isolated islands of a high tin phase in the filament region"*, perhaps referring to the decomposition of the high-Sn

---

[a] Although given what I have exposed up to now, it is very clear that the IGC's heat treatment was *also* a suggestion from Cogan.

phase "Nausite"[a]. They also described this high-Sn phase as *"lath-like"*, a description that matches the porous structure of the decomposition of Nausite. The heat treatment used in this paper was the same as that introduced by Schwall *et al.*[150] but they also attempted slightly shorter times, as suggested by Higuchi *et al.*[157]. The shorter heat treatment version used by Dietderich *et al*[114] is shown Figure 37.
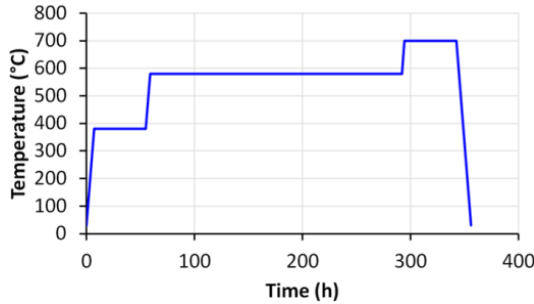

Figure 37 The shorter heat treatment version of Higuchi *et al.*[157] used by Dietderich *et al*[114].

I must point out that although they found the ~200°C heat treatment ineffective, they also found that "*some homogenization heat treatment (e.g. 380°C+580°C) is useful before the high temperature reaction treatment*". Finally, something that you may have already guessed: the highest J_c was seen at the highest temperature A15 reaction (700°C). The relevant information from this influential paper is summarized in Table 7.

Table 7 Lessons learned and relevant information from Dietderich *et al*[114] , 1985

Author and date	Dietderich *et al.*[114], 1985
Company or research group	LBNL
Wire type	IGC's distributed-barrier Internal-Tin
Mixing isothermal steps used	• 200 hours at 200°C, 33 hours at 375°C, and 218 hours at 580°C • 120 hours at 200°C, 24 hours at 380°C, and 233 hours at 580°C • 48 hours at 380°C, and 233 hours at 580°C
Reference	Schwall *et al.*[150]
Justification for mixing steps	Minor changes and some omissions
Conclusion (regarding mixing)	200°C reaction is useless, but some homogenization is useful
Conclusion (regarding J_c)	J_c is mostly determined by the A15 reaction

---

[a] We will introduce Nausite [$(Nb_{0.75}Cu_{0.25})Sn_2$] in a later chapter

3. 5. 3 (f) Smathers et al.[133], 1990

By the time MJR switched to Internal-Tin, a stepped heat treatment was already an assumed necessity for this technology—and since Teledyne had also reached the conclusion that *"Large Kirkendall voids are detrimental to the wire"* back when the first Bronze-Process MJR patents were made[132], it was only natural for them to attempt a stepped heat treatment as well. However, it appears Teledyne's reasons for using a stepped heat treatment were more focused on the prevention of voids than the need for mixing since their isothermal step at 220°C for 100 hours was designed to *"wet the phase boundaries[134]"* in order to avoid the formation of large Kirkendall voids at the Cu/Sn interphase, and the 340°C isothermal step for 48 hours was to prevent the formation of the δ phase (something that was based on External-Tin fears[139]). The heat treatment schedule used by Smathers *et al.*[133] is shown in Figure 38. The relevant information from this influential paper is summarized in Table 8.
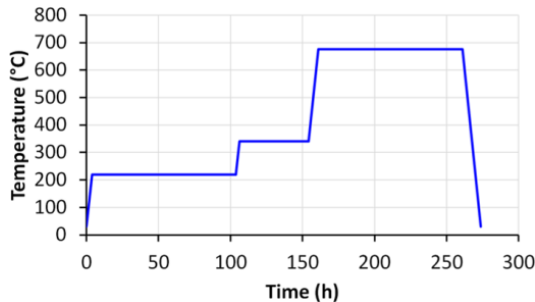

Figure 38 The heat treatment schedule used by Smathers *et al.*[133].

Table 8 Lessons learned and relevant information from Smathers *et al.*[133],1990

Author and date	Smathers *et al.*[133],1990
Company or research group	Teledyne
Wire type	MJR distributed-barrier Internal-Tin
Mixing isothermal steps used	100 hours at 220°C and 48 hours at 340°C
Reference	(none)
Justification for mixing steps	• 220°C: *"wetting of the phase boundaries to avoid porosity"* • 340°C: Not disclosed but most likely attempting to avoid the δ phase.
Conclusion (regarding mixing)	Large Kirkendall voids are detrimental to the wire
Conclusion (regarding J_c)	J_c is mostly determined by the A15 reaction. Final heat treatment should be at *"about less than 800°C for not less than about 100 to 200h."*

3. 5. 3 (g) Gregory et al.[158], 1991

Amid this fear of Kirkendall voids, IGC teamed up with BNL to explore the effects of a hot isostatic press (HIP) on the void formation during wire heat treatment. Using IGC's single-barrier Internal-Tin wires, with a shorter version of the previously established heat treatment by Schwall *et al.*[150], they found that *"the bulk of the porosity in internal tin material appears to result from the formation of the bronze rather than from the Kirkendall effect which takes place during the formation of the Nb₃Sn"*[158], a nice observation, but one that did not specify the benefits of avoiding porosity, in fact they *"showed improved J_c in low field range, above 15 T the opposite effect appeared to be true"*[158]—a baffling result that was to be explored further, but never confirmed. The two heat treatment schedules used by Gregory *et al.*[158] are shown in Figure 39
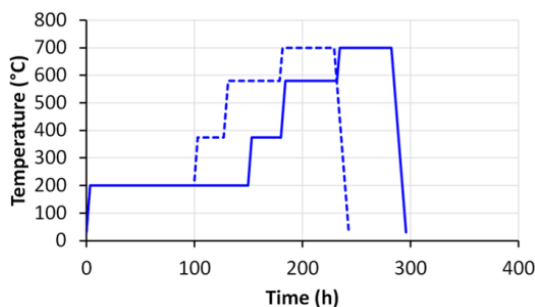

Figure 39 The two heat treatment schedules used by Gregory *et al.*[158].

The relevant information from this influential paper is summarized in Table 9. Notice that they attempted a shorter heat treatment too, possibly influenced by Higuchi *et al.*[157]—however they did not attempt skipping the 200°C step as suggested by Dietderich *et al.*[114] from LBNL.

3. 5. 3 (h) The race for ITER

Once ITER established the requirements for the wires to be used in the Tokamak in 1995[81], the U.S. Department of Energy encouraged IGC (the best Internal-Tin manufacturer in the US at the time) to improve their wires for the ITER machine. This, of course, entailed the need to optimize the heat treatment and ultimately find a *"common heat treatment for all ITER conductors"*[91]. As you may have already guessed, this task was not an easy one; the huge amount of information, reaction temperatures, reaction times, wire types, and erred assumptions that have

accumulated over the decades, led to a *wild-goose empirical chase* that took IGC in several different directions—finally landing on a "tossed salad" heat treatment that uses almost all temperature holds mentioned here.[a]

Table 9 Lessons learned and relevant information from Gregory *et al.*[158], 1991

Author and date	Gregory *et al.*[158], 1991
Company or research group	IGC and BNL
Wire type	IGC's single-barrier Internal-Tin
Mixing isothermal steps used	146 hours at 200°C, 27 hours at 375°C and 48 hours at 580°C 96 hours at 200°C, 24 hours at 375°C and 48 hours at 580°C
Reference	Schwall *et al.*[150]
Justification for mixing steps	Shorter times perhaps influenced by Higuchi et. al.[157]
Conclusion (regarding mixing)	Pores form during mixing, not during A15 reaction
Conclusion (regarding J_c)	Decreasing porosity narrows J_c distribution and increases low-field J_c (ambiguous)

In one of their studies (Gregory *et al.*[91], 1996), they skipped all but the 375°C isothermal step. IGC also explored ramp rates[b], and confirmed that a faster ramp rate decreased hysteresis loss—albeit acknowledging that a fast ramp rate is not practical for full-sized ITER coils. In a later study (Gregory *et al.*[161], 1997), IGC explored (further) the effects of using a hot isostatic press (despite being impractical for ITER as well) and found that most of the porosity was formed around 450°C (as suggested by Cogan *et al.*[139] one decade earlier).

The interesting thing about this observation of porosity at 450°C is that it was found on wires that were not meant to be tested for I_c. These wires were reacted at 450°C (with or without the HIP) for 48 hours to compare (metallographically) the porosity formed. Using this method they noticed that the HIP-reacted samples had significantly less pores, to which IGC said *"large voids…are obviously a matter of some concern"*, despite there being no significant difference in their J_c.[c]

The search for an ideal stepped heat treatment kept going on until the early 2000s, and during this time period IGC did not specify or justify many of their isothermal step choices. Perhaps the most interesting (yet counterintuitive) decisions

---

[a] It is worth reminding the reader that this heat treatment is for single-barrier Internal-Tin

[b] Since they seem to affect hysteresis loss[159]

[c] Mechanical properties don't seem to be affected by pores either as shown in ref [162], so why are we so afraid of voids?

IGC made regarding heat treatments was to implement a 460°C isothermal step to their wires (Pyon and Kanithi[163], 2003). This isothermal step, according to Cogan et al.[139] and Gregory et al.[161], would produce a significant amount of voids. So why was it chosen? It may have something to do with the fact that the voids prevent a certain degree of filament bridging and therefore hysteresis loss could be improved. Or perhaps IGC, (just like OST did in Zhang et al.[137] 1999) found empirically that this isothermal step could improve wire properties in the end. Either way, despite not reporting any justification, the final heat treatment schedule chosen for ITER[164] uses the following heat treatment (shown in Figure 40):

1. 50 hours at 210°C,
2. 25 hours at 340°C,
3. 25 hours at 450°C, and
4. 100 hours at 575°C.
5. A15 reaction (varies).
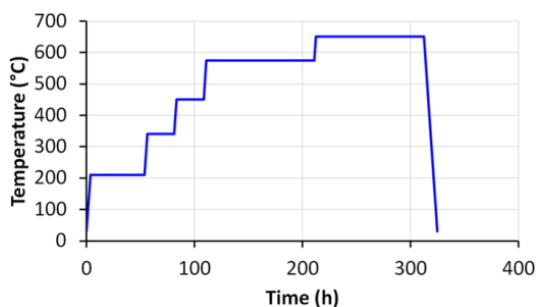
Figure 40 The final heat treatment schedule chosen for ITER wires.

Table 10 highlights the different papers which have included any of the ITER temperature holds (or similar temperatures), with their justifications. Figure 41 shows the timeline of the heat treatment evolution.

I apologize for stressing this so much, but I must point this out again: all these studies found that the most influential reaction was the A15 reaction, yet this did not stop research groups from attributing mystical benefits to poorly understood kinetic Cu-Sn mixing reactions.

Table 10 The different ITER temperature holds and all the studies that had used them previously

| Reaction temperature	Authors using this reaction	Justification
~ 210°C	• Cogan et al.[139], 1983 • Schwall et al.[150], 1983 • Higuchi et. al.[157], 1984 • Dietderich et al.[114], 1985 • Smathers et al.[133], 1990 • Gregory et al.[158], 1991 • Zhang et al.[137] 1999	Transforming the pure Sn into the η phase, although in most cases this was not mentioned perhaps because the explanation is obvious.
~ 340°C	• Cogan et al.[139], 1983 • Schwall et al.[150], 1983 • Higuchi et. al.[157], 1984 • Dietderich et al.[114], 1985 • Smathers et al.[133], 1990 • Gregory et al.[158], 1991 • Gregory et al.[91], 1996 • Gregory et al.[161], 1997 • Zhang et al.[137] 1999	Most likely to avoid the δ phase, although some studies went above its formation temperature to increase the reaction rate.
~ 450°C	• Gregory et al.[161], 1997 • Zhang et al.[137], 1999 • Pyon and Kanithi[163], 2003	High amounts of porosity formed perhaps helping to reduce hysteresis.
~ 575°C	• McInturff and Larbalestier, 1975 • Cogan et al.[139], 1983 • Schwall et al.[150], 1983 • Higuchi et. al.[157], 1984 • Dietderich et al.[114], 1985 • Gregory et al.[158], 1991 • Zhang et al.[137], 1999	Homogenization of Sn
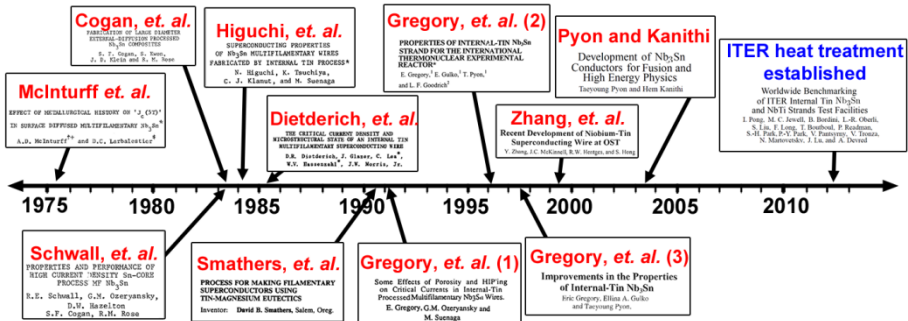
Figure 41 Timeline of the heat treatment evolution

3. 5. 3 (i) Oxford Superconducting Technologies

As I have mentioned before, between 1997 and 2001, OST was experimenting with pretty much all viable fabrication methods of the time[116]. As far as their ITER

wire goes, OST chose a heat treatment very similar to IGC's—given that the U.S. Department of Energy was aiming for one common heat treatment. However, as far as their MJR product, their heat treatment of choice went from 220°C/100h + 340°C/48h plus the A15 reaction (used back in the Teledyne days[133]), to 200°C/6h + 350°C/18h + 450°C/28h + 580°C/60h plus the A15 reaction[137]. This new MJR heat treatment had a similar effect to those previously reported in other wire types using temperature holds at 450°C and 580°C, that is, a lower hysteresis loss and a better distribution of the Sn before A15 reaction[a]

A curious thing that can be pointed out here is that by the late 1990s, *none* of the Internal-Tin studies had suggested an isothermal step near 408°C, the melting point of the η phase. I say "curious" because if we follow the rhetoric (or belief) that has ruled the stepped heat treatments up to now, one would expect that an isothermal step near 408°C would be highly desired to mitigate the melting of the η phase—a phase transformation that involves the biggest volumetric change in the system with an expansion of ~9.4%[b]. This expansion is quite significant compared to the ~2.59% expansion at the melting of pure Sn[167] (which according to my calculations of Appendix B is in fact ~0.18% when a small amount of Cu is added).

OST was the first Internal-Tin manufacturer to suggest an isothermal step near the melting point of the η phase, and they chose to have a 48 hour isothermal step at 400°C in order to transform the η phase as much as possible into the ε phase. They also chose a 48 hour isothermal step at 210°C in order to transform the pure Sn into the η phase[138] (see Appendix B for other reasoning behind the 215°C step). Figure 42 shows the standard heat treatment used in RRP® wires since 2005.[168]

3.6   *The RRP® revolution*

The development of the RRP® technology was a game-changer for the High Energy Physics community. In only four years, RRP® went from being just as good as MJR[116] to reaching the highest J_c ever produced in a Nb₃Sn wire[93]—becoming the best prospect for the first particle collider using Nb₃Sn magnets[169]. As it will be seen in the next chapter the RRP® sub-element design and heat treatment have remained

---

[a] However it must be mentioned that the conclusions of "a better distribution of Sn" were reached indirectly, this has never been quantified.

[b] From a specific volume of 0.119 cm³/g of the η phase[165] to a specific volume of 0.130 cm³/g of liquid Cu-Sn (50 at.%Sn) at 408°C[166].

the same for a decade, and most of OST's efforts have been aimed towards stacking more sub-elements to reduce D_{eff} while retaining wire integrity and enhancing piece length[94].
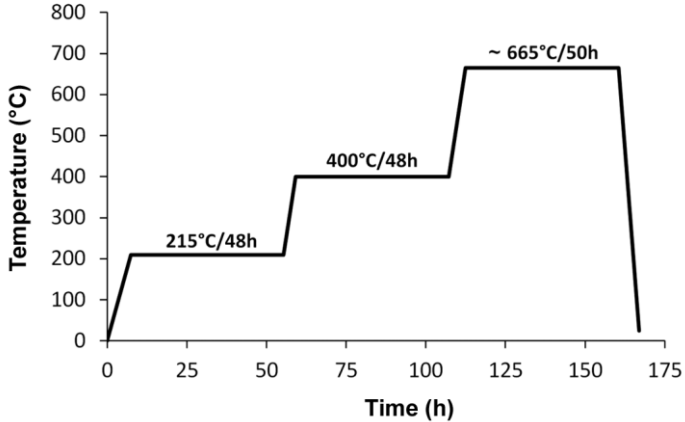

Figure 42 The standard heat treatment for RRP® wires since 2005.

3.7 Conclusion

Internal-Tin wires come in many flavors, and it appears from this extensive literature review that different wires have evolved under similar assumptions despite their significant differences. The fast evolution of the technology and the restrictive demands of large projects like ITER and the LHC have led to heat treatment goals that are not very clear at the moment. In a later chapter of this thesis we will explore the RRP® mixing heat treatment in further detail, and it will be shown that none of the claims of Internal-Tin heat treatments shown in this chapter (and Appendix B) apply to RRP® wires.

Chapter 4 - The Restacked Rod Process

——Success is going from failure to failure without losing your enthusiasm——

Winston Churchill

Over the last few decades the US Department of Energy has been encouraging the improvement of RRP® wires through the Conductor Development Program (CDP) with the ultimate goal of Nb_3Sn use for particle accelerator magnet fabrication[85, 92, 151, 170]. As we saw in previous chapters, RRP® currently holds the J_c record[93] of a Nb_3Sn wire (~3000 A/mm^2 at 12 T and 4.2 K). However, particle accelerator magnets require a much smaller D_{eff} than these record-holding RRP® wires. The issue, however, is that the J_c of RRP® wires tends to degrade significantly as its sub-element size, D_s, is reduced[a]. This trend is depicted in Figure 43 (using 15 T J_c values), and as you can see the drop is quite alarming given the demanding requirements for the FCC.

In this chapter, I would like to explore the different aspects of RRP® wires that have enabled OST (Bruker-OST since early 2017) to produce a wire which is currently meeting the specifications for the Hi-Lumi LHC—but which (as shown in Figure 43) still needs significant optimization for the FCC or similar high energy future particle colliders.

4.1   Sub-element properties

As I have shown in previous chapters, RRP® is a distributed-barrier Internal-Tin wire. In other words, it is an array of sub-elements composed of a Sn core surrounded by Nb filaments inside a Cu matrix and a Nb barrier. A sketch of a standard sub-element cross section is shown in Figure 44, as well as a backscattered electron image of a *fully reacted* sub-element. (RRP® reaction will be covered in a later chapter).

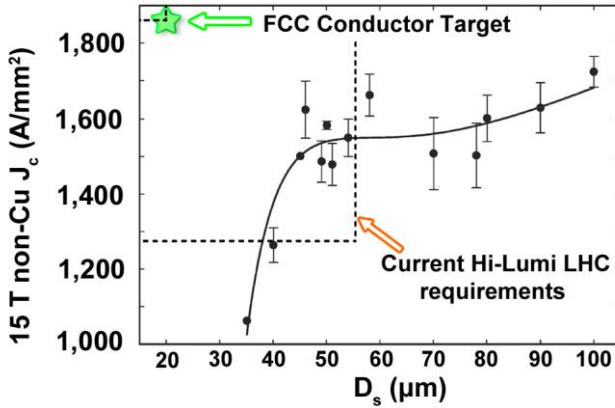[a] In RRP® wires, D_s essentially the same as D_{eff}

Figure 43 The critical current density of RRP® wires as a function of sub-element size showing a strong drop in J_c below 50 μm. Boxes for the Hi-Lumi LHC and the FCC targets are shown.
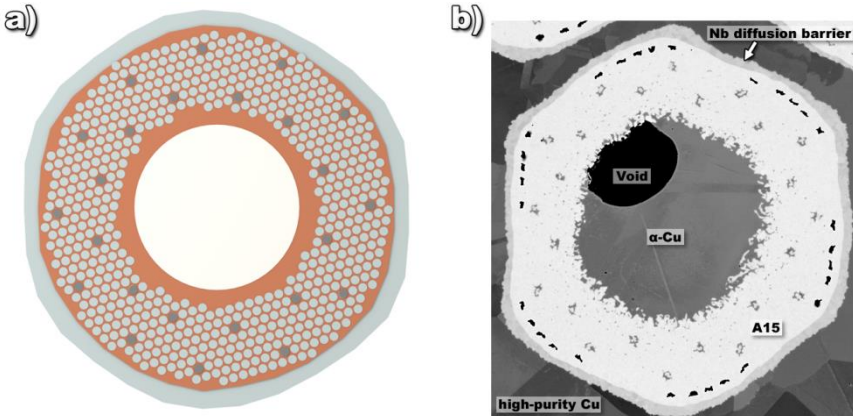

Figure 44 (a) A sketch of a standard sub-element cross section. (b) a fully reacted RRP® sub-element showing the monolithic Nb₃Sn ring that is formed after reaction.

I have also shown, that an Internal-Tin sub-element design can vary significantly regarding its filament size, Cu-channel thickness, Sn core size, number of filaments, etc. (see Figure 32 on page 50). In order to keep track of all these variables Bruker-OST has standardized a few sub-element parameters. Among the most important ones are:

1. Sn percent inside the barrier (wt.% Sn),
2. Nb to Sn atomic ratio (Nb:Sn),
3. and, Local area ratio (LAR)

Below I will explain how each one of these sub-element parameters are

measured—and elaborate on their potential impacts on wire properties.

4. 1. 1   Sn percent inside the barrier

I must start by saying that all the values of 'Sn percent inside the barrier' in this thesis will be given in *atomic percent* Sn, simply because it will make it easier to compare to later measurements [a]. This measurement is done by making a hypothetical mix of all the Cu and the Sn inside the sub-element and reporting the wt.% Sn (or at.% Sn) of such mixture. Figure 45 shows the sub-element parts that play a role in this measurement. As you can see, this value is mostly a function of the size of the Sn core with respect to the Cu annulus [b] and the size of the Cu-channel[c]. It should also be mentioned that the few Cu hexes between the filament pack and the barrier (often called Cu fillers) may have an impact on this measurement.
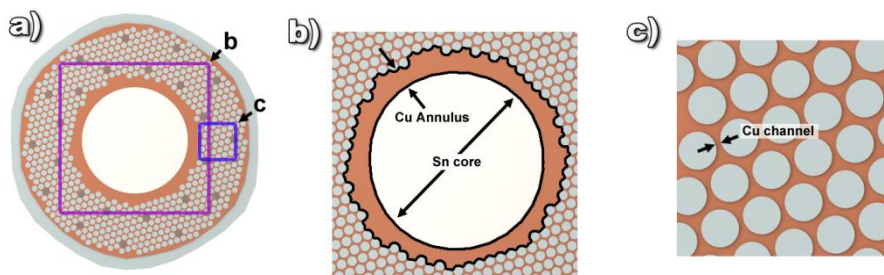
Figure 45 (a) A sketch of an RRP® sub-element with (b) a closer look at the Sn core and the Cu annulus, as well as (c) a closer look at the Cu channel. These are the main sources of Cu and Sn in the sub-element.

It has been established that the recommended ratios for optimum design are 34.9 to 44.9 at.% Sn[138], and that increasing the Sn content in the sub-element is one of the most important drivers of higher J_c[103]. However, it has been suggested that too much Sn can result on something called Nb filament dissolution[151]. We will talk about Nb dissolution in a later chapter since it appears to be an important source of the J_c degradation during wire reaction.

---

[a] In the RRP® patent[138] this value is given in *weight percent* Sn

[b] The size of the Sn core and the Cu annulus can have slight variations depending on tolerances in the gun-drilled hole dimensions and the Sn rod size.

[c] The Cu-channel size is controlled by the size of the Cu-sheath during the fabrication of the monofilament.

4. 1. 2   Nb to Sn atomic ratio

The Nb:Sn atomic ratio is another important parameter. Ideally one would want this ratio to be 3:1 since Nb_3Sn is precisely a 3:1 compound. The problem is that this measurement includes the Nb diffusion barrier, therefore a complete reaction of a 3:1 Nb:Sn atomic ratio would mean a complete consumption of the diffusion barrier—leaving the high-purity Cu extremely vulnerable to poisoning. For this reason, the Nb:Sn atomic ratio value is recommended[138] to be slightly larger (*i.e.* sub-stoichiometric). A value between 3.1 and 3.6 is recommended in order to preserve the integrity of the diffusion barrier and the RRR of the wires.

The standard sub-element design uses a Nb:Sn atomic ratio of 3.4, however, it was shown[85] in 2014 that a value of 3.6 can protect the RRR significantly with only a 2-3% sacrifice in J_c.

4. 1. 3   Local area ratio

The local area ratio (LAR) is mostly determined by the size of the Cu-sheath of the monofilament during fabrication. Figure 46(a) shows a Cu-Clad Nb monofilament similar to the one we saw in Figure 18 (page 30) for a Nb-Ti wire. The LAR is the ratio between the Cu area and the Nb area of this monofilament. Figure 46(b) shows how the LAR ends up affecting the final stack dimensions. The recommended[138] LAR range is between 0.15 and 0.25.

LAR has been of significant concern lately because, as the sub-elements get smaller and Cu-channel thickness is reduced, adjacent Nb filaments can come into contact and produce wire breakages[94].
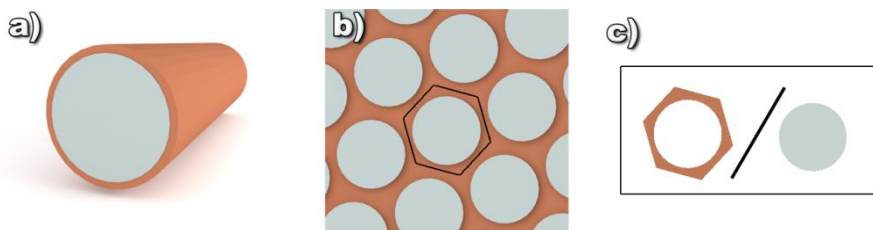

Figure 46 Sketches of (a) a Cu-Clad Nb monofilament before extrusion and shaping, (b) its final stacked dimensions yielding (c) the sub-element local area ratio.

LAR will become of important consideration later on in this thesis work when we discuss the mixing heat treatment of RRP® wires.

4.2   Reduced Sn sub-elements

Bruker-OST has attempted a few experimental billets[a] with slight variations in the above-mentioned parameters. However, there has only been one sub-element design change whose properties justified their implementation. These new sub-elements came to be known as 'reduced Sn' sub-elements, and are obtained simply by using a smaller Sn rod during sub-element fabrication. The result is a Nb:Sn atomic ratio of 3.6 instead of 3.4; which produce a wire of superior RRR (with a mild reduction in J_c). These reduced Sn billets are currently reaching 2,900 A/mm^2 in a sub-element size of 55 μm and their RRR is over 150. However, the J_c trend shown in Figure 43 at the beginning of this chapter is still a concern.

4.3   Restack number

There is one wire parameter I have not talked about yet: the number of restacked sub-elements used for a particular wire or billet. In RRP® wires (just like most superconducting wires) the different components are stacked using a grid of *hexagonal centered numbers*. In such configuration, increasing the rows of stacked elements increases the number of elements as follows:

$$Equation\ (1) \qquad N = 3n(n-1) + 1$$

where n is the number of stacked rows and N is the number of hexagonal placeholders. A few examples of hexagonal stacks are shown in Figure 47.
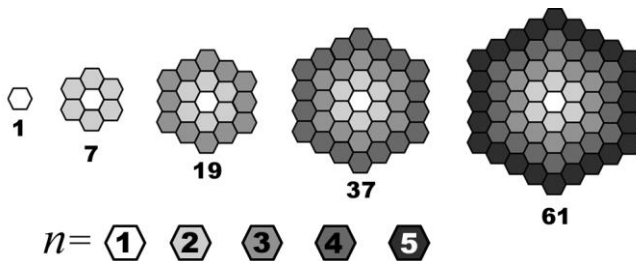

Figure 47 Stack counts (N) of hexagonal centered numbers according to the number of stacked rows, n.

An RRP® stack of five hexagonal rows is often called a 61-stack, since there are 61 placeholders. However, if you recall, a stabilizing Cu fraction between 50% and

55% is required for accelerator magnet applications. Therefore, some of these placeholders must be Cu hexagons instead of sub-elements. The nomenclature of an RRP® wire is therefore complete by adding another number to the name—signifying the number of sub-elements. The most common configurations are 54/61, 90/91, 108/127, 144/169, and 198/217; where the first number is the number of sub-elements and the second number is the stack count. A cross section of a 108/127 stack is shown in Figure 48. Notice that the 19 placeholders in the center are made of Cu.
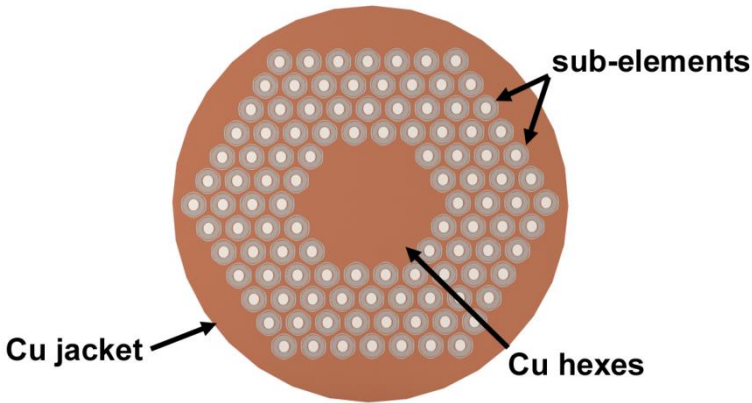
Figure 48 A (sketch) cross section of a 108/127 stack RRP® wire.

4.4   *Restacking benefits and issues*

There are two ways of reducing D_s in RRP® wires: either drawing down the wire to a smaller size, or, using a higher stack count. Unfortunately a wire which is too small may present complications during Rutherford cabling and magnet manufacturing (because of its reduced strength); therefore the preferred method of reducing D_s is using a higher stack count. The present design for particle accelerator applications is either a 108/127 stack or a 144/169 stack[a] between 0.9 and 0.7 mm in wire diameter. Figure 49 shows backscattered electron images of various (fully reacted) RRP® wire cross sections at different sizes.

---

[a] There were several 169-stack experimental billets manufactured (between 2014 and 2016) with a few sub-elements from the corners replaced by Cu—making them 132/169. This stack configuration was thought to improve wire RRR, but it later shown to be of little efficacy. Today a 144/169 stack is preferred.
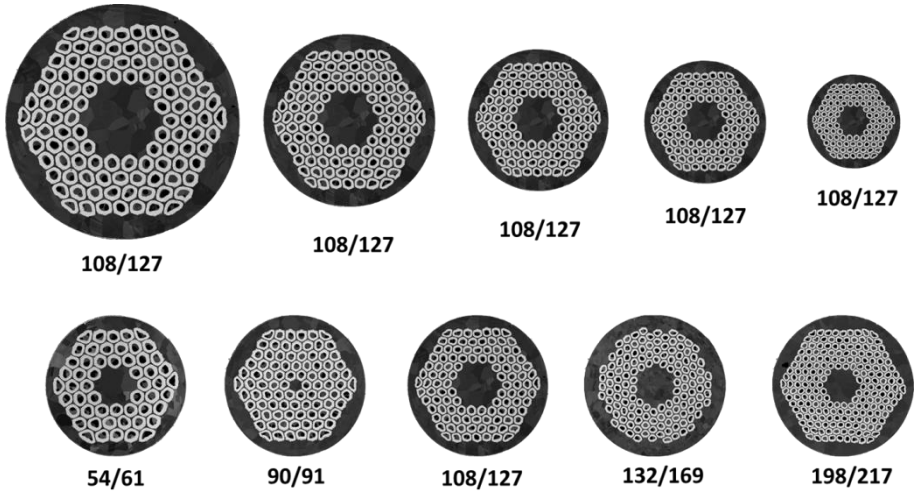
Figure 49 Backscatter electron images of fully reacted RRP® wires showing a wide range of sub-element sizes. The top images are of a 108/127 billet at different wire diameters, and the bottom images are of various billets with different stack counts at the same wire diameter.

Equation (2) is commonly used[171] for calculating the D_s of a particular RRP® wire,

$$Equation\ (2) \qquad D_s = \frac{D_w}{\sqrt{N(1+R)}}$$

where D_w is the wire diameter, N is the number of sub-elements, and R is the Cu:Non-Cu ratio. Using current wire specifications[85] this equation yields the sub-element sizes shown in Table 11 for the different wire diameters and stack counts.

Table 11 Sub-element sizes in μm for the different RRP® stack configurations with a Cu:Non-Cu ratio of 1.2.

Wire diameter (mm)	54/61 stack	90/91 stack	108/127 stack	132/169 stack	198/217 stack
2.0	202	154	129	115	100
1.5	151	116	97	87	75
1.0	101	77	65	58	50
0.85	86	66	55	49	43
0.7	71	54	45	40	35
0.5	50	39	32	29	25

Over the last few decades, Bruker-OST has made significant improvements in wire fabrication—leading to billets of considerable lengths even at high stack counts[85, 92]. However, their main concern lately has been the trend shown at the

beginning of this chapter (in Figure 43).

Whether it is drawing wires down or stacking higher sub-element numbers, this trend towards lower J_c at smaller D_s remains, and has haunted RRP® for many years[92]. It has been suggested that as the sub-elements get smaller, certain features such as the absolute size of the diffusion barrier, or the Cu channel thickness, are affecting the reaction in a negative way, resulting in either a loss of Sn to the cryostabilizer[94] and/or the formation of low quality A15 during reaction[172, 173]. I will explore the source of this trend in a later chapter.

4.5 Conclusion

RRP® wires have shown significant advances regarding wire fabrication in the past decade, but the sub-element design has remained virtually unchanged. In order to meet FCC specifications, regardless of wire fabrication, we must understand why the J_c drops so drastically with D_s. I believe at this point the reader should be very familiar with the history, the fabrication, and the particle collider requirements of RRP® wires. It has certainly taken me a significant portion of this thesis work to introduce the subject of my work. But I believe it was necessary in order to understand the heat treatment optimization and the possible design optimizations discussed in later chapters. In the following chapter (chapter 5) I will introduce several metallography and microscopy methods used to study potential RRP® wire improvements. Once the methods are understood, I will proceed to the results and conclusions of this thesis work (in chapters 6 and 7).

Chapter 5 - Digital image Analysis for Superconductors

——There were many scientific instruments[in the Voyagers], ultraviolet and infrared spectrometers, devices to measure charged particles and magnetic fields and the radio emission from Jupiter–but the most productive have been the two television cameras, designed to take tens of thousands of pictures of the planetary islands in the outer solar system——

Carl Sagan

As it will become clear later in this thesis, a large amount of digital image analysis was required to quantify the subtle changes in phase transformations and wire properties obtained when different heat treatments are applied to RRP® wires. The techniques behind the automated processes used to acquire statistically satisfactory and reproducible sets of measurements are described in this chapter.

5.1   The link between superconductivity and microscopy

In superconductivity, just like in almost every branch of science, images are essential for the basic understanding physical principles. Most of the advanced characterization techniques used in superconductors—such as magnetization measurements[174], x-ray diffraction[175], and heat capacity measurements[176]—are difficult to interpret without the visual support from images of the features behind the measurements. Furthermore, there are certain phenomena of superconductivity that have been understood further thanks to microscopic images; among these we have flux pinning[177], flux penetration[178], grain boundaries as current suppressors[179–181], secondary phases as current suppressors[182], wire heat treatment issues[183], etc. Additionally, the quantification of images through image analysis (IA) can provide important measurements such as filament sizes and Cu to non-Cu ratios.

All in all, superconductivity and microscopy go hand in hand—and in this chapter, I would like to explore the outstanding and ever-expanding capabilities of microscopy and IA. In doing so I will also introduce the specific techniques I have used over the last couple of years to study and understand the RRP® wire

fabrication and heat treatment.

Now, in order to continue the historical theme of this thesis work, I would like to give a brief recapitulation of the IA software upraise.

5.2   The history of image analysis

The incredible power found in today's open-source IA software is mostly owed to one man: Wayne Rasband[184]. Rasband has been developing IA software from the moment digital images first became available to the public in the mid 1980's. His first IA prototype software used images of 512-by-512 pixels on a PDP-11 "minicomputer"[a]. This prototype was developed for the National Institutes of Health (hence its name NIH Image). A few years later, once the Mac II came along in 1987, Rasband moved to this new and advanced platform developing the base-code for what today is known as ImageJ or FIJI.

Rasband was a visionary; he knew that as long as NIH Image had a robust (yet simple) base-code and interphase, he could have it preform complex tasks through additional features called plug-ins and macros which the users could develop and implement themselves[b]. This was a very innovative idea at the time, and Rasband's open-source philosophy (although not named as such back then) enabled NIH Image to move to the PC platform rather quickly—catching up with Mac by the early 1990's.

However, because most of the adaptations to PC were done by a corporation called Scion, the PC adaptation of NIH Image was a closed-source software, and when the bugs arose, there were not enough Scion workers to fix them. Rasband knew he was the only one who could fix this—by writing his own code for PC—in order to keep his open-source mantra, but it seemed like a monumental task. It was not until the Java platform came along in the mid-90's with its *'write once, run anywhere'* slogan, when Rasband decided to work on a new NIH Image code. He named it Image-'J' (after Java), and although this software had several issues throughout its development[c], Rasband managed to keep his open-source vision intact.

---

[a] Which under today's standards is far from "mini".

[b] Plug-ins are user developed extensions of the open-source code, and macros are scripts that can perform a series of repetitive and/or complex tasks.

[c] Mainly due to the evolution of Java itself.

Today, the ever-expanding ImageJ is known as FIJI[185], after a group biologists took control of most of the code and the maintenance of the software. But despite biologists representing the largest population of FIJI users, most of the advanced plug-ins and macros are just as useful for material science and metallography.

5.3   *Sample preparation is essential*

Allow me to take a few steps back from the IA process. Before IA we must have an image, and, in order to take an image of a superconductor wire, one must prepare a *metallographic sample*. This is done by placing the wire inside a phenolic resin (to hold the sample in place), and polishing a mirror-like finish of the sample surface, or rather, its cross section.

However, this sample preparation process can affect the outcome (*i.e.* the image) in many ways. For example, it can slightly alter shapes, it can introduce foreign particles to the sample, or it can hide features within the sample. Such considerations are even more critical in exploratory studies where one is not sure what the measurements might reveal. Figure 50 shows two images of the same RRP® sub-element (at an early fabrication step) where the filaments appear to have different sizes after IA—because of the different sample preparation techniques.
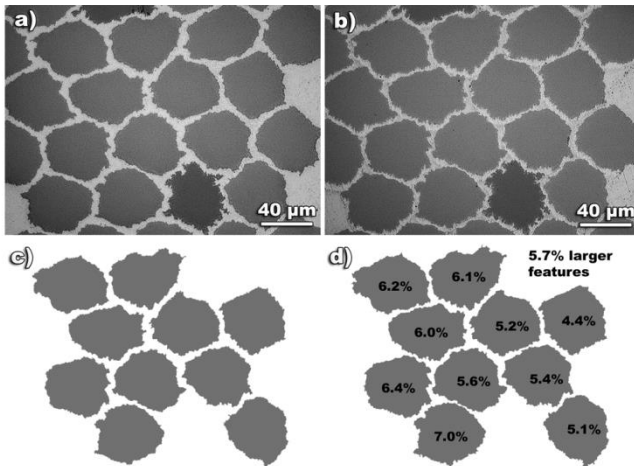
Figure 50 Light microscope images of two identical RRP® filaments (at an early step of the fabrication) using (a) a proper sample preparation and (b) a sample preparation with excessive force. (c) and (d) show the isolated filament sections from (a) and (b) respectively. The dimensional difference quantified in d) is an artificial effect obtained from a poor metallographic preparation.

Other than mild dimensional effects, certain sample features can be missed or misinterpreted if the sample preparation is not optimal. One of the most representative cases of misleading conclusions from poorly prepared samples can be observed in Bi-2212 wires. An impatient sample preparation technique on this soft composite wire can smear the silver and other wire components into the Kirkendall voids, leading to the wrong conclusions about the porosity formed during reaction. Figure 51 shows the *same wire* polished using a quick-and-dirty technique and a more elaborate and patient technique. The difference is clear.
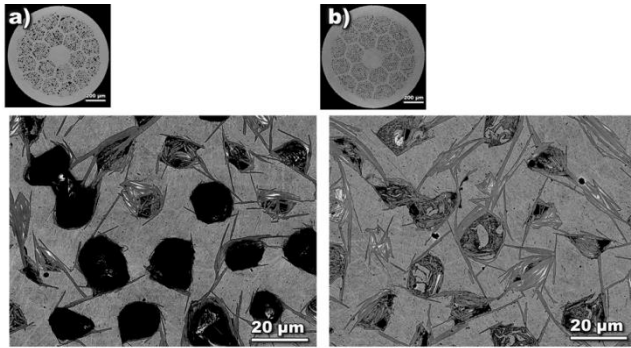
Figure 51 Images of the same Bi-2212 wire (fabricated by Bruker-OST) showing significantly different contents of voids (or bubbles) depending on the polishing technique. The image in (a) is a properly prepared sample, and the image in (b) is a sample prepared using excessive force and short polishing times.

Sample preparation of course may vary depending on what is being sought after, but the examples above show that there are consequences to quick and impatient metallographic techniques that one must be aware of.

5.4   *Backscattered electron images*

Backscattered electron images have the advantage of being sensitive to the average atomic number (Z) of the components in the image. This 'Z-contrast' gives backscatter electron images a major advantage for IA because of the stark shade difference between components (as it was observed in Figure 44(b) on page 69 for a fully reacted RRP® wire).The bulk of the IA studies done for this thesis work were done on backscattered electron images taken with a Field Emission Scanning Electron Microscope (FESEM). For this reason, I will not discuss other image types[a].

---

[a] For more information on this subject please refer to reference [186].

5.5 Image properties

All digital images are discretized in small boxes called picture elements or pixels[a]. A pixel has an area of one squared pixel which (for simplicity) is also called pixel. Therefore, the resolution of a digital image can be described in two ways: either by the total number of horizontal and vertical pixels, or by the total number of (square) pixels. For example, an image which is 3072 × 2304 pixels is also said to be a 7 megapixel image.

5. 5. 1 Intensity values and bit depth

Aside from having a dimension of one pixel by one pixel, a pixel has an *intensity value*. This value can be represented either by a single number in the case of grayscale images, or by a combination of three RGB (red, green, and blue) values in the case of color images[b].

Additionally, when talking about digital images one often talks about bit-depth. Bit-depth is the range of intensity values which a single pixel can have. In the so-called 8-bit space, each pixel in the image has an intensity value between *black* (with a value of zero) and *white* (with a value of 255)[c]. Any number in between 0 and 255 is a shade of gray with a particular intensity value. In color images, each pixel has three values—and can be regarded as three 8-bit images—therefore they are called "24-bit color images" (that is 8 × 3).

However, for 16-bit (grayscale) images, a pixel has the option of having any of 2^{16} shades of gray, where 0 is black and 65,535 is white. The difference is astonishing, a 16-bit image can have an incredible level of detail which is far richer than what the human eye can discern, but through IA, a 16-bit space image offers an incredible capability of detecting minute differences in intensity values.

5. 5. 2 Histograms

A histogram is another useful way to visualize the information of a digital image file. In its most basic definition, a histogram is a population chart where the vertical axis represents the pixel frequency and the horizontal axis represents (in this case) the intensity value. To illustrate this simple definition, a histogram of a small picture

---

[a] In 3-D images such as MRI scans the most basic unit is called voxel after "volume element".

[b] An alternative to RGB is CMYK which uses four numbers.

[c] The name 8-bit comes from the fact that the binary form of 256 is 11111111 (eight ones)—or 2^8

(17×13 pixels) is shown in Figure 52. Notice that there are only 255 intensity values, meaning this is an 8-bit image. Then, Figure 53 shows a much larger 16-bit image where the histogram is significantly richer. This particular image is an image of a few filament bundles (and the diffusion barrier) of a fully reacted Bronze-Process wire.
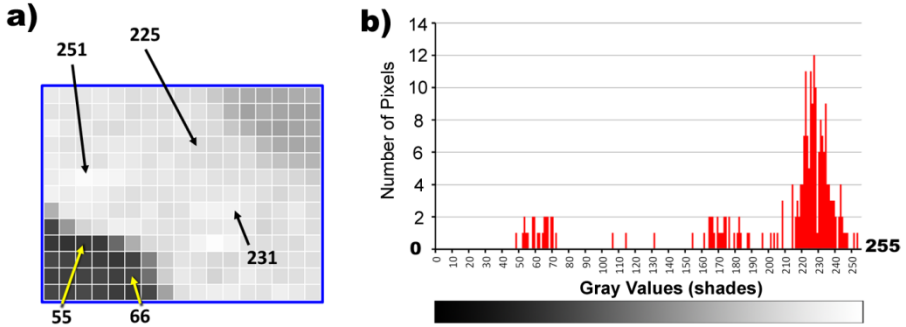

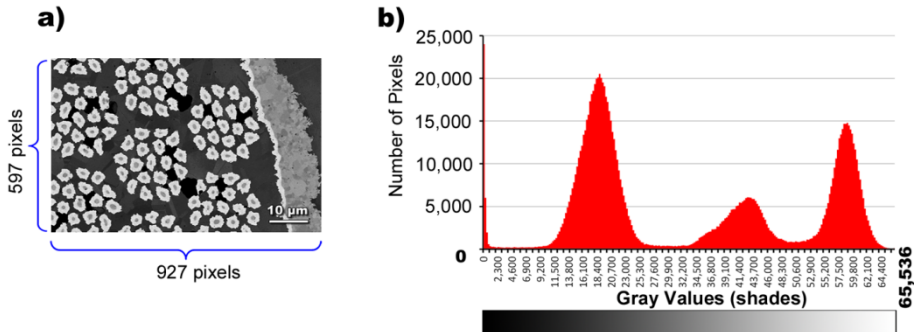Figure 52 (a) A 221-pixel image showing some gray values and (b) the histogram of the image in 8-bit space.

Figure 53 (a) A backscattered electron image of a Bronze-Process ITER wire cross section taken in 16-bit space showing (b) the histogram of the image.

5.6   Image analysis

Now that I have shown you the properties of basic digital images and their histograms, allow me to explain how these are used to isolate the different components of superconductors in order to extract useful measurements.

5. 6. 1   Feature recognition

By looking at Figure 53, it is very easy to see that the histogram appears to be separating the pixels in groups (or peaks). This is extremely useful because when we isolate the pixels belonging to a particular peak, we can produce a separate image.

This is in fact one of the most common algorithms used in IA: separating a histogram into multiple *"binary images"* in which the individual components are represented by black pixels with everything else being white[a]. Figure 54 shows an image which has been separated into binary images of each component according to their Z-contrast as seen in the histogram.
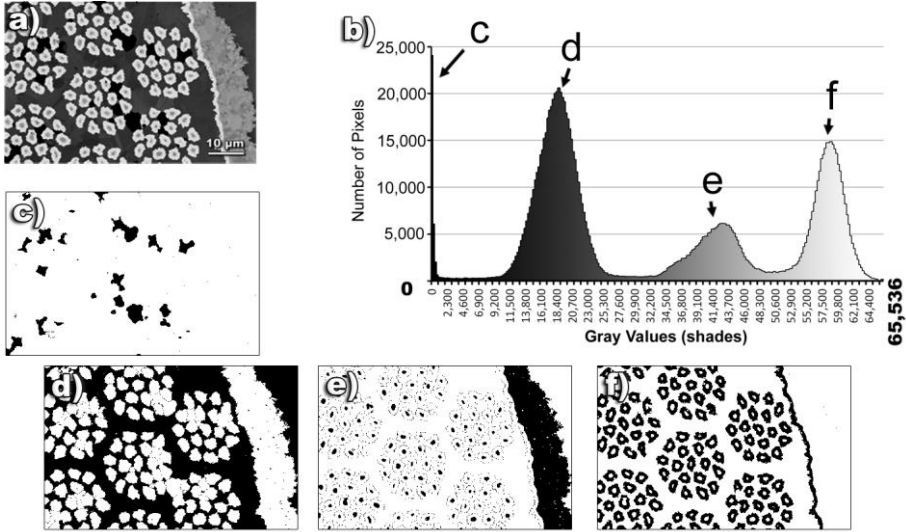

Figure 54 (a) An SEM image of a Bronze-Process ITER wire and its (b) histogram showing different regions of gray values which can be easily separated into binary images of (c) the Kirkendall voids, (d) the α-bronze and the high-purity Cu, (e) the Nb diffusion barrier and the unreacted Nb filament cores, and (f) the Nb_3Sn.

5. 6. 2 Binary image algorithms

As described in section 5.5 a pixel is a unit of area, meaning that an image (*i.e.* an array of pixels) represents an area as well. And just like in any two-dimensional plane, one can perform simple measurements—such as the distance between two points, or two-dimensional (area) measurements. Obtaining these, and other more complex measurements, is the essence of IA. And binary images are particularly useful since they have a sharp boundary (black to white) precisely where the isolated feature begins and where it ends.

However, such binary images need to be adequately produced using thresholding algorithms and other non-invasive IA algorithms in order to extract useful and representative measurements. Allow me to explore these algorithms:

---

[a] The name binary image comes from the fact that black can be regarded as 0 and white as 1.

5. 6. 2 (a) Thresholding

A threshold, by definition, is a point at which a quantity stops (or starts) meeting a criteria. In IA we want to set these criteria so that they include a particular feature associated with a peak distribution in the histogram. In other words, one uses the histogram to select the pixels that belong to a particular component (peak) as it was done for Figure 54. However, histograms often have slight overlaps between components which can complicate the thresholding operation. Using statistical principles based on histogram shape, relative heights, image entropy, position, etc.[187], FIJI has 16 different thresholding algorithms that can produce different selections. Choosing the right algorithm can result in a very accurate and reproducible binary image[a].

Nonetheless, despite there being plenty of algorithms that work in different situations, the easiest (and most reproducible) thresholding operation will always be that which involves *only two peaks*. To get to this advantageous situation, one must use the IA software to perform the thresholding operation on specific parts of the image[b]. An example of this is shown in Figure 55 for a fully reacted Internal-Tin (ITER) wire. Notice that when the thresholding operation is done on the entire image, it produces a binary image with incomplete features, while the thresholding operations for the component boundaries produce neatly defined features.

Notice that in order to obtain the complete features of Figure 55 we must "fill-in" the thresholded features since the threshold was applied to the boundaries only.

5. 6. 2 (b) Fill-holes

A *Fill-holes* algorithm is recommended for cases like those of Figure 55 where solidifying the features is desired. Such algorithm identifies white pixels that are completely surrounded by black pixels and "fills" them in with black to *complete* the feature. Another example where fill holes comes in handy is shown in Figure 56 where the automatic threshold applied to the entire image of a fully reacted 132/169 RRP® wire has produced sub-elements with empty cores.[c]

---

[a] The word *reproducible* in this sentence is essential

[b] Preferably the pixels containing the boundary between the relevant components

[c] Notice that in this case the thresholding algorithm has been applied to the entire image—which contains more than two peaks—but the threshold is acceptable since it falls well within the valley of the two main components of interest
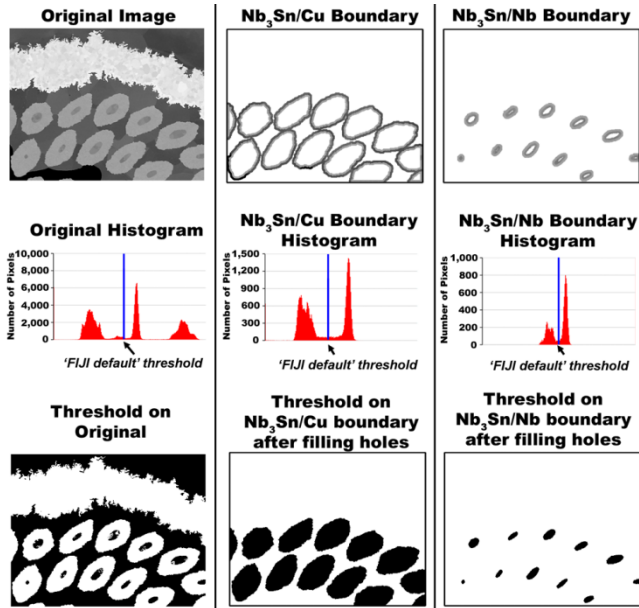
Figure 55 FIJI's default threshold applied to three different regions of an image. On the left case the entire image is used, while on the middle and the right cases only certain selections are used. The accuracy of the threshold is shown by the histogram and the resulting binary images.
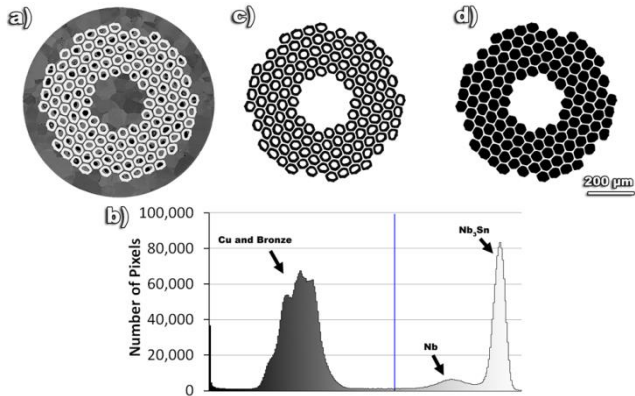

Figure 56 (a) A transverse cross section of a fully reacted 132/169 RRP® wire to which an automated threshold has been applied, producing an acceptable guess between the two main regions of the (b) histogram. This threshold resulted in a (c) binary image to which a fill holes algorithm can be applied to produce a (d) binary image of the subelement features in their entirety.

5. 6. 2 (c) Filtering by feature values

It is very common for a threshold operation to produce small features that are not intended to be measured. This can happen with dust, voids, scratches, and other sample features that may or may not be introduced by the polishing procedure.

84

Either way, the removal of such features (often very small) in binary images is desirable. To do this, certain algorithms measure all the particle areas in the binary image and *reject* those under (or above) a specific area value. These algorithms also have the option of removing those features at the edge of the image—since they are most likely incomplete and not representative. Figure 57 shows an example of a Bronze-Process ITER wire where a very small piece of filament was trapped inside a Kirkendall void. This small piece was taken out of the binary image using a reject features algorithm.
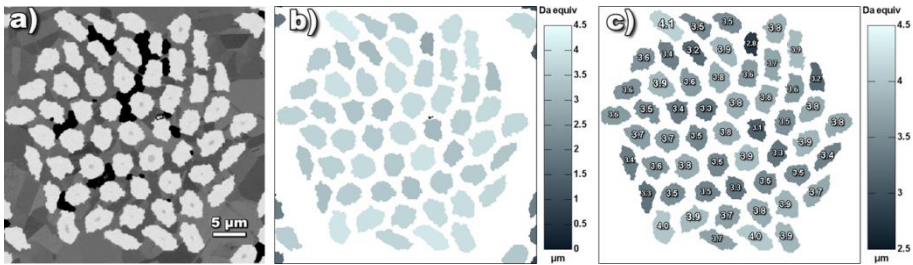
Figure 57 (a) A filament bundle of a Bronze-Process ITER wire. The filaments were thresholded and color coded in (b), while they were thresholded, filtered by size, and color coded in (c). Notice that the corrected range shows more valuable information as the variation easier to see. Notice that the color scales of (b) and (c) are different.

5. 6. 2 (d) Outlines

Outline algorithms do precisely what their name implies; they outline whatever features are in a binary image. Figure 58 shows the diffusion barrier of an ITER Bronze-Process wire that has been outlined.

5.7 Capabilities of image analysis

Below I would like to discuss several aspects of measurements commonly performed on superconducting wires.

5. 7. 1 Area fractions

As it was shown in section *2. 2. 1,* one of the most important specifications for superconductors is the stabilizer-to-superconductor ratio. Figure 59 shows the Cu to Non-Cu ratio for all eight ITER wire manufacturers, obtained using IA algorithms. These area fraction measurements are also useful for many other features relevant to superconductor properties such as secondary phase fractions, void fractions, unreacted fractions, etc.
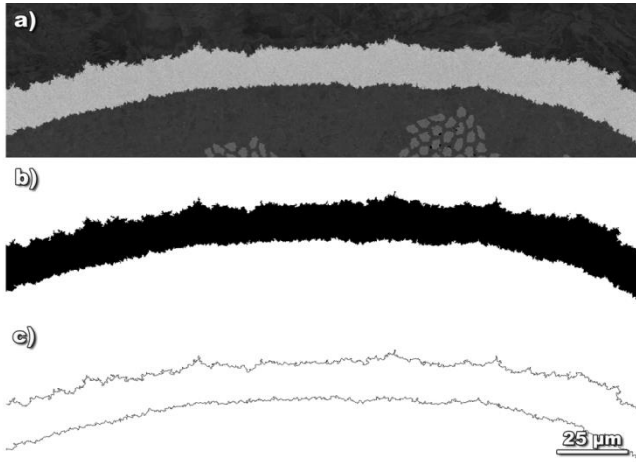
Figure 58 (a) The Ta diffusion barrier of a Bronze-Process ITER wire which is thresholded in (b), and outlined in (c).
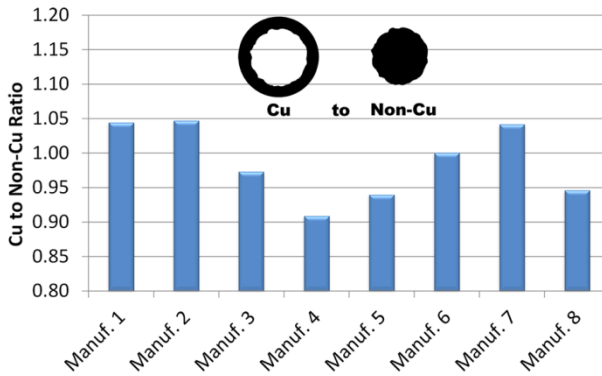

Figure 59 Cu to Non-Cu ratios of all eight ITER wire manufacturers

5. 7. 1 (a) Filament uniformity (sausaging)

If you recall the fabrication steps of superconductors outlined in section *2. 2. 2*, a filament stack such as the one shown in Figure 19(b) (page 33) often comes from the same monofilament (Figure 19(a)). And if the monofilament is large enough, the entire wire stack may come from the same piece as well. So when we take an image of a wire cross section, we are looking at several cuts (made during wire fabrication) of the same monofilament—after it has been drawn down to final size (Figure 19(c)). This means that measuring all the filament areas of a single wire cross section can be

regarded as performing multiple measurements along the length of a filament[a].

The usefulness of such measurement is that the spread of this population of filament areas can provide us with a very good idea of the filament size inhomogeneity *along the length* of the wire. This inhomogeneity is called *sausaging*, and is represented by the sketch in Figure 60
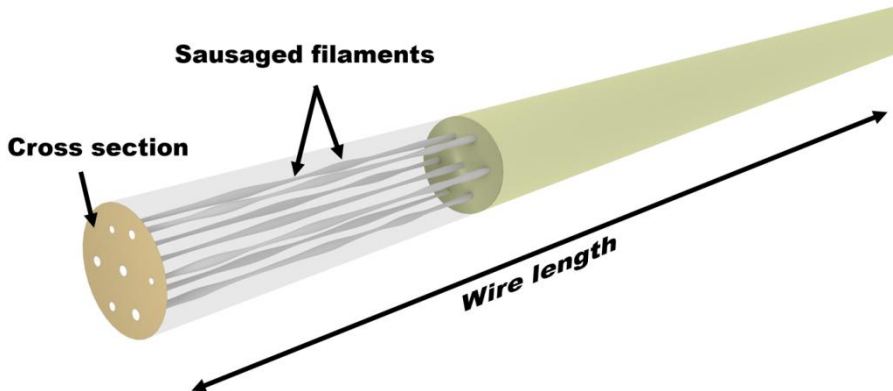

Figure 60 Sketch of a wire length depicting very dramatic filament sausaging.

Using wire cross sections to estimate the degree of sausaging has shown to be representative of wire performance in many cases, especially in Nb-Ti wires where the large number of filaments and their ductility produces very homogeneous shapes[188]. Figure 61 shows filament area measurements of two similar ITER wires, where one of the manufacturing processes has produced more outliers in the cross sectional area measurements and therefore more sausaging.

5. 7. 2   *Examples of more complex measurements*

As I mentioned in section 5.2, FIJI's open source philosophy allows users to create macros of their own—enabling more complex analyses. Below are two examples of macros we have developed at the ASC in order to study superconductors.

---

[a] That is if we assume that each neighboring filament in the wire cross section is regarded as the same filament but a couple of millimeters further down the length, which is a very common assumption to make once the fabrication steps are understood.

5. 7. 2 (a) Using non-binary images

In the next chapter I will discuss an important aspect of RRP® wire heat treatment in which two Cu-Sn phases (η and ε) are coexisting in the sub-element core (with some Kirkendall voids as well). Finding the area fractions of these three components (η, ε, and voids) allows me to determine the amount of Cu and Sn present in the core[a]. A very useful way to measure the area fractions of these phases is by giving a value of 0 to the phases in the core are that are not of interest, and a value of 100 to the desired phase fraction. In doing so, I can measure the average intensity value of the sub-element core area—which should be equivalent to the percentage of non-black pixels—and therefore the percentage of that particular phase. Figure 62 is an example of such measurement.
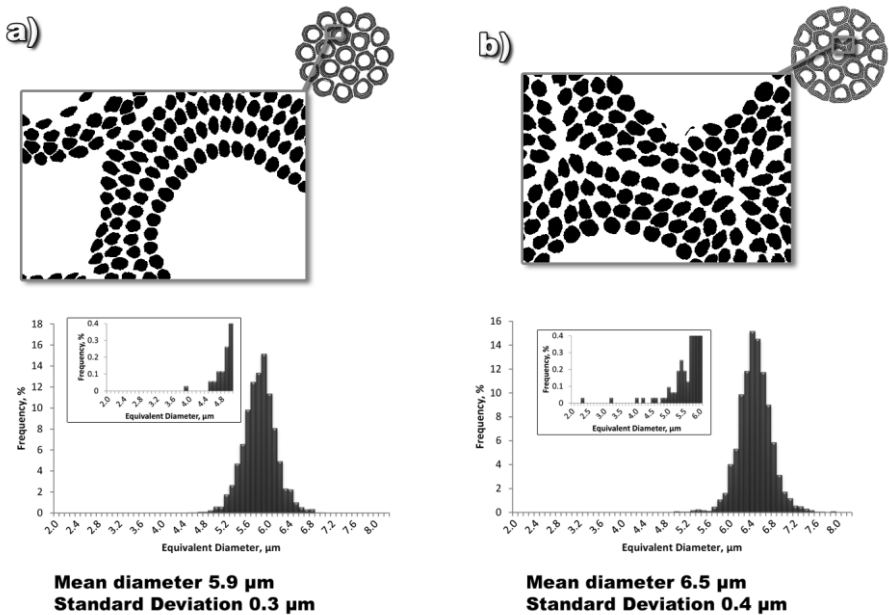
Figure 61 Binary images of Nb$_3$Sn filaments from two ITER manufacturers (more than 1000 filaments each). The wire on the right shows locally pinched filaments that contribute to a larger standard deviation.

5. 7. 2 (b) Using x-y coordinates of outlines

Another useful macro developed at the ASC uses outlines of features (recall section *5. 6. 2 (d)*). This macro measures the closest distance between two outlines at

---

[a] Since they are essentially line compounds (see Figure 27 in page 64)

every point, and therefore produces a very large amount of thickness measurements with a significant statistical distribution as shown in Figure 63.
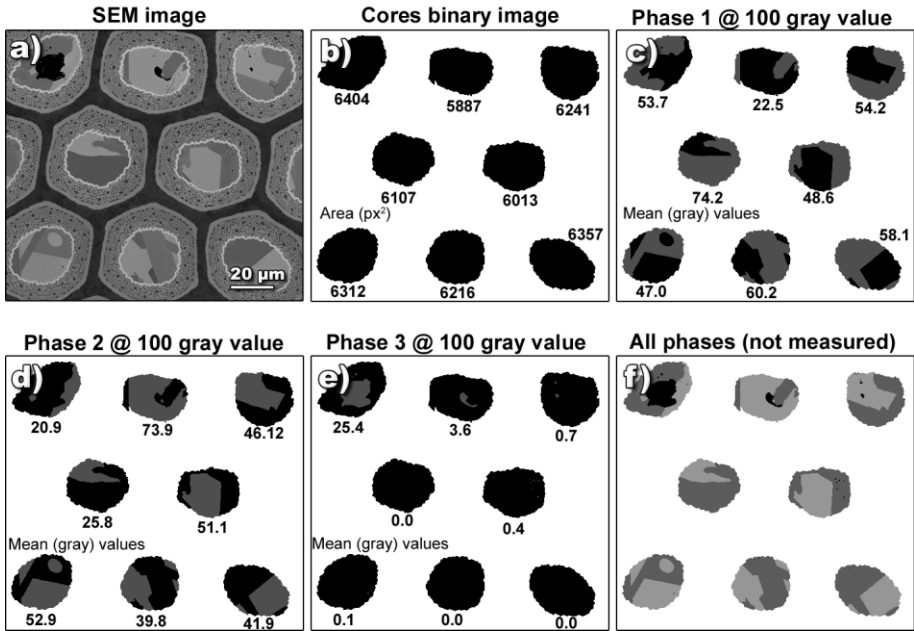

Figure 62 (a) An SEM image of RRP® sub-elements during reaction having three different phases inside the cores (namely η, ε, and voids). (b) A binary image of the cores used to establish the regions of interest and to measure the areas of each. (c), (d) and (e) are images of the different phases colored using a gray value of 100 and leaving the rest black. The mean gray values represent the percentage of each phase in each core. (f) is a composite image of all phases colored for emphasis.

5.8   Conclusion

The phrase *"a picture is worth a thousand words"* is somewhat of a subjective statement. But as it was shown above, after IA, an image is definitely worth a thousand measurements. That is the power of IA, and when combined with a properly designed experiment it can reveal important details of superconductor wires. In the next chapter the power of IA will be applied to phase transformations during RRP® wire reaction in order to understand and optimize the "mixing heat treatment" for high J_c strands.
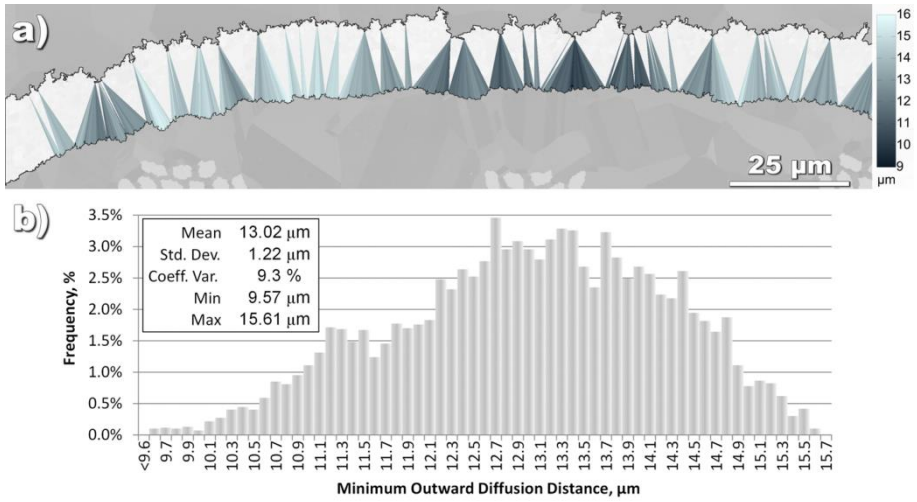
Figure 63 (a) An outlined Ta diffusion barrier in a Bronze-Process wire where the minimum outward diffusion distances have been obtained using a macro (the minimum distance lines have been color coded according to length). (b) The statistical distribution of the measured distances.

Chapter 6 - RRP® Heat Treatment Exploration

——The significant problems we face cannot be solved at the same level of thinking we were when we created them——

Albert Einstein

As I mentioned in Chapter 3, the RRP® heat treatment has remained virtually unchanged for over a decade[a]. Since 2005, only the *A15 reaction* has undergone some minor changes in order to tailor electromagnetic properties such as critical current density, J_c, upper critical field, B_{c2}, and residual resistivity ratio, RRR. However, there are certain restrictions on the time and temperature flexibility of the A15 reaction step—mainly because of the vulnerability of the cryostabilizer Cu to poisoning by Sn[189]. For example, a long A15 reaction (>50 hours) at high temperatures (≥670°C) can produce a high J_c by stimulating Sn diffusion and increasing the extent of the reaction, but unfortunately this often breaches the diffusion barriers and degrades the RRR of the high-purity Cu[b]. Therefore, a rule of thumb (which has existed since the beginning of RRP®[168]) is to keep A15 reaction under 60 hours and below 670°C—despite resulting in about 90% of the critical current capability of the wires.

There are other considerations such as the fact that higher temperatures can stimulate grain growth and therefore lower the flux-pinning potential of Nb_3Sn[c]. On the other hand, lower temperatures may not drive enough Sn diffusion—causing inhomogeneities in its distribution across the A15 ring which often result in a lower performance at higher fields[176, 190].

---

[a] See Figure 42 on page 87 for the standard heat treatment profile.

[b] It is worth reminding the reader at this point that the barriers are meant to react *partially* and contribute to the Nb_3Sn fraction; nonetheless an incomplete reaction of the Nb barrier is necessary to preserve RRR.

[c] Flux-pinning is an important property for the prevention of flux-jumps which are sources of heat during magnet operation (as it was discussed in section *2. 2. 1*).

To complicate matters further, finding a balance of electromagnetic properties is even more difficult as the sub-elements get smaller. Not only the sharp drop in J_c mentioned in Chapter 4 but also the RRR limitations dictated by the smaller thickness of the diffusion barrier[94]. So, despite several attempts made in the past decade to improve the A15 reaction, there is only a very small window between 650°C and 665°C (under 50 hours)[a] that has been empirically optimized to fit the varying sub-element size—at the cost of a lower of J_c at lower temperatures or a loss of RRR at higher temperatures.

6.1   The mixing steps

Variations of the mixing steps for the RRP® heat treatment have never been suggested, perhaps because of the difficult past the mixing steps have had in general (see Chapter 3). The lack of a consistent justification for their use in other Internal-Tin wires, and the wide variety of temperatures and times used over the years, make it almost impossible to optimize any mixing step empirically[b]. Moreover, the unfounded justifications for such mixing steps, makes one wonder whether they are necessary at all—especially when one departs from the assumption that Kirkendall voids are counterproductive[191] or that Cu-Sn mixing is the goal of these isothermal steps[153].

Nonetheless, there is one consequence of mixing that has remained true for all high-J_c Internal-Tin wires, and it does seem to be related to kinetic transformations occurring below 600°C: Nb dissolution.

6. 1. 1   The reality of dissolution

Since the IGC days, micrographs of high-J_c Internal-Tin wires have revealed pieces of disconnected Nb$_3$Sn found near the inner wall of the A15 ring. These disconnected pieces have been observed in IGC's Internal-Tin wires[114], in MJR wires[192], in RRP® wires[151], and in other Internal-Tin wires fabricated by smaller vendors[193].

Back in 1985 the microscopic structures that preceded these disconnected pieces of Nb$_3$Sn were once described as *"lath-like"*, and it was very much suspected that liquid Sn was their source[114]. It was later found (in 2002) that the formation of a

---

[a] This temperature range is slightly higher for Ta doped (older) wires.

[b] The most common scientific tool for Internal-Tin heat treatment exploration by far.

Sn-Nb-Cu ternary phase (now called Nausite [a]) was somehow related to Nb dissolution as well. However, it was unclear whether the dissolution caused Nausite or the other way around[192].

Bruker-OST certainly acknowledged the importance of this issue; as they pointed out in 2003 that *"dissolution of the Nb filaments is more extensive in the higher J_c design, due to the higher Sn content of that wire"*[151], a statement that suggests liquid Sn was the main driver of the Nb dissolution. It was not until 2011 that a materials science group in CERN (Pong, *et al.*[172], *2011*) pointed out that the Nausite phase ultimately transforms into Nb_3Sn and that the lath-like features identified years earlier (Dietderich *et al*[114], *1985*) were a result of the decomposition of the Nausite. It was also noticed that the most probable sequence of phase transformations was Nausite→$NbSn_2$→Nb_6Sn_5→Nb_3Sn[175]. Figure 64(a) shows an image of an RRP® sub-element with a significant amount of these lath-like features—now known to be a result of Nausite decomposition[175]. Figure 64(b) shows the disconnected pieces of Nb_3Sn identified as Nb dissolution for many years.
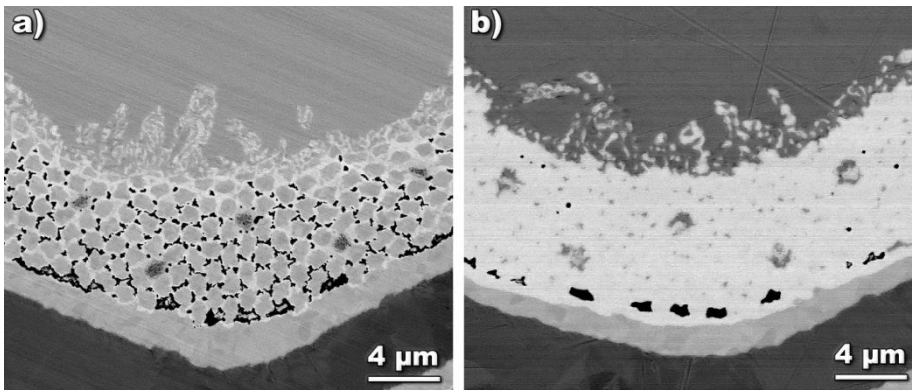
Figure 64 (a) A partially reacted RRP® sub-element showing features (between the core and the filaments) of what used to be Nausite. At this point in the reaction (at around 550°C or three hours after the end of the 400°C step) this Nausite has decomposed into a very porous structure of $NbSn_2$. (b) A partially reacted RRP® sub-element after 8 hours at 665°C showing a few disconnected pieces of Nb_3Sn previously identified as Nb dissolution and now associated with the decomposition of the Nausite phase.

Even as early as 2003, Bruker-OST pointed out that *"It is anticipated that additional improvements could be obtained by further reducing the effect of Nb*

---

[a] Named after Michael Naus, an ASC graduate student who discovered this phase. It was recently found that the proper chemical formula is $(Nb_{0.75}Cu_{0.25})Sn_2$.

filament dissolution"[151], but this did not turn out to be a straight forward task—given that their understanding of the mixing heat treatment was very limited, and a proper study of the Nausite formation had not been done before this thesis work.

6. 1. 2   *Sn and Cu diffusion*

In 2013, a key finding regarding the RRP® mixing heat treatment steps flew in the face of all preconceived notions of Cu-Sn mixing and void formation. At CERN, Pong *et al.*[156], *2013*, examined partially reacted RRP® subelements and noticed that the outward Sn diffusion seemed to come to a halt during the 400°C step when a ring of Nausite formed at the boundary between the Nb filament pack and the sub-element core. Such a situation from my own study is shown in Figure 65.
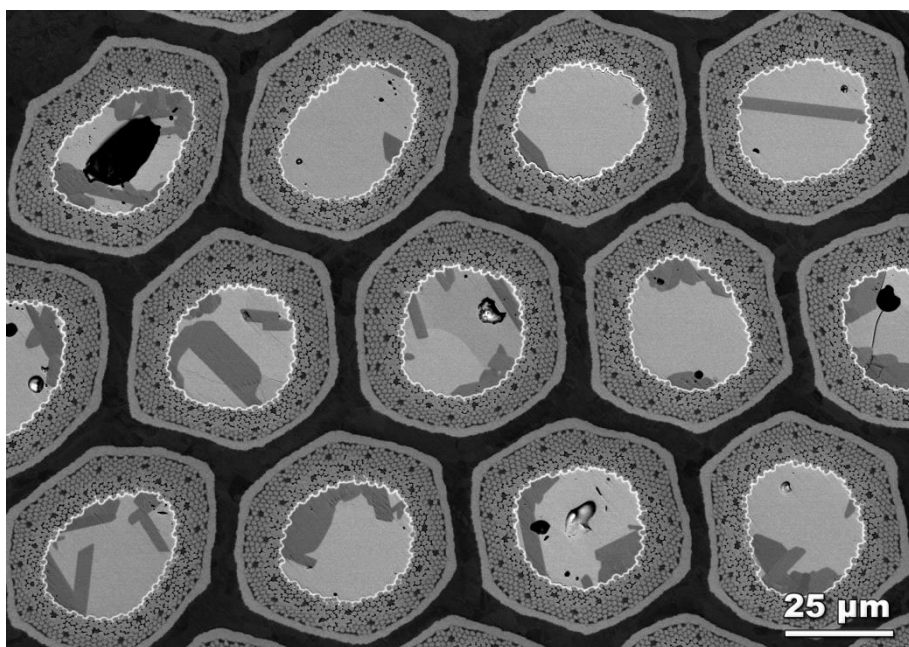
Figure 65 A group of partially reacted RRP® sub-elements (8 hours into the 400°C step) showing a continuous ring of Nausite sitting between the filament pack and the Cu-Sn core.

This ring of Nausite later came to be known as the *"Nausite membrane"* and (given our confused preconceptions about Cu-Sn mixing) it was rather an inconvenience, since it prevents the mixing of Cu and Sn within the Nb filaments—a circumstance that has been sought ever since the birth of Internal-Tin wires[150].

Furthermore, Pong *et al.*[156]*, 2013* also noticed that right before the A15 reaction[a] there appears to be a great deal of Kirkendall voids surrounding the Nb filaments. Such a state can be observed above in Figure 64(a).

So, aside from the Sn being trapped inside the core prior to the A15 reaction (because of the Nausite membrane), the Cu appears to have left the filamentary pack, leaving the filaments almost completely surrounded by Kirkendall voids. This certainly makes one wonder why we have spent so much time in a *"proper homogenization of the bronze"*[150] (around the filaments) when it does not even occur in these wires. Such an observation also incites the baffling question of: How can the A15 reaction carry on if the filaments are sitting between Kirkendall voids?

6. 1. 3   *Sn bursts*

One last aspect of the mixing steps that I would like to recall for the reader is the so-called Sn burst phenomenon. The 215°C step, other than initiating the Sn diffusion, is said to set up the conditions necessary to prevent a pressure buildup during the melting of Sn at 227°C. However, as it is shown in Appendix B, the melting of a mixture of Sn with a few percent Cu (as is the case of RRP® Sn cores) results in a very mild expansion (lower than half a percent) which is very *unlikely* to cause a pressure high enough to break the Cu/Nb composite surrounding the Sn-rich core.

So, if an adequate mixing of the Sn around the filaments is not a result of the mixing steps, and the expansion of Sn during melting disagrees with the suspected mechanisms of a Sn-burst, why do we bother mixing?

6. 1. 4   *Mixing step observations*

It appears there is a fundamental misconception surrounding the mixing steps. Not only were these designed to initiate a kinetic process that does not happen (Cu-Sn mixing in the filamentary pack) but they also seem to prevent an issue that has never been reported in RRP® wires (Sn bursts). Given these observations, allow me to present the exploratory studies which have revealed the true purpose of a mixing heat treatment in RRP® wires, and which have shed some light on the root cause of the sharp J_c drop shown at the beginning of Chapter 4 (page 69).

---

[a] Effectively at zero hours into the A15 step

6.2 RRP® heat treatment explorations

Following the footsteps of Pong et al.[156], 2013, I designed an experiment in which small pieces of RRP® wires were heat treated inside quartz tubes pumped to very high vacuum (~10^{-6} Pa) and then filled with Argon at 300 Torr. The tubes were pulled out of the furnace at various times during the heat treatment and immediately "quenched" in water for metallographic preparation and image analysis. Micrographs of sub-elements at the end of the three heat treatment steps are shown in Figure 66.
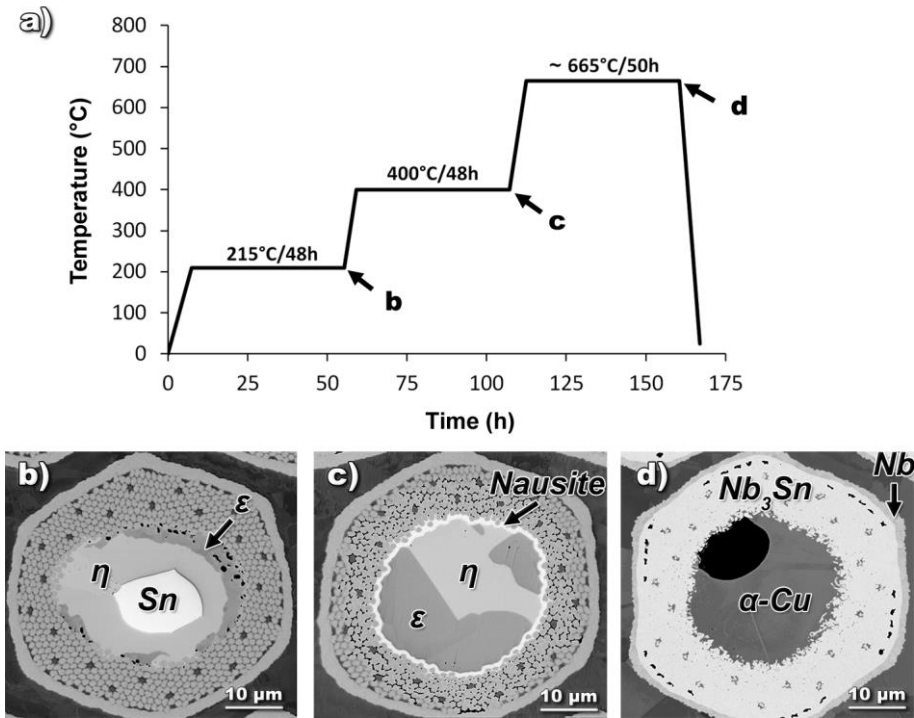
Figure 66 The morphologies found in RRP® sub-elements after each one of the isothermal steps in the heat treatment.

6. 2. 1 The 215°C step

The micrographs I took during the 215°C step certainly revealed that this step behaves as expected. The Sn in the core slowly diffuses out into the Cu annulus with a thermodynamically coherent front of Sn, η, ε, and α (in that order). There is only one thing that was unexpected here. Often times, towards the end of this step, the η-phase penetrates a few rows of filaments creating what seems to be a Sn-rich

phase—which given its high Z-contrast is likely to be Nausite. Figure 67 shows the 215°C step at 0 hours, 24 hours, and 48 hours.
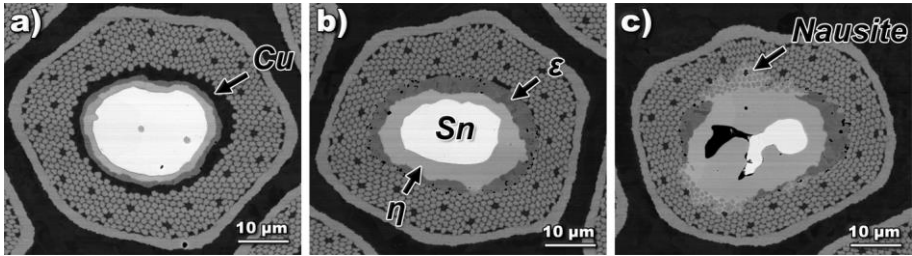
Figure 67 Partially reacted sub-elements showing the Sn diffusion during the 215°C step at (a) 0 hours, (b) 24 hours, and (c) 48 hours.

6. 2. 1 (a) Skipping the 215°C step

Exploring alternatives to this heat treatment, I removed the 215°C step and heat treated a few billets for I_c testing. After such heat treatment (48 h at 400°C and 50 h at 665°C), I noticed that the electromagnetic properties of these wires were not much different from the standard heat treatment. Table 12 shows the change in J_c of these billets when skipping the 215°C step.

Table 12 Various billets of different wire diameters and stack configurations showing a very low change in J_c when skipping the 215°C step.

Billet ID	Stack	Wire diameter (mm)	Approx. sub-element size (μm)	ΔJ_c (12 T) when skipping the 215°C step
16630	132/169	0.85	50	3%
16630	132/169	0.7	41	0%
16630	132/169	0.6	35	3%
16315	132/169	0.85	50	0%
16315	132/169	0.7	41	2%
16315	132/169	0.6	35	0%
17563	108/127	0.85	56	-7%
17563	108/127	0.778	51	-4%
14753	108/127	0.85	55	-5%
14753	108/127	0.778	50	-4%

Perhaps the most surprising observation of this experiment is the fact that the Nausite membrane formation between the filament pack and the core seen in Figure 65 and Figure 66(c) is the preferred arrangement regardless of whether the 215°C step was used or not. This happens even after the η-phase has penetrated the filament pack as it did in Figure 67(c). Any penetration seems to recede once it reaches 400°C, and the Nausite membrane forms within a few hours (as shown in Figure 68), completely erasing the effects of the 215°C step.
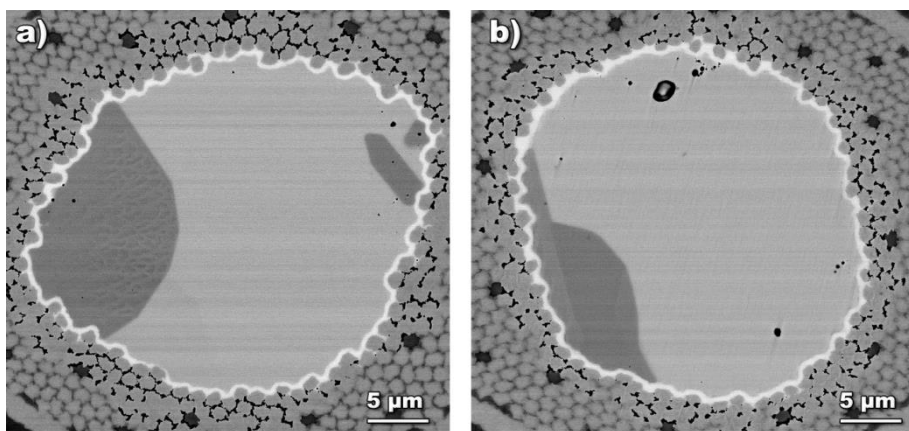
Figure 68 Two nearly identical Nausite membranes formed after 8 hours into the 400°C step using (a) the standard heat treatment and (b) a heat treatment skipping the 215°C.

6. 2. 2   The 400°C step

There are two aspects of the 400°C step that are worth taking a closer look at. The first one has to do with the prevention (or mitigation) of Nausite growth, and the second one is something that was noticed almost immediately after taking a few micrographs. As far as Nausite growth goes, it would be of great interest to find out how fast it grows given that Nb dissolution is a result of it. And as far as the second observation goes, it was rather surprising to see that there is an appreciable inward Cu diffusion *through* the Nausite membrane during the 400°C step[a]. A sequence of sub-elements during the 400°C step is shown in Figure 69, notice the increase in Nausite thickness and the reduction of η content (indicative of an a higher Cu content) as a function of time.

This Cu-flux across the solid Nausite membrane is a strange kinetic mechanism that resembles that of biological cell membranes—allowing water into the cell (or in this case Cu) while locking everything else in place—which is why I have thought of this as *"Cu osmosis"*.

---

[a] Which is something that Pong *et. al.*[156], *2013* observed only above 415°C (during the ramp to A15 temperatures).
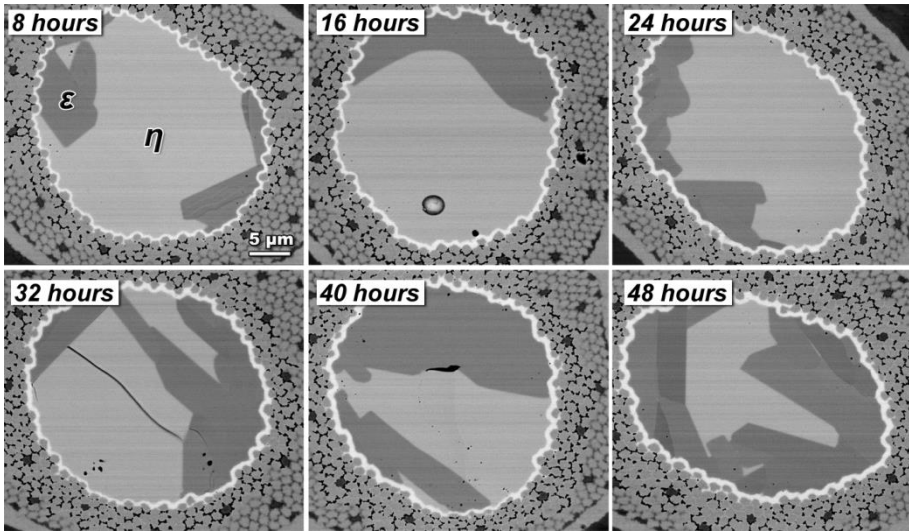
Figure 69 A sequence of sub-elements during the 400°C step as a function of time.

6. 2. 2 (a) Nausite growth rate

Using the tools described in section *5. 7. 2*, I measured the Nausite membrane thickness of various sub-elements across multiple wires and noticed that its growth (at least in this particular sub-element design) agrees very well with a power law growth:

$$\textit{Equation (3)} \qquad x(T,t)=k(T)t^n$$

where x is the thickness of the Nausite membrane, T is the temperature, t is time, n is the growth exponent, and k is the coefficient of the Arrhenius equation shown below:

$$\textit{Equation (4)} \qquad k=k_0 \, e^{\left(\frac{Q_g}{RT}\right)}$$

where k^0 is a constant, Q_g is the activation (formation) energy, and R is the universal gas constant. Figure 70 shows the Nausite membrane thickness[a] at various temperatures, where each data point is an average of more than eleven thousand measurements done via IA on high magnification images. Each image covering three fully formed membranes[b]. Least-square fits were added to the data points of

---

[a] Formed in billet 16315 at 0.85 mm in diameter, see Table 12 for stack and D_s information

[b] The error bars in this graph are the standard deviations of these measurements

the heat treatments (at or above 370°C), giving a power law growth exponent, n, of 0.27. Additionally, using the power law combined with Equation (4), the activation energy of Nausite was found to be 98.27 kJ/mol. With this, the layer thickness values for temperatures below 370°C were predicted and later confirmed as shown by the single data points in Figure 70 for 360°C and 350°C. A table with multiple values of Nausite layer thickness (calculated using *Equation (3)*) can be found in Appendix C.
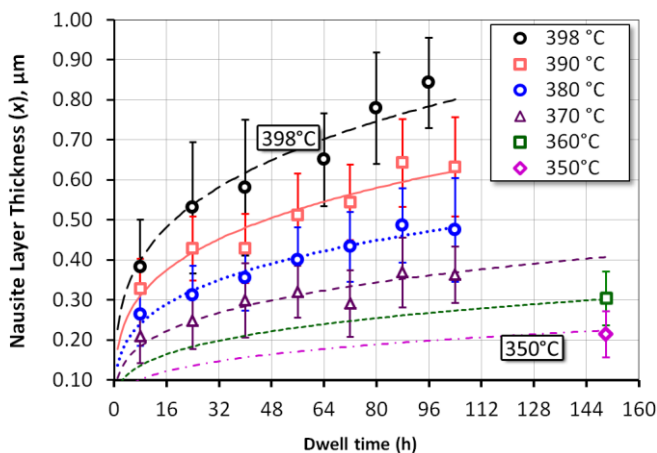

Figure 70 Nausite layer thickness measured using IA algorithms with least-square fits for data points at or above 370°C. Predicted traces for values below 370°C were added and later confirmed.

6. 2. 2 (b) Cu diffusion

The Cu diffusion on the other hand has proven to be slightly different. Using the phase fraction measurement techniques described in section *5. 7. 2*, I was able to measure the at.% Sn inside the Nausite membranes of various billets, and noticed that as the Cu flows into the core, the at.% Sn drops at a very similar rate across various temperatures. Figure 71 shows the at.% Sn[a] as a function of time at different temperatures. Each data point was taken from an image covering over 30 sub-elements of the same wire cross section and the error bars in the graph are the standard deviations of a single image. It is important to keep in mind that the Sn locked up in the Nausite membrane is not included in this measurement, therefore some of the at.% Sn change is also related to the loss of Sn to the Nausite membrane given that Nausite is 66 at.% Sn, 25 at.% Nb, and 8 at.% Cu[194].

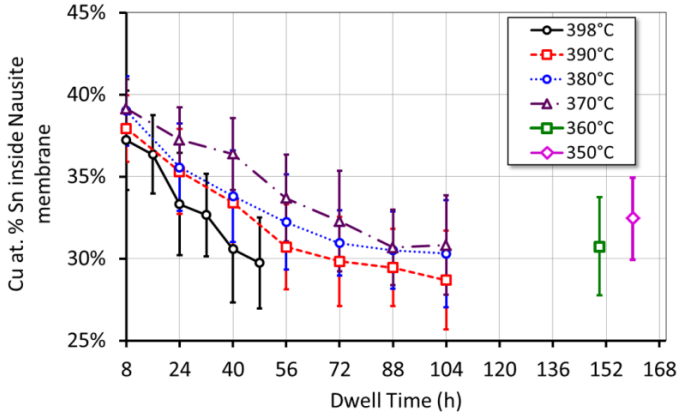[a] For billet 16315 at 0.85 mm in diameter, see Table 12 for stack and D_s information

Figure 71 The change in at.% Sn inside the Nausite membrane as a function of time for various temperatures.

Unlike the Nausite membrane growth rate (which is constant across multiple billets and wire sizes), the at.% Sn drop rate seems to have slight variations across billets, and a notably slower drop rate for smaller sub-elements of the same billet. In other words, Cu diffusion is less effective in smaller sub-elements. However, using a lower temperature and a longer time seems to even out the total amount of Cu diffused in. This effect can be observed in the final values of at.% Sn (at different isothermal steps) shown in Table 13. As you can see, the *at.% Sn variation* across sub-element diameters (standard deviation row) is much smaller for lower temperatures and longer times—and it seems to minimize somewhere around 28 at.% Sn.

Table 13 The final at.% Sn inside the Nausite membrane of two 132/169 stack wires at different wire diameters.

	398°C 48 h	390°C 104 h	380°C 104 h	370°C 104 h	360°C 150 h	350°C 400 h
16315 @ 0.85 mm	29.7%	28.7%	30.3%	30.8%	30.7%	28.2%
16315 @ 0.70 mm	31.6%	29.4%	30.5%	31.4%	30.1%	27.9%
16315 @ 0.60 mm	31.3%	29.8%	31.5%	32.0%	30.2%	28.3%
St. Dev.	**1.0%**	**0.6%**	**0.7%**	**0.6%**	**0.3%**	**0.2%**
16630 @ 0.85 mm	33.5%	29.4%	29.9%	32.6%	32.2%	28.7%
16630 @ 0.70 mm	32.5%	31.2%	30.7%	32.5%	31.7%	28.6%
16630 @ 0.60 mm	32.2%	29.6%	31.6%	31.7%	32.1%	28.5%
St. Dev.	**0.7%**	**1.0%**	**0.9%**	**0.5%**	**0.3%**	**0.1%**

6. 2. 3   Liquefaction of the η-phase

As discussed in section *3. 5. 3 (i)* (see page 65), the liquefaction of the η-phase at 408°C has been one of the main reasons why a 400°C step was used in the first place. The goal (under traditional beliefs of Cu-Sn mixing), was to transform as much η as possible into ε by mixing the Sn and the Cu within the filaments. What the literature has failed to show until now is that this mixing does not happen within the filaments, rather, it happens inside the cores thanks to the Nausite membrane. But regardless of where it happens, I have found that lowering the temperature of the "400°C step" (which I now refer to as the Cu diffusion step) is still beneficial.

During my "quench" experiments I found that there is a secondary source of Nausite formation (other than the membrane growth). This additional Nausite formation is most likely the root cause of the "lath-like" features previously reported[a]. Such Nausite formation happens during a very short window of time after the liquefaction of the η-phase—when the liquid Cu-Sn is in intimate contact with the Nausite ring. Figure 72(a) shows an example of this secondary Nausite formation event which is most likely the source of the porous structures seen in Figure 72(b).
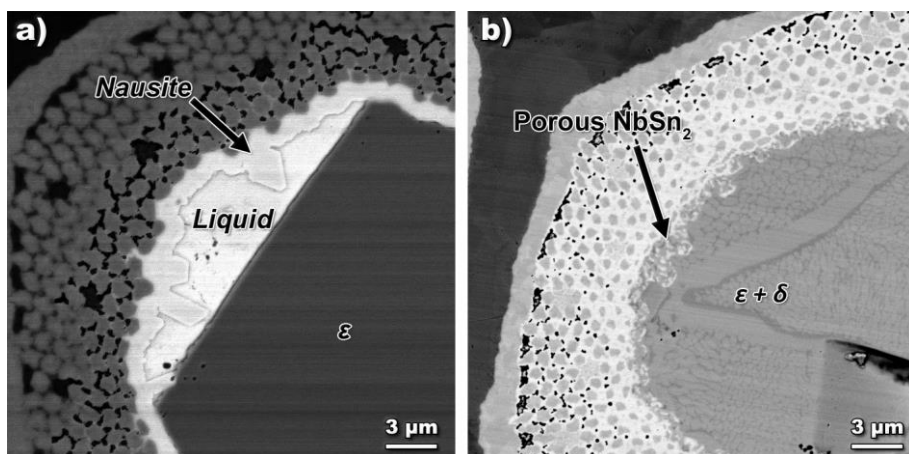
Figure 72 Partially reacted sub-elements at (a) 500°C upon ramp up and (b) at the end of the ramp when the temperature reached the final step target of 665°C.

The speed at which this secondary Nausite grows is worth highlighting. The presence of liquid inside RRP® wires rarely exceeds three hours (during the

---

[a] Identified by Dietderich *et. al*[114], *1985*, and later shown to be a result of Nausite decomposition by Pong, *et. al.*[172], *2011*,

ramp-up to A15 temperature), yet it is enough to produce these large Nausite grains and increase the membrane thickness further.

6. 2. 4   *Nausite as a metastable phase*

Nausite is certainly a very mysterious phase. Only recently its crystal structure was identified[194], and its Cu/Sn selectivity is indeed interesting. Unfortunately I was not able to contribute much information regarding the properties of this phase other than the fact that above 408°C it is a metastable phase, and it decomposes over time. This was observed when performing a differential thermal analysis (DTA) with two different ramp rates. As shown in Figure 73 there is a slight jump in the *differential temperature rate of change*, dΔT/dT, above 500°C most likely associated with Nausite decomposition. Such a jump happens at different temperatures depending on the ramp rate, suggesting that this decomposition is time-dependent—as it happens roughly two hours after the liquefaction of η.
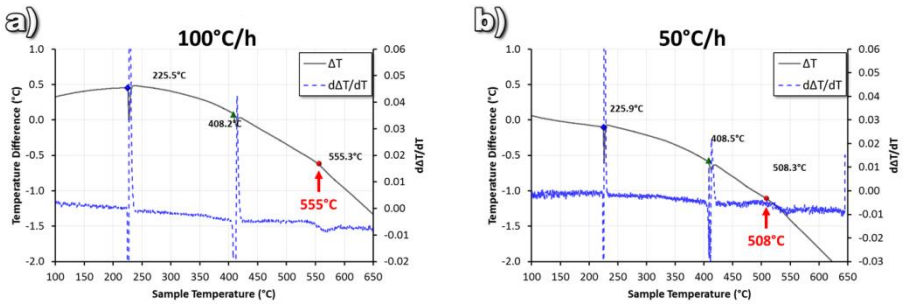
Figure 73 Differential thermal analysis of two RRP® wires ramped to 650°C at (a) 100°C/h and (b) 50°C/h. The difference in the Nausite decomposition events suggest that it is not temperature dependent.

6. 2. 5   *Nausite as a source of large grain A15*

Another downside of Nausite formation is that even when it transforms into Nb_3Sn that is *not* disconnected from the A15 ring, it tends to produce large grain Nb_3Sn—which (as I have mentioned before) has low flux-pinning capabilities. A portion of a fractured surface of a sub-element's A15 ring is shown in Figure 74 where a row of large grains can be seen towards the inner side (left side) of the A15 ring. It is very likely that all these large grains came from the decomposition of Nausite and that their contribution to transport current is very small.
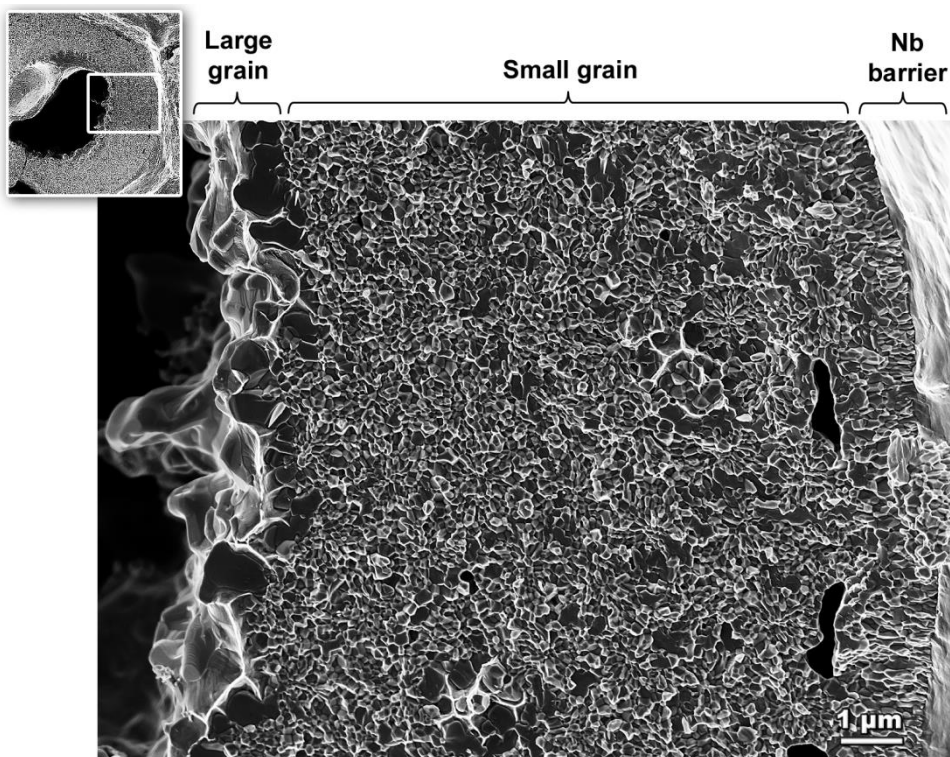
Figure 74 A fractured surface of a fully reacted sub-element showing a row of large grains on the inner side of the A15 ring.

6.3   *Heat treatment optimization*

In the above section I have reported a great deal about the pros and the cons of Nausite, but I think the most important thing to remember is that Nausite is not a desired phase[a]. It wastes Sn and Nb on disconnected large-grain Nb_3Sn which does not contribute to transport current. However, the Nausite membrane configuration *does* present an opportunity to mix the Cu-Sn inside the sub-element cores—rather than the filament pack—effectively reducing the amount of η-phase and therefore reducing the chances of secondary Nausite formation.

Knowing this, a heat treatment which promotes Cu diffusion and suppresses the Nausite membrane growth was made our goal. Initial attempts to redesign the heat treatment have already been done using a Cu mixing step of 370°C for 108 h and have shown a significant increase in the J_c of RRP® wires, despite using the same

[a] My apologies to Mike Naus

104

A15 step. Figure 75 shows the improved J_c values compared to the graph shown in Chapter 4.
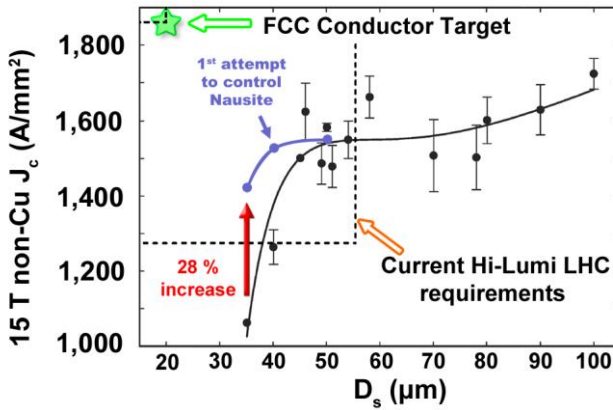
Figure 75 Adding the new heat treatment values to Figure 43. The purple data points are those using a heat treatment with a Cu diffusion step of 108 h at 370°C and an A15 step of 50 hours at 665°C.

As you can see, a heat treatment which promotes Cu diffusion and hinders Nausite growth can have a significant impact on J_c. But unfortunately wires with smaller sub-elements are still showing an important drop in J_c. One of the reasons for this can be seen in Table 13 (page 101) because even when using 108 h at 370°C the smaller sub-elements still have a slightly higher amount of Sn (~1 at.% Sn more) which should result in a larger amount of Nausite grains formed after liquefaction.

Another reason is that the Nausite membrane represents a much larger area fraction for smaller sub-elements. This is illustrated by the simplified sketch in Figure 76(a), and represented by *Equation (5)* which is plotted in Figure 76(b), where A_N is the Nausite membrane area, A_S is the area of the sub-element, r is the ratio of the core diameter to the sub-element diameter[a], and x, as before, is the Nausite layer thickness.

$$\text{Equation (5)} \qquad \frac{A_N}{A_S} = \frac{x(2D_S r - x)}{D_S^2}$$

If we are to reduce the sub-element size below 40 μm we must aim for a heat treatment that produces the thinnest Nausite layer possible and which promotes Cu diffusion. Below 350°C the slow Cu diffusion is likely to result in a heat treatment

---

[a] A_N includes the Nausite membrane and assumes the area is a circle

that is too long for magnet production. However, using 350°C for 400 hours allows for a complete diffusion of Cu for all sizes (see Table 13 on page 101) and produces a considerably thinner Nausite layer (see Table 14 in page 120). I have not had the time to test such heat treatment for I_c, but it will most likely present further improvements, even if the same A15 step is used.
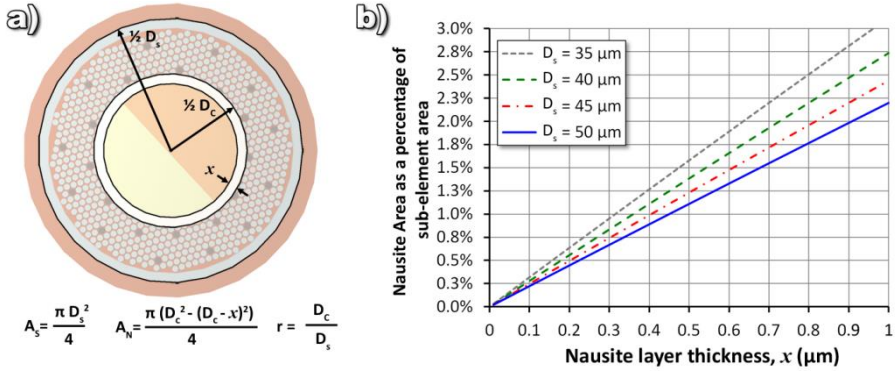
Figure 76 (a) A simplified sketch of a sub-element showing the relevant variables of *Equation (5)*. (b) Area fraction of Nausite as a function of layer thickness.

6.4   Conclusion

Despite my skepticism regarding earlier literature on the mixing steps, I have found that Cu-Sn mixing is indeed a possibility in RRP® wires—even if it does not occur in the manner that the earlier literature expected it to happen. Thanks to the Nausite membrane, a very peculiar kinetic mechanism allows the Cu to diffuse into the sub-element core and to decrease the fraction of η-phase present before crossing the 408°C line. Unfortunately a complete consumption of the η-phase is not a possibility in the current sub-element design, however an at.%Sn in the core of ~28%[a] is achievable using a Cu diffusion step of 400 hours at 350°C—even at sub-element diameters of 35 μm.

With regards to the 215°C mixing step, my experiments indicate that it has no value in these composites, and it wastes valuable time that could be used for Cu diffusion ~370°C or below. Unfortunately, convincing the magnet community that Sn bursts are not a threat has been rather difficult. I often find resistance to the idea of a heat treatment that crosses the melting point of pure Sn without an isothermal

---

[a] Which is only 3 at.%Sn units away from total consumption of η (see Figure 27 in page 64).

step because of the few anecdotal instances in which a magnet has been compromised at the expense of a defective wire. But Sn bursts have never been observed in RRP® wires, and if they have never leaked during the unavoidable melting of the η-phase (present after the standard 48 hours at 400°C), I highly doubt they will leak during the melting of Sn. Besides, the few Sn bursts that remain in the memories of magnet manufacturers were never investigated as to say whether they happened during the melting of Sn or during the melting of η.[a]

It might seem harmless to still use a 215°C/48 h step as "Sn burst insurance", since it does not affect J_c. However, we saw in Chapter 3 how a simple assumption can lead to a complete misunderstanding of a technological feature and may thwart advancement for decades. Furthermore, we are scientists, and we should base our decisions on evidence—not belief—and at the moment the available evidence *does not* seem to point to the melting of Sn as a threat to RRP® wires.

---

[a] Furthermore, about 27% of the Sn is never consumed by the 215°mixing step so it will melt regardless.

Chapter 7 - A Look into the Future

——We must not cease from exploration, and the end of all our exploring will be to arrive where we started and know the place for the first time——

T. S. Eliot

Given the complexity of the RRP® reaction, it is not surprising that it has taken us a long time to understand what really happens during the mixing steps. We now know that Kirkendall voids are *not* an issue for this type of wire, and that the Nb filaments *do not* need to be surrounded by a homogeneous mix of Cu-Sn in order to form a homogeneous fully-dense ring of Nb_3Sn. However, the mechanism of the Nb_3Sn reaction itself is still a mystery. The Sn appears to have enough connectivity (within the void-rich, Cu-depleted matrix of the filament pack) to rapidly form a ring of Nb_3Sn which appears fully reacted even after 8 hours (see Figure 64 on page 93)[a]. This rapid Sn mobility seems to be a surface effect, as suggested by the bright phase surrounding the Nb filaments in Figure 64(a). Notice that this high Z-contrast phase is present surrounding every filament and appears to be the 'highway' used by Sn to react even on the inside of the diffusion barrier (farthest from the original Sn source) very early into the A15 reaction step.

But regardless of the A15 reaction mechanism, the most relevant finding of this thesis work is that one of the most important sources of J_c degradation does not have to do with the A15 reaction itself—but with series of kinetic transformations happening before it. These kinetic transformations are a result of a premature attack on the Nb (by Sn-rich phases) resulting on the production of Nausite: the root of large grain A15 in RRP® wires.

7.1   Advantages of RRP® over other high-J_c technologies

It should be mentioned that large grain A15 is not unique to RRP® wires.

---

[a] Although it appears fully reacted in 8 hours, the extra 42 hours are essential to homogenize the Sn and drive B_{c2} up.

Powder-in-Tube[195], as well as a similar technology called Tube-Type[196], have even more serious issues regarding an excessive formation of large grain A15. In their case, the rapid diffusion of Sn quickly overwhelms the Nb, and although there is little time for much Nausite to form (because there are no isothermal steps), a significant amount of $NbSn_2$ forms during the first few hours of the A15 reaction. The result of this early transformation is a thick layer of large grain A15 on the inside of the tube. A sketch of an unreacted and a reacted filament of these two tube technologies is shown in Figure 77, where a much thicker large grain region is observed compared to the one seen in Figure 74 for RRP®.
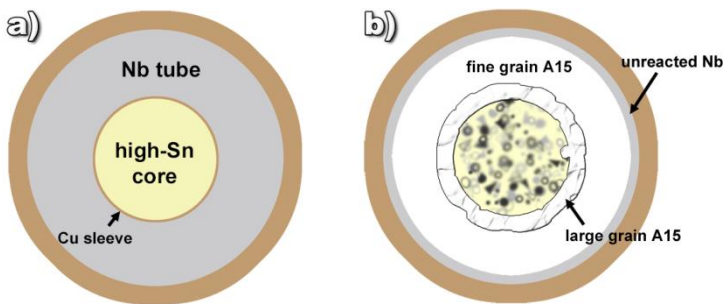
Figure 77 (a) A sketch of an unreacted filament of a generic Powder-in-Tube or Tube-Type wire and its (b) reacted version showing a very thick layer of large grain A15.

It all seems to come down to the fact that whenever Nb is exposed *locally* to a highly concentrated amount of Sn (whether it is η, Nausite, Liquid-Sn, or $NbSn_2$), a sequence of events unfolds which results in large grain A15. The word "locally" in the previous sentence is very important because in the case of Powder-in-Tube and Tube-Type (which are ruled by outward Sn diffusion only), the $NbSn_2$ large-grain layer seems to grow until the layer itself becomes a buffer zone separating the Sn-rich core from the Nb. As this happens, the local concentration of Sn on the outside of this large grain layer must be low enough for Nb_3Sn to form for the rest of the reaction.

For these tube technologies this means that a sacrificial inner ring of large grain is unavoidable because an outwardly-diffusing high-Sn source will always drive a high concentration of Sn at the reaction front—saturating the Nb and triggering the formation of Nausite and eventually $NbSn_2$ (depending on the temperature). The only way to prevent a high local concentration of Sn and therefore prevent Nausite or $NbSn_2$ is to have a low-Sn core—as it was done for ITER Internal-Tin wires[191], and, as it was done for certain Powder-in-Tube wires which used Nb_6Sn_5 powder

instead of $NbSn_2$ power[197]. The problem with either one of these approaches is that these wires are often low J_c, precisely because of their low Sn content. But the beauty of the RRP® sub-element configuration (and its Nausite membrane), is that it allows us to freeze the outward diffusion of Sn momentarily, while the Cu diffuses into the core and transforms the high-Sn core into a low-Sn core as shown schematically in Figure 78. This is the true *mixing of Cu-Sn* in RRP® wires, a holy grail that we had been looking for in the wrong place.[a]
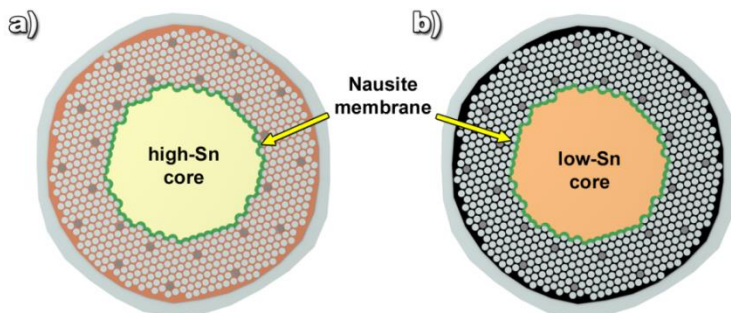
Figure 78 Simplified sketches of RRP® sub-elements undergoing the Cu diffusion step. The sub-element in (a) shows the starting configuration of this step and the sub-element in (b) shows the end configuration. Phase transformations are not shown for simplicity.

7.2   *Possible design changes*

A logical next step for this study would be a slight reduction of the Sn content such that a full transformation of the core into the ε-phase (25 at.%Sn) becomes possible, but as we saw in Chapter 6, the current 'reduced Sn' sub-element design reaches a minimum of ~28 at.%Sn after a Cu diffusion step of 400 hours at 350°C. I have also had the chance to measure the minimum Sn content in a 'standard Sn' billet, and such sub-elements seem to reach a minimum of ~30 at.%Sn after the same Cu diffusion step.

Unfortunately these slightly elevated Sn contents above the stoichiometric composition of the ε-phase contain enough η-phase to cause further Nausite formation. So the question is:

> *What sub-element modifications should be done in order to have*
> *a fully ε-phase core after the Cu-diffusion step?*

---

[a] Among the filaments

7. 2. 1   *Increasing the Cu content*

I have calculated that *if* the Nb:Sn atomic ratio is kept constant (as well as their absolute amounts[a]), we would need to increase the Cu amount by 4.9% of the sub-element area in the case of the reduced Sn sub-element design and 7.3% in the case of the standard Sn sub-element design. The result would be to allow a complete transformation of the cores into the ε-phase at the expense of a sub-element which is 4.9% or 7.3% larger (depending on the amount of Sn). It is difficult to estimate the effect that such design change would have on J_c because the sub-element area itself increases, but since there is no liquefaction of η, the entire reaction can be controlled better.

However, adding Cu to the sub-element is more complicated than it seems. One might be tempted to increase the *local area ratio* (LAR) to increase the Cu content, but this can also affect the *Nb to Sn atomic ratio*, as well as the *Sn percent inside the barrier*. This was the case of a recent sub-element design change in which the LAR was increased, but unfortunately this also lowered the Nb:Sn atomic ratio—which may explain the low RRR values produced by this prototype wire[198].

7. 2. 2   *Increasing the Cu channel thickness is not a necessity*

One of the first hypotheses put forth in order to explain the lower 'Cu diffusion rate' in smaller wires (*i.e.* the slightly higher final at.% Sn in small D_s wires shown in Table 13), was that the Cu channel thickness may be getting thin enough to slow down the flow of Cu into the core. However, this does not seem to be an issue when using the heat treatment proposed (400 hours at 350°C). Figure 79 shows the at.% Sn using both the standard heat treatment and the proposed heat treatment for the same wire at three different sizes. Notice that the data points for the proposed heat treatment are much closer together and their error bars smaller—while the standard heat treatment produces a larger scatter and larger error bars. This is an indication that the variation of Cu diffusion across sub-element sizes can be mitigated by using a lower temperature, and therefore the Cu-channel thickness is not an issue yet.

---

[a] I can't show any calculations of this because of my non-disclosure agreement with Bruker-OST.
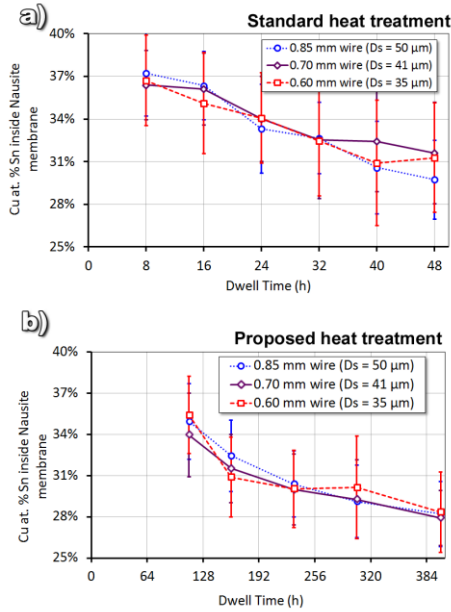
Figure 79 The at.% Sn evolution for the same wire at different sizes when using (a) the standard heat treatment and (b) the proposed heat treatment. Notice that the error bars and the measurement variation are much smaller for the proposed heat treatment.

7.3   *A closer look at the A15 reaction*

If we have found a more optimum mixing heat treatment that promises a more effective use of the Sn, Nb, and Cu, even at small sub-element sizes, the next step would be to optimize the A15 formation step. As I mentioned at the beginning of Chapter 6 the A15 reaction has only been slightly modified over the years to accommodate the sub-element size reduction. There have been a few other attempts to find better reaction times and temperatures[176, 189, 190], but these have been carried out on old large-D_s RRP® billets before Ti doping was implemented, and they were done—as usual—using an empirical approach.

Nonetheless I believe we have enough information to make an educated guess for a better A15 reaction step at this point. Instead of fixing one variable (time) and sweeping across the other (temperature)[a], we should first step back and consider what we are aiming for.

---

[a] Which is a technique that has taken us nowhere, and has in fact exposed some pretty scary situations in extreme circumstances such as the so-called strain irreversibility cliff[199]

The ultimate goal of the A15 step is to have enough Sn diffusion to homogenize the Sn (and the dopant) across the Nb$_3$Sn ring. This is more effectively achieved when using high temperatures, but this often results in low RRR as well as low pinning-force[176]. A low temperature on the other hand, has been shown to produce significant Sn gradients across the A15 ring and therefore an unsatisfactory high-field performance (*i.e.* low B_{c2})[189]. However, there are two things that we need to consider about these low temperature attempts. The first is rather obvious; the Sn mobility is significantly reduced at lower temperatures, and there has not been enough time for it to homogenize adequately[a]. Therefore, a longer time must be used if one is to lower the temperature and expect the same extent of homogenization.

The second aspect we need to consider is that all these low temperature attempts have been done on Ta doped wires. It has been shown that Ti has the ability to increase the extent of the reaction[126, 200] and that it allows for similar diffusion extent when lower temperatures are used[201]. Therefore we should explore the possibilities of Ti doping keeping in mind that the reaction itself is more effective.

Arup Ghosh, who has been one of the key investigators of RRP® A15 heat treatment optimization, has suggested (before retiring from his position at BNL) to attempt a heat treatment of 400 hours at 620°C[202]. Such heat treatment is currently being tested at Bruker-OST and unfortunately its results could not be reported in time for this thesis work.

If such an A15 step is successful, the new RRP® heat treatment may end up being: 400 hours at 350°C and 400 hours at 620°C, as shown in Figure 80. Minor modifications to this heat treatment may be done to adjust for sub-element size. For example, a slightly shorter A15 step can be used if the RRR of small sub-elements is compromised or vice versa for larger sub-elements. Also, if a very thin Nausite membrane is desired (as it should for smaller size sub-elements) lowering the Cu diffusion step 5 to 10°C but increasing the time to 500 or 600 hours could be an option once the sub-element size is reduced closer to the 25 μm FCC targets.

---

[a] In fact, all these attempts show outstanding RRR values[189] even when using steps close to 100 hours[176], suggesting there is still much room for improvement.
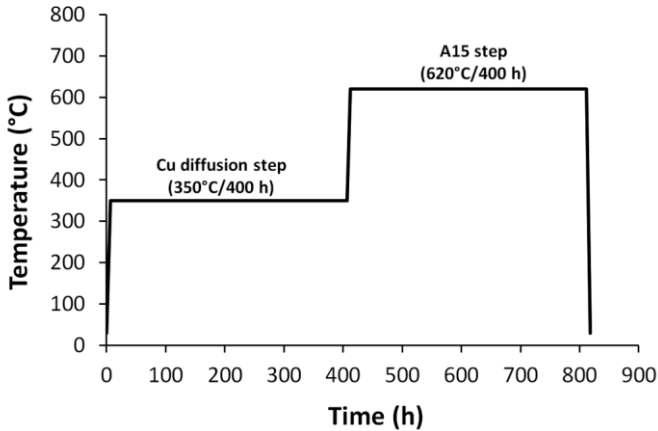
Figure 80 The proposed heat treatment for future RRP® wires.

7.4   Conclusion

Without considering the success or the failure of the A15 step proposed above or the expected improvements from the proposed Cu diffusion step, over the past three years I have managed to identify an important root cause for the detrimental J_c drop that has haunted RRP® wires for decades. As a result, my first attempt at a Cu diffusion optimization has shown a J_c increase of ~28% in wires with a sub-element size of 35 µm (see Figure 75 in page 105). Nonetheless, the FCC targets are still far from those currently obtainable—and significant improvements need to be done if we are to successfully implement Nb₃Sn wires for particle physics applications. Going above 3000 A/mm^2 at 25 µm[a] means that these 25 µm sub-elements need to be slightly more efficient than their 85 µm versions[93]—and we are not certain whether the J_c degradation comes *only* from the issues highlighted here or if it comes from other unknown dimensional, chemical, or physical effects. Nonetheless, the fact that such record has been achieved in large D_s RRP® wires (with this identical sub-element design) is a testament that the possibility still exists and that if we pay enough attention to the details we might be able to make the necessary adjustments to achieve the demanding FCC goal.

As we come to the end of this thesis work, I would like to highlight a few things related to the approaches taken for this research project:

---

[a] Which is roughly the FCC target (although nowadays it is preferred to use the 16 T value of 1500 A/mm^2)

First, the extensive history presented in the first chapters of this thesis, was not just a retelling of a story that has been told a thousand times, but rather a crucial part of the critical thinking that led to my findings. I found that in order to truly think outside the box one needs to understand what the box is made of; which in this case it was made of 40-years of Internal-Tin and External-Tin wire history.

Second, in order for me to break the deep-seated beliefs and the empirical approaches that had plagued Internal-Tin studies for many years, I had to challenge tradition and common wisdom; I had to step outside my comfort zone and spend long hours digging through the scientific literature knowing that it could lead nowhere. But it did.

And finally, the most important (and perhaps surprising) fact of what you have witnessed here is that *anybody* could have done this. All I did was notice something odd, find out where it came from, and record how it happened. It was only a matter of taking the time to observe with patience and ask the right questions. As Isaac Newton once said, *"if I have seen further it is by standing on the shoulders of giants"* the only difference here is that I have leaned-over, closer to the giant's ear, and whispered: *"Tell me Mr. Giant, where have you been…? "*.

I truly hope you have enjoyed reading this thesis work as much as I have enjoyed writing it, and I cannot thank you enough for reading this far. I hope the passion that I have spilled all over this document has impacted you enough to encourage you to take a more curious approach to the problems that lay ahead of us, free from prejudice, preconceived notions, and constraints…

Appendix A – Symbols and Acronyms

Symbol	Definition
α-phase	Cu(Sn) solid solution
ε-phase	Cu_3Sn
δ-phase	$Cu_{41}Sn_{11}$
η-phase	Cu_6Sn_5
A15	Nb_3Sn structure or often Nb_3Sn itself
at.% Sn	atomic percent tin
B_c	critical field
B_{c2}	upper critical field
Cu	copper
D_{eff}	filament diameter
D_s	sub-element diameter
eV	electron volt
FCC	Future circular collider
IA	Image analysis
k	Arrhenius equation coefficient
LAR	local area ratio
Mg	magnesium
n	Power law growth exponent
Nb	niobium
Nb:Sn	niobium to tin atomic ratio
Q_g	Activation energy
R	Universal gas constant
RRR	residual resistivity ratio
Sn	tin
Ti	titanium
T	Temperature
t	time
wt.% Sn	weight percent tin
x	Nausite layer thickness

Appendix B - Melting of Cu-Sn (98.2 at.%Sn)

There have been a few instances in magnet manufacturing history where Internal-Tin wires (particularly Internal-Tin MJR wires) appear to have leaked a large amount of Sn and have severely poisoned the stabilization Cu of neighboring wires—rendering the magnet useless. These instances have come to be known as "Sn-bursts", and the *melting* of Sn has for many years been thought of as the phase transformation responsible for such catastrophes. Unfortunately, these are instances which have never been adequately recorded, and given the confusion of the Internal-Tin heat treatment exposed in Chapter 3, a very common (unfounded) conclusion has been that a ~215°C heat treatment step can produce enough Cu-Sn mixing to prevent a pressure buildup by transforming the Sn into η or ε before crossing the 232°C line (melting point of Sn). In this Appendix, I want to look a little further into the melting of Sn, in order to see if its expansion upon melting is enough to justify the Sn bursts, and whether it is a real threat to RRP® wires.

The melting of pure Sn is indeed known to produce a volumetric expansion of about 2.59%[167]—from a specific volume of 0.1398 cm^3/g (when solid) to a specific volume of 0.1434 cm^3/g (when liquid) at 232°C. However, RRP® sub-element cores are *not* made of pure Sn; they often have slightly less than 1 wt.% Cu[138], and it has been shown recently that a small amount of Cu can make liquid Sn slightly denser than its pure form—from a specific volume of 0.1434 cm^3/g (in the pure case) to a specific volume of 0.1412 cm^3/g in the case of a solution of Cu 98.2 at.%Sn at 232°C[166]. Such liquid is 1.5% denser than liquid pure Sn.

Following this approach of considering the effects of small traces of Cu on metallic Sn, let us consider the tetragonal lattice of *solid* Sn shown in Figure 81a, with a specific volume of 0.1398 cm^3/g[167]. Now, because the relative atomic radius difference of Cu and Sn, Cu is expected to be a substitutional impurity as shown in Figure 81b. This means that the volume of a single cubic centimeter of pure Sn where 1.8% of the atoms have been replaced by Cu should be less dense (*i.e.* have a higher specific volume). Furthermore, it has been shown that the lattice parameter, *a*, can increase about 0.5% when ~1.8% of the atoms have been replaced by Cu[203]— increasing the specific volume further.
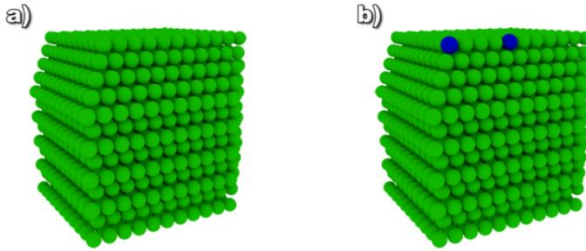
Figure 81 (a) An array of the tetragonal crystal structure of solid Sn and (b) a similar array but with a few percent of the atoms as substitutional impurities of Cu (blue atoms).

Equation (6) shows the calculation of the atomic mass of a solid solution of Cu 98.2 at.%Sn where A_{Sn} and A_{Cu} are the atomic masses of Sn and Cu respectively.

$$\text{Equation (6)} \qquad A_{Cu\ 98.2\ at.\%Sn} = \left(A_{Sn} \times \frac{98.2}{100}\right) + \left(A_{Cu} \times \frac{1.8}{100}\right)$$

With A_{Sn} and A_{Cu} being 118.69 and 63.54 g/mol respectively[204], equation Equation (6) yieds the following:

$$A_{Cu\ 98.2\ at.\%Sn} = 117.697\ ^g/_{mol}$$

Which is 0.8% less dense than pure Sn. Now, since we know pure solid Sn has a specific volume of 0.1398 cm³/g, and we are assuming all the Cu atoms are substitutional (*i.e.* negligible volume change), then:

$$\text{Equation (7)} \qquad V_m^{\ Cu\ 98.2\ at.\%Sn(s)} = V_m^{\ Sn} + \left(V_m^{\ Sn} \times 0.8\%\right)$$

yielding

$$V_m^{\ Cu\ 98.2\ at.\%Sn(s)} = 0.1410\ ^{cm^3}/_g$$

So, the melting of a solid solution of Cu 98.2 at.%Sn from a solid specific volume of 0.1410 cm³/g (Equation (7)) to a liquid specific volume of 0.1412 cm³/g (ref [166]) yields an expansion of 0.18%—much lower than the 2.59% expansion of pure Sn[167]. Therefore it appears the pressure build-up that has been thought as the mechanism for Sn bursts is not as extreme as it once was thought. e will revisit other sources of Sn bursts in Chapter 6.

Appendix C - Nausite layer thicknesses

Table 14 Nausite membrane thickness in µm for various temperatures and times.

Temperature→ Time↓	398°C	390°C	380°C	370°C	360°C	350°C	340°C
25	0.544	0.423	0.327	0.251	0.186	0.138	0.101
50	0.657	0.511	0.395	0.302	0.224	0.166	0.122
100	0.793	0.616	0.477	0.365	0.270	0.200	0.147
150	0.885	0.688	0.532	0.408	0.302	0.224	0.164
200	0.957	0.744	0.575	0.441	0.326	0.242	0.177
250	1.017	0.790	0.611	0.468	0.347	0.257	0.189
300	1.068	0.830	0.642	0.492	0.364	0.270	0.198
350	1.114	0.866	0.670	0.513	0.380	0.282	0.207
400	1.155	0.898	0.694	0.532	0.394	0.292	0.214
450	1.192	0.927	0.717	0.549	0.407	0.301	0.221
500	1.227	0.954	0.738	0.565	0.419	0.310	0.228
550	1.259	0.979	0.757	0.580	0.430	0.318	0.234
600	1.289	1.002	0.775	0.594	0.440	0.326	0.239

References

1   C. Sagan, *Cosmos*. Ballantine Books, 1985.

2   R. Boyle, *New experiments physico-mechanical, touching the spring of the air, and its effects, made, for the most part, in a new pnuematical engine*, Third. London: printed by Miles Flesher, 1682.

3   F. Hauksbee, *Physico-mechanical experiments on various subjects: containing an account of several surprizing phaenomena touching light and electricity, producible on the attrition of bodies*. London: Printed by R. Brugis, 1709.

4   A. Volta, "On the Electricity Excited by the Mere Contact of Conducting Substances of Different Kinds. In a Letter from Mr. Alexander Volta, F. R. S. Professor of Natural Philosophy in the University of Pavia, to the Rt. Hon. Sir Joseph Banks, Bart. K. B. P. R. S.," *Philos. Trans. R. Sosciety 1800*, vol. 90, pp. 403–431, Jan. 1800.

5   M. Faraday, "On some new Electro-Magnetical Motions, and on the Theory of Magnetism," *Q. J. Sci. Lit. Ats*, vol. 12, no. 24, pp. 414–422, Sep. 1821.

6   N. Tesla, "A New System of Alternate Current Motors and Transformers," *Trans. Am. Inst. Electr. Eng.*, vol. V, no. 10, pp. 308–327, Jul. 1888.

7   H. Hertz, *Electric Waves: Being Researches on the Propagation of Electric Action with Finite Velocity Through Space*. Dover Publications, 1893.

8   W. Crookes, "On Radiant Matter I," *Pop. Sci. Mon.*, vol. 16, pp. 13–24, Nov. 1879.

9   J. J. Thomson, "Cathode Rays," *Electr. - Wkly. Illus. J. Electr. Eng. Ind. Sci.*, vol. 39, no. 4, pp. 104–109, May 1897.

10 J. Hershel, "On the Hyposulphurous Acid and its Compounds," *Edinb. Philos. J.*, vol. 1, pp. 8–29, Jun. 1819.

11 H. Becquerel, "Sur les radiations emises par phosphorescence," *Comptes Rendus Hebd. Académie Sci.*, vol. 102, no. 5, pp. 420–421, Jun. 1896.

12 H. Becquerel, "Sur les radiations invisibles émises par les corps phosphorescents," *Comptes Rendus Hebd. Académie Sci.*, vol. 102, no. 5, pp. 501–503, Jun. 1896.

[13] W. Röntgen, "On a New Kind of Rays," *Science*, vol. 3, no. 59, pp. 227–231, Feb. 1896.

[14] L. Boltzmann, "Weitere Studien über das Wärmegleichgewicht unter Gasmolekülen," *Sitzungsberichte Akad. Wiss.*, vol. 66, pp. 275–370, Oct. 1872.

[15] A. Einstein, "Investigations on the theory of the brownian movement," *Dover Publ. Inc*, no. Translated by A. D. Cowper, 1905.

[16] E. Rutherford, "The Retardation of the Velocity of the Alpha Particles in Passing Through Matter," *Philos. Mag. Ser. 6*, vol. 12, no. 67, pp. 134–147, Jul. 1906.

[17] E. Rutherford, "Uranium radiation and the electrical conductivity produced by it," *Philos. Mag. Ser. 5*, vol. 47, no. 284, pp. 109–169, Jan. 1899.

[18] E. Rutherford, "The scattering of α and β particles by matter and the structure of the atom," *Philos. Mag. Ser. 6*, vol. 21, no. 125, pp. 669–688, May 1911.

[19] N. Bohr, "On the Constitution of Atoms and Molecules, Part I," *Philos. Mag.*, vol. 26, no. 151, pp. 1–24, 1913.

[20] N. Bohr, "On the Constitution of Atoms and Molecules, Part III Systems containing several nuclei," *Philos. Mag.*, vol. 26, no. 155, pp. 857–875, 1913.

[21] W. Pauli, "Über den Zusammenhang des Abschlüsses der Elektronengrüppen im Atom mit der Komplexstruktur der Spektren," *Z. Für Phys.*, vol. 31, no. 1, pp. 765–783, Feb. 1925.

[22] W. Heisenberg, "Über den anschaulichen Inhalt der quantentheoretischen Kinematik und Mechanik," *Z. Phys.*, vol. 43, pp. 172–198, Mar. 1927.

[23] E. Rutherford, "Collision of alpha particles with light atoms : IV. An anomalous effect in nitrogen," *Philos. Mag. Ser. 6*, vol. 37, no. 222, p. 581, 1919.

[24] E. Rutherford and J. Chadwick, "The disintegration of elements by α particles," *Philos. Mag. Ser. 6*, vol. 44, no. 261, pp. 417–432, Sep. 1922.

[25] J. Chadwick, "Possible Existence of a Neutron," *Nature*, vol. 129, p. 312, Feb. 1932.

[26] O. Hahn and F. Strassmann, "Über den Nachweis und das Verhalten der bei der Bestrahlung des Urans mittels Neutronen entstehenden Erdalkalimetalle," *Naturwissenschaften*, vol. 27, no. 1, pp. 11–15, Jan. 1939.

[27] V. F. Hess, "Über Beobachtungen der durchdringenden Strahlung bei sieben Freiballonfahrten," *Phys. Z.*, vol. 13, pp. 1084–1091, 1912.

[28] A. L. Cortie, "Sir Norman Lockyer, 1836-1920," *Astrophys. J.*, vol. 53, p. 233, May 1921.

[29] F. Hoyle, "On Nuclear Reactions Occuring in Very Hot STARS. I. the Synthesis of Elements from Carbon to Nickel.," *Astrophys. J. Suppl. Ser.*, vol. 1, p. 121, Sep. 1954.

[30] G. Lemaître, "The Beginning of the World from the Point of View of Quantum Theory," *Nature*, vol. 127, no. 3210, May 1931.

[31] G. Gamow, "Expanding Universe and the Origin of Elements," *Phys. Rev.*, vol. 70, no. 7–8, pp. 572–573, Oct. 1946.

[32] C. D. Anderson, "The Positive Electron," *Phys. Rev.*, vol. 43, no. 6, pp. 491–494, Mar. 1933.

[33] P. a. M. Dirac, "The Quantum Theory of the Electron," *Proc. R. Soc. Lond. Math. Phys. Eng. Sci.*, vol. 117, no. 778, pp. 610–624, Feb. 1928.

[34] C. T. R. W. M. A. F.R.S, "LXXV. The condensation method of demonstrating the ionisation of air under normal conditions," *Philos. Mag. Ser. 6*, vol. 7, no. 42, pp. 681–690, Jun. 1904.

[35] S. H. Neddermeyer and C. D. Anderson, "Note on the Nature of Cosmic-Ray Particles," *Phys. Rev.*, vol. 51, no. 10, pp. 884–886, May 1937.

[36] C. M. G. Lattes, H. Muirhead, G. P. S. Occhialini, and C. F. Powell, "Process Involving Charged Mesons," *Nature*, vol. 159, pp. 694–697, 1947.

[37] G. D. Rochester and C. C. Butler, "Evidence for the Existence of New Unstable Elementary Particles," *Nature*, vol. 160, pp. 855–857, Dec. 1947.

[38] J. D. Cockcroft and E. T. S. Walton, "Experiments with High Velocity Positive Ions," *Proc. R. Soc. Lond. Math. Phys. Eng. Sci.*, vol. 129, no. 811, pp. 477–489, Nov. 1930.

[39] J. D. Cockcroft and E. T. S. Walton, "Experiments with High Velocity Positive Ions. (I) Further Developments in the Method of Obtaining High Velocity Positive Ions," *Proc. R. Soc. Lond. Math. Phys. Eng. Sci.*, vol. 136, no. 830, pp. 619–630, Jun. 1932.

[40] E. Lawrence, "Method and apparatus for the acceleration of ions," US1948384 A, 20-Feb-1934.

[41] K. M. G. Siegbahn, "Nobel Prize in Physics 1939 - Presentation Speech," 1939.

[42] E. M. McMillan, "The Synchrotron—A Proposed High Energy Particle Accelerator," *Phys. Rev.*, vol. 68, no. 5–6, pp. 143–144, Sep. 1945.

[43] H. R. Crane, "The Racetrack: A Proposed Modification of the Synchrotron," *Phys.Rev.*, vol. 69, pp. 542–542, 1946.

[44] W. Brobeck, "Design Study for a Ten-Bev Magnetic Accelerator," *Rev. Sci. Instrum.*, vol. 19, no. 9, pp. 545–551, Sep. 1948.

[45] E. J. Lofgren, "The Proton Synchrotron," *Science*, vol. 111, no. 2882, pp. 295–300, Mar. 1950.

[46] E. J. Lofgren, "Experiences with the Bevatron," *Lawrence Berkeley Natl. Lab.*, Apr. 1956.

[47] O. Chamberlain, E. Segrè, C. Wiegand, and T. Ypsilantis, "Observation of Antiprotons," *Phys. Rev.*, vol. 100, pp. 947–950, Nov. 1955.

[48] E. D. Courant, M. S. Livingston, and H. S. Snyder, "The Strong-Focusing Synchroton—A New High Energy Accelerator," *Phys. Rev.*, vol. 88, no. 5, pp. 1190–1196, Dec. 1952.

[49] D. A. Glaser, "Some Effects of Ionizing Radiation on the Formation of Bubbles in Liquids," *Phys. Rev.*, vol. 87, no. 4, pp. 665–665, Aug. 1952.

[50] F. Reines and C. L. Cowan, "The Neutrino," *Nature*, vol. 178, no. 4531, pp. 446–449, Sep. 1956.

[51] M. Gell-Mann, "A schematic model of baryons and mesons," *Phys. Lett.*, vol. 8, no. 3, pp. 214–215, Feb. 1964.

[52] E. D. Bloom, D. H. Coward, H. DeStaebler, J. Drees, G. Miller, L. W. Mo, et al., "High-Energy Inelastic e−p Scattering at 6° and 10°," *Phys. Rev. Lett.*, vol. 23, no. 16, pp. 930–934, Oct. 1969.

[53] G. Aad, T. Abajyan, B. Abbott, J. Abdallah, S. Abdel Khalek, A. A. Abdelalim, et al., "Observation of a new particle in the search for the Standard Model Higgs boson with the ATLAS detector at the LHC," *Phys. Lett. B*, vol. 716, no. 1, pp. 1–29, Sep. 2012.

[54] R. A. Beth and C. Lasky, "The Brookhaven Alternating Gradient Synchrotron," *Science*, vol. 128, no. 3336, pp. 1393–1401, Dec. 1958.

[55] R. Wilson, "The Tevatron." FERMILAB-TM-0763, 01-Feb-1978.

[56] P. F. Chester, "Superconducting magnets," *Rep. Prog. Phys.*, vol. 30, no. 2, p. 561, 1967.

[57] H. Rogalla and P. H. Kes, *100 Years of Superconductivity*. Taylor & Francis, 2011.

[58] CERN. Geneva. The LHC Study Group, "Design study of the Large Hadron Collider (LHC) : a multiparticle collider in the LEP tunnel." Geneva : CERN, 1991. - 212 p., 06-Jun-1991.

[59] L. Rossi, "Superconductivity: its role, its success and its setbacks in the Large Hadron Collider of CERN," *Supercond. Sci. Technol.*, vol. 23, no. 3, p. 034001, Mar. 2010.

[60] G. E. Gallagher-Daggitt, "Superconductor Cables for Pulsed dipole Magnets." Rutherford High Energy Report, RHEL-M-A25, 1973.

[61] R. M. Scanlan, J. Royet, and R. Hannaford, "Fabrication of Rutherford-Type Superconducting Cables for Construction of Dipole Magnets," Lawrence Berkeley Lab., CA (USA), LBL-24321; CONF-880653-1, May 1988.

[62] E. Barzi and A. V. Zlobin, "Research and Development of Wires and Cables for High-Field Accelerator Magnets," *IEEE Trans. Nucl. Sci.*, vol. 63, no. 2, pp. 783–803, Apr. 2016.

[63] M. Garber and W. Sampson, "Critical current anisotropy in NbTi cables," *IEEE Trans. Magn.*, vol. 21, no. 2, pp. 336–338, Mar. 1985.

[64] A. V. Tollestrup, R. E. Peters, K. Koepke, and R. H. Flora, "Coil Extension, Deformation and Compression during Excitation in Superconducting Accelerator Dipole Magnets," *IEEE Trans. Nucl. Sci.*, vol. 24, no. 3, pp. 1331–1333, Jun. 1977.

[65] D. J. Kevles, "Big Science and Big Politics in the United States: Reflections on the Death of the SSC and the Life of the Human Genome Project," *Hist. Stud. Phys. Biol. Sci.*, vol. 27, no. 2, pp. 269–297, 1997.

[66] S. C. Snowdon, "Design of Superconducting High Energy Beam Line Dipole-Magnetostatics," *IEEE Trans. Nucl. Sci.*, vol. 24, no. 3, pp. 1257–1259, Jun. 1977.

[67] S. C. Snowdon, "Mechanical and Thermal Stresses in Superconducting Accelerator and Beam-Line Magnets," *IEEE Trans. Nucl. Sci.*, vol. 24, no. 3, pp. 1254–1256, Jun. 1977.

68 P. Lefèvre, and T. Pettersson, Eds., *The Large Hadron Collider*. CERN Desktop Publishing Service, 1995.

69 D0 Collaboration, V. M. Abazov, B. Abbott, M. Abolins, B. S. Acharya, M. Adams, et al., "Observation of the Doubly Strange *b* Baryon Ω_b^-," *Phys. Rev. Lett.*, vol. 101, no. 23, p. 232002, Dec. 2008.

70 A. R. Kantrowitz and Z. J. J. Stekly, "A New Principle for the Construction of Stabilized Superconducting Coils," *Appl. Phys. Lett.*, vol. 6, no. 3, pp. 56–57, Feb. 1965.

71 F. P. Levi, "Permanent Magnets Obtained by Drawing Compacts of Parallel Iron Wires," *J. Appl. Phys.*, vol. 31, no. 8, pp. 1469–1471, Aug. 1960.

72 P. F. Dahl, G. H. Morgan, and W. B. Sampson, "Loss Measurements on Twisted Multifilamentary Superconducting Wires," *J. Appl. Phys.*, vol. 40, no. 5, pp. 2083–2085, Apr. 1969.

73 D. R. Dietderich, S. E. Bartlett, S. Caspi, P. Ferracin, S. A. Gourlay, H. C. Higley, et al., "Correlation between strand stability and magnet performance," *IEEE Trans. Appl. Supercond.*, vol. 15, no. 2, pp. 1524–1528, Jun. 2005.

74 V. V. Kashikhin and A. V. Zlobin, "Magnetic instabilities in Nb_3Sn strands and cables," *IEEE Trans. Appl. Supercond.*, vol. 15, no. 2, pp. 1621–1624, Jun. 2005.

75 P. J. Lee and B. Strauss, *100 Years of Superconductivity - 11.2 Nb-Ti from beginnings to perfection*. Taylor & Francis, 2011.

76 J. W. Ekin, "Strain Effects in Superconducting Compounds," in *Advances in Cryogenic Engineering Materials*, A. F. Clark and R. P. Reed, Eds. Springer US, 1984, pp. 823–836.

77 N. Mitchell, "Assessment of conductor degradation in the ITER CS insert coil and implications for the ITER conductors," *Supercond. Sci. Technol.*, vol. 20, no. 1, p. 25, Jan. 2007.

78 A. Godeke, M. C. Jewell, C. M. Fischer, A. A. Squitieri, P. J. Lee, and D. C. Larbalestier, "The upper critical field of filamentary Nb_3Sn conductors," *J. Appl. Phys.*, vol. 97, no. 9, p. 093909, May 2005.

79 T. G. Berlincourt and R. R. Hake, "Upper Critical Fields of Transition Metal Alloy Superconductors," *Phys. Rev. Lett.*, vol. 9, no. 7, pp. 293–295, Oct. 1962.

80 K. Tachikawa and P. J. Lee, *100 Years of Superconductivity - 11.3 History of Nb_3Sn and Related A15 Wires*. Taylor & Francis, 2011.

[81] N. Mitchell, P. Bruzzone, M. Spadoni, M. Nishi, A. Shikov, and J. Minervini, "Strand production and benchmark testing for the ITER model coils," *IEEE Trans. Appl. Supercond.*, vol. 5, no. 2, pp. 905–908, 1995.

[82] R. M. Scanlan, D. R. Dieterich, and H. C. Higley, "Conductor development for high field dipole magnets," *IEEE Trans. Appl. Supercond.*, vol. 10, no. 1, pp. 288–293, 2000.

[83] A. Devred, I. Backbier, D. Bessette, G. Bevillard, M. Gardner, C. Jong, et al., "Challenges and status of ITER conductor production," *Supercond. Sci. Technol.*, vol. 27, no. 4, p. 044001, Apr. 2014.

[84] A. Ballarino and L. Bottura, "Targets for R&D on Nb_3Sn conductor for High Energy Physics," *IEEE Trans. Appl. Supercond.*, vol. PP, no. 99, pp. 1–1, 2015.

[85] M. B. Field, Y. Zhang, H. Miao, M. Gerace, and J. A. Parrell, "Optimizing Conductors for High Field Applications," *IEEE Trans. Appl. Supercond.*, vol. 24, no. 3, pp. 1–5, 2014.

[86] M. Suenaga, K. Tsuchiya, and N. Higuchi, "Superconducting critical current density of bronze processed pure and alloyed Nb_3Sn at very high magnetic fields (up to 24 T)," *Appl. Phys. Lett.*, vol. 44, no. 9, pp. 919–921, May 1984.

[87] A. Kikuchi and H. Taniguchi, "Development of New High Tin Content Bronze Alloys and Improved Bronze-Processed Nb_3Sn Wires," *ICEC24-ICMC2012*, 2012.

[88] F. R. Fickett, *Standards for measurement of the critical fields of superconductors*. National Bureau of Standards, 1985.

[89] P. X. Zhang, J. F. Li, J. W. Liu, C. G. Li, K. Zhang, X. D. Tang, et al., "Fabrication and characterization of internal Sn and bronze-processed Nb_3Sn strands for ITER application," *Supercond. Sci. Technol.*, vol. 23, no. 3, p. 034013, 2010.

[90] T. Miyatake, Y. Murakami, H. Kurahashi, S. Hayashi, K. Zaitsu, B. Seeber, et al., "Influence of Wire Parameters on Critical Current Versus Strain Characteristics of Bronze Processed Superconducting Wires," *IEEE Trans. Appl. Supercond.*, vol. 22, no. 3, pp. 4805005–4805005, Jun. 2012.

[91] E. Gregory, E. Gulko, T. Pyon, and L. F. Goodrich, "Properties of Internal-Tin Nb_3Sn Strand for the International Thermonuclear Experimental Reactor," in *Advances in Cryogenic Engineering Materials*, vol. 42, L. T. Summers, Ed. Springer US, 1996, pp. 1319–1328.

92 J. A. Parrell, Y. Zhang, M. B. Field, and S. Hong, "Development of Internal Tin Nb$_3$Sn Conductor for Fusion and Particle Accelerator Applications," *IEEE Trans. Appl. Supercond.*, vol. 17, no. 2, pp. 2560–2563, 2007.

93 J. A. Parrell, M. B. Field, Y. Zhang, and S. Hong, "Advances in Nb$_3$Sn strand for fusion and particle accelerator applications," *IEEE Trans. Appl. Supercond.*, vol. 15, no. 2, pp. 1200–1204, 2005.

94 J. A. Parrell, Y. Zhang, M. B. Field, M. Meinesz, Y. Huang, H. Miao, et al., "Internal Tin Conductors Engineered for Fusion and Particle Accelerator Applications," *IEEE Trans. Appl. Supercond.*, vol. 19, no. 3, pp. 2573–2579, 2009.

95 C. van Beijnen and J. Elen, "Multifilament Nb$_3$Sn superconductors produced by the E.C.N. technique," *IEEE Trans. Magn.*, vol. 15, no. 1, pp. 87–90, Jan. 1979.

96 T. Boutboul, L. Oberli, A. den Ouden, D. Pedrini, B. Seeber, and G. Volpini, "Heat Treatment Optimization Studies on PIT Strand for the NED Project," *IEEE Trans. Appl. Supercond.*, vol. 19, no. 3, pp. 2564–2567, Jun. 2009.

97 L. Bottura, G. de Rijk, L. Rossi, and E. Todesco, "Advanced Accelerator Magnets for Upgrading the LHC," *IEEE Trans. Appl. Supercond.*, vol. 22, no. 3, pp. 4002008–4002008, Jun. 2012.

98 S. I. Bermudez, G. Ambrosio, A. Ballarino, E. Cavanna, R. Bossert, D. Cheng, et al., "Second-Generation Coil Design of the Nb$_3$Sn low-β Quadrupole for the High Luminosity LHC," *IEEE Trans. Appl. Supercond.*, vol. 26, no. 4, pp. 1–5, Jun. 2016.

99 L. D. Cooley, A. K. Ghosh, D. R. Dietderich, and I. Pong, "Conductor Specification and Validation for High-Luminosity LHC Quadrupole Magnets," *IEEE Trans. Appl. Supercond.*, vol. 27, no. 4, pp. 1–5, Jun. 2017.

100 M. Benedikt and F. Zimmermann, "Status and Challenges of the Future Circular Collider Study," CERN, Geneva, CERN-ACC-2016-0005, Jan. 2016.

101 O. S. Brüning, P. Collier, P. Lebrun, S. Myers, R. Ostojic, J. Poole, et al., *LHC Design Report*. Geneva: CERN, 2004.

102 D. Schoerling, H. Bajas, M. Bajko, A. Ballarino, M. Benedikt, S. Izquierdo Bermudez, et al., "Strategy for Superconducting Magnet Development for a Future Hadron-Hadron Circular Collider at CERN." Proceedings of Science, The European Physical Society Conference on High Energy Physics, Jul-2015.

[103] J. A. Parrell, M. B. Field, Y. Zhang, and S. Hong, "Nb$_3$SnConductor Development for Fusion and Particle Accelerator Applications," *AIP Conf. Proc.*, vol. 711, no. 1, pp. 369–375, Jun. 2004.

[104] M. Benedikt and F. Zimmermann, "Towards Future Circular Colliders," Dec. 2015.

[105] B. T. Matthias, T. H. Geballe, S. Geller, and E. Corenzwit, "Superconductivity of Nb$_3$Sn," *Phys. Rev.*, vol. 95, no. 6, pp. 1435–1435, Sep. 1954.

[106] A. R. Kaufmann and J. J. Pickett, "Multifilament Nb$_3$Sn Superconducting Wire," *J. Appl. Phys.*, vol. 42, no. 1, pp. 58–58, Jan. 1971.

[107] J. K. Hulm and R. D. Blaugher, "Superconducting Solid Solution Alloys of the Transition Elements," *Phys. Rev.*, vol. 123, no. 5, pp. 1569–1580, Sep. 1961.

[108] H. E. Cline, R. M. Rose, and J. Wulff, "Niobium-Thorium Eutectic Alloy as a High-Field, High-Current Superconductor," *J. Appl. Phys.*, vol. 34, no. 6, pp. 1771–1774, Jun. 1963.

[109] D. Larbalestier, P. Madsen, J. Lee, M. Wilson, and J. Charlesworth, "Multifilamentary niobium tin magnet conductors," *IEEE Trans. Magn.*, vol. 11, no. 2, pp. 247–250, Mar. 1975.

[110] M. N. Wilson, C. R. Walters, J. D. Lewin, and P. F. Smith, "Experimental and theoretical studies of filamentary superconducting composites," *J. Phys. Appl. Phys.*, vol. 3, no. 11, p. 1517, 1970.

[111] M. Suenaga and W. B. Sampson, "Superconducting Properties of Multifilamentary Nb$_3$Sn Made by a New Process," *Appl. Phys. Lett.*, vol. 20, no. 11, pp. 443–445, Jun. 1972.

[112] M. Suenaga, O. Horigami, and T. S. Luhman, "Effects of Sn concentration on the critical current density of Nb$_3$Sn formed at the Nb–(Cu–Sn alloy) interface," *Appl. Phys. Lett.*, vol. 25, no. 10, pp. 624–627, Nov. 1974.

[113] S. Fürtauer, D. Li, D. Cupid, and H. Flandorfer, "The Cu–Sn phase diagram, Part I: New experimental results," *Intermetallics*, vol. 34, pp. 142–147, Mar. 2013.

[114] D. R. Dietderich, J. Glazer, C. Lea, W. V. Hassenzahl, and J. Morris, J. W., "The critical current density and microstructural state of an internal tin multifilamentary superconducting wire," *IEEE Trans. Magn.*, vol. 21, no. 2, pp. 297–300, Mar. 1985.

[115] Y. Hashimoto, K. Yoshizaki, and M. Tanaka, "Processing and properties of superconducting Nb_3Sn filamentary wires," *Proc. Fifth Int. Cryog. Eng. Conf. ICEC*, no. Kyoto, 1974.

[116] M. Field, R. Hentges, J. Parrell, Y. Zhang, and S. Hong, "Progress with Nb_3Sn conductors at oxford instruments, superconducting technology," *IEEE Trans. Appl. Supercond.*, vol. 11, no. 1, pp. 3692–3695, Mar. 2001.

[117] C. H. Rosner, "Intermagnetics Remembered: from Superconductor-Based GE Spin-Off to Billion Dollar Valuation," *IEEECSC ESAS Eur. Supercond. News Forum*, no. 9, Jan. 2012.

[118] M. I. Agafonova, V. V. Baron, and E. M. Savitskii, "Structure and Properties of Niobium-Tin Alloys," *Izvest Akad Nauk SSSR Otd. Tekh Nauk Met Topl.*, vol. Vol: No. 5, Sep. 1959.

[119] T. B. Reed and H. C. Gatos, "Synthesis and Superconducting Properties of Nb_3Sn_2 and Nb_2Sn_3," *J. Appl. Phys.*, vol. 33, no. 8, pp. 2657–2657, Aug. 1962.

[120] L. L. Wyman, J. R. Cuthill, G. A. Moore, J. J. Park, and H. Yakowitz, "Intermediate Phases in Superconducting Niobium-Tin Alloys," *J. Res. Natl. Bur. Stand. Sect. Phys. Chem.*, vol. 66A, no. 4, Jul. 1962.

[121] J. P. Charlesworth, I. Macphail, and P. E. Madsen, "Experimental work on the niobium-tin constitution diagram and related studies," *J. Mater. Sci.*, vol. 5, no. 7, pp. 580–603, Jul. 1970.

[122] C. Segal, C. Tarantini, Z. H. Sung, P. J. Lee, B. Sailer, M. Thoener, et al., "Evaluation of critical current density and residual resistance ratio limits in powder in tube Nb_3Sn conductors," *Supercond. Sci. Technol.*, vol. 29, no. 8, p. 085003, 2016.

[123] R. E. Enstrom, "Superconducting Properties of Nb_6Sn_5 and of Multiphase Nb–Sn Alloys," *J. Appl. Phys.*, vol. 37, no. 13, pp. 4880–4882, Dec. 1966.

[124] J. E. Kunzler, E. Buehler, F. S. L. Hsu, and J. H. Wernick, "Superconductivity in Nb_3Sn at High Current Density in a Magnetic Field of 88 kgauss," *Phys. Rev. Lett.*, vol. 6, no. 3, pp. 89–91, Feb. 1961.

[125] C. L. Kolbe and C. H. Rosner, "Processing and superconducting properties of Nb_3Sn wires," *Met Soc Conf*, vol. 19, pp. 17–33, 1963.

[126] K. Tachikawa, T. Asano, and T. Takeuchi, "High-field superconducting properties of the composite-processed Nb_3Sn with Nb-Ti alloy cores," *Appl. Phys. Lett.*, vol. 39, no. 9, pp. 766–768, Nov. 1981.

[127] B. Zeitlin, G. Ozeryansky, and K. Hemachalam, "An overview of the IGC Internal Tin Nb_3Sn conductor," *IEEE Trans. Magn.*, vol. 21, no. 2, pp. 293–296, Mar. 1985.

[128] M. Suenaga, "Metallurgy of Continuous Filamentary A15 Superconductors," in *Superconductor Materials Science: Metallurgy, Fabrication, and Applications*, S. Foner and B. B. Schwartz, Eds. Springer US, 1981, pp. 201–274.

[129] E. F. Nippes, *Metals Handbook Ninth Edition Volume 6: Welding, Brazing, and Soldering*, 9th edition. Metals Park, Ohio: Asm Intl, 1983.

[130] J. C. McKinnell, D. B. Smathers, M. B. Siddall, and P. M. O'Larey, "Improved superconducting critical current density in modified jelly roll Nb_3Sn by the application of niobium (Nb) diffusion barriers," *IEEE Trans. Appl. Supercond.*, vol. 5, no. 2, pp. 1768–1772, Jun. 1995.

[131] W. K. McDonald, "Composite construction process and superconductor produced thereby," US4262412 A, 21-Apr-1981.

[132] W. K. McDonald, "Expanded metal containing wires and filaments," US4414428 A, 08-Nov-1983.

[133] D. B. Smathers, "Process for making filamentary superconductors using tin-magnesium eutectics," US4973527 A, 27-Nov-1990.

[134] D. Smathers, "Private Communication." 05-Sep-2016.

[135] R. Hentges, K. R. Marken, Y. Zhang, J. Lichtenwalner, and S. Hong, "Recent progress in Nb_3Sn development at Oxford Superconducting Technology," *IEEE Trans. Appl. Supercond.*, vol. 5, no. 2, pp. 303–306, Jun. 1995.

[136] D. B. Smathers, P. M. O'Larey, M. M. Steeves, and M. O. Hoenig, "Production of tin core modified jelly roll cable for the MIT Multipurpose Coil," *IEEE Trans. Magn.*, vol. 24, no. 2, pp. 1131–1133, Mar. 1988.

[137] Y. Zhang, J. C. McKinnell, R. W. Hentges, and S. Hong, "Recent development of niobium-tin superconducting wire at OST," *IEEE Trans. Appl. Supercond.*, vol. 9, no. 2, pp. 1444–1446, Jun. 1999.

[138] M. Field, J. Parrell, Y. Zhang, and S. Hong, "Critical current density in Nb_3Sn superconducting wire," US20060081307 A1, 20-Apr-2006.

[139] S. Cogan, S. Kwon, J. Klein, and R. Rose, "Fabrication of large diameter external-diffusion processed Nb_3Sn composites," *IEEE Trans. Magn.*, vol. 19, no. 3, pp. 1139–1142, May 1983.

[140] A. McInturff and D. Larbalestier, "Effect of metallurgical history on '$J_c(5T)$' in surface diffused multifilamentary Nb$_3$Sn," *IEEE Trans. Magn.*, vol. 11, no. 2, pp. 259–262, Mar. 1975.

[141] H. E. Cline, B. P. Strauss, R. M. Rose, and J. Wulff, "Superconductivity of a Composite of Fine Niobium Wires in Copper," *J. Appl. Phys.*, vol. 37, no. 1, pp. 5–8, Jan. 1966.

[142] M. Suenaga, W. Sampson, and T. Luhman, "Fabrication techniques and properties of multifilamentary Nb$_3$Sn conductors," *IEEE Trans. Magn.*, vol. 17, no. 1, pp. 646–653, Jan. 1981.

[143] Z. Mei, A. J. Sunwoo, and J. W. Morris, "Analysis of low-temperature intermetallic growth in copper-tin diffusion couples," *Metall. Trans. A*, vol. 23, no. 3, pp. 857–864, Mar. 1992.

[144] S. Cogan, D. S. Holmes, and R. M. Rose, "On the elimination of Kirkendall voids in superconducting composites," *Appl. Phys. Lett.*, vol. 35, no. 7, pp. 557–559, Oct. 1979.

[145] C. C. Tsuei, "Ductile Superconducting Copper-Base Alloys," *Science*, vol. 180, no. 4081, pp. 57–58, Apr. 1973.

[146] S. Foner, E. J. M. Jr, B. B. Schwartz, R. Roberge, and J. L. Fihey, "High-field critical current in insitu multifilamentary Cu-Sn-Nb alloys," *Appl. Phys. Lett.*, vol. 31, no. 12, pp. 853–854, Dec. 1977.

[147] D. Finnemore, J. Verhoeven, E. Gibson, and J. Ostenson, "Nb$_3$Sn composites with submicrometer filaments," *IEEE Trans. Magn.*, vol. 15, no. 1, pp. 693–694, Jan. 1979.

[148] K. Hemachalam and M. Pickus, "Studies on filamentary Nb3Sn wires fabricated by the infiltration method," *IEEE Trans. Magn.*, vol. 13, no. 1, pp. 466–469, Jan. 1977.

[149] W. Fietz, "Nb$_3$Sn in 1978: State of the art," *IEEE Trans. Magn.*, vol. 15, no. 1, pp. 67–75, Jan. 1979.

[150] R. Schwall, G. Ozeryansky, D. Hazelton, S. Cogan, and R. Rose, "Properties and performance of high current density Sn-core process MF Nb$_3$Sn," *IEEE Trans. Magn.*, vol. 19, no. 3, pp. 1135–1138, May 1983.

[151] J. A. Parrell, Y. Zhang, M. B. Field, P. Cisek, and S. Hong, "High field Nb$_3$Sn conductor development at Oxford Superconducting Technology," *IEEE Trans. Appl. Supercond.*, vol. 13, no. 2, pp. 3470–3473, 2003.

[152] A. Petrovich and B. A. Zeitlin, "Multifilamentary Nb$_3$Sn Composites Incorporating a High-Tin Bronze," in *Advances in Cryogenic Engineering*, K. D. Timmerhaus, R. P. Reed, and A. F. Clark, Eds. Springer US, 1978, pp. 398–405.

[153] M. T. Naus, M. C. Jewell, P. J. Lee, and D. C. Larbalestier, "Lack of influence of the Cu-Sn mixing heat treatments on the super-conducting properties of two high-Nb, internal-Sn Nb$_3$Sn conductors," presented at the Advances in Cryogenic Engineering ICMC, 2002, vol. 614, pp. 1016–1023.

[154] T. Yamashina and M. Kajihara, "Quantitative Explanation for Uphill Diffusion of Sn during Reactive Diffusion between Cu-Sn Alloys and Nb," *Mater. Trans.*, vol. 3, p. 829～837, Mar. 2006.

[155] Aloke, T. Laurila, and V. Vuorine, "Microstructure, Diffusion and Growth Mechanism of Nb$_3$Sn Superconductor by Bronze Technique," in *Superconductor*, A. Moyses, Ed. Sciyo, 2010.

[156] I. Pong, L.-R. Oberli, and L. Bottura, "Cu diffusion in Nb$_3$Sn internal tin superconductors during heat treatment," *Supercond. Sci. Technol.*, vol. 26, no. 10, p. 105002, Oct. 2013.

[157] N. Higuchi, K. Tsuchiya, C. J. Klamut, and M. Suenaga, "Superconducting Properties of Nb$_3$Sn Multifilamentary Wires Fabricated by Internal Tin Process," in *Advances in Cryogenic Engineering Materials*, A. F. Clark and R. P. Reed, Eds. Springer US, 1984, pp. 739–746.

[158] E. Gregory, G. M. Ozeryansky, and M. Suenaga, "Some Effects of Porosity and Hip'ing on Critical Currents in Internal-Tin-Processed Multifilamentary Nb$_3$Sn Wires," Brookhaven National Lab., Upton, NY (United States), BNL-46846; CONF-9110306--1, Jan. 1991.

[159] R. L. S. M. Suenaga, "Effects of temperature ramp rate during heat treatment on hysteresis loss and critical current density of internal tin processed wires," *US-Jpn. Workshop Kyoto*, Feb. 1995.

[160] D. R. Dietderich, W. V. Hassenzahl, and J. W. M. Jr, "The Relationship between Critical Current and Microstructure of Internal Tin Wire," in *Advances in Cryogenic Engineering Materials*, R. P. Reed and A. F. Clark, Eds. Springer US, 1986, pp. 881–888.

[161] E. Gregory, E. A. Gulko, and T. Pyon, "Improvements in the properties of internal-tin Nb$_3$Sn," *IEEE Trans. Appl. Supercond.*, vol. 7, no. 2, pp. 1498–1503, Jun. 1997.

[162] N. Cheggour, P. J. Lee, L. F. Goodrich, Z.-H. Sung, T. C. Stauffer, J. D. Splett, et al., "Influence of the heat-treatment conditions, microchemistry, and

microstructure on the irreversible strain limit of a selection of Ti-doped internal-tin Nb_3Sn ITER wires," *Supercond. Sci. Technol.*, vol. 27, no. 10, p. 105004, 2014.

[163] T. Pyon and H. Kanithi, "Development of Nb3Sn conductors for fusion and high energy physics," *IEEE Trans. Appl. Supercond.*, vol. 13, no. 2, pp. 3474–3477, Jun. 2003.

[164] I. Pong, M. C. Jewell, B. Bordini, L. Oberli, S. Liu, F. Long, et al., "Worldwide Benchmarking of ITER Internal Tin and Nb-Ti Strands Test Facilities," *IEEE Trans. Appl. Supercond.*, vol. 22, no. 3, pp. 4802606–4802606, 2012.

[165] A. S. for Metals, *Metals Handbook, Volume 8: Metallography, Structures and Phase Diagrams. 8th Edition*, 8th ed edition. American Society for Metals, 1973.

[166] P. Fima, "Surface tension and density of liquid Sn–Cu alloys," *Appl. Surf. Sci.*, vol. 257, no. 2, pp. 468–471, Nov. 2010.

[167] K. Bornemann and P. Siebe, "Dichtemessungen von Metallen und Legierungen - bei hohen Temperaturen mit besonderer Berucksichtigung des flussigen Zustandes. III. Messungen nach dem Dilatometerverfahren. Das System Sn-Bi.," *Z Met.*, vol. 14, p. 329, Aug. 1922.

[168] A. K. Ghosh, E. A. Sperry, L. D. Cooley, A. M. Moodenbaugh, R. L. Sabatini, and J. L. Wright, "Dynamic stability threshold in high-performance internal-tin Nb_3Sn superconductors for high field magnets," *Supercond. Sci. Technol.*, vol. 18, no. 1, p. L5, Jan. 2005.

[169] R. M. Scanlan and D. R. Dietderich, "Progress and plans for the U.S. HEP conductor development program," *IEEE Trans. Appl. Supercond.*, vol. 13, no. 2, pp. 1536–1541, Jun. 2003.

[170] D. R. Dietderich and A. Godeke, "Nb_3Sn research and development in the USA – Wires and cables," *Cryogenics*, vol. 48, no. 7–8, pp. 331–340, Jul. 2008.

[171] D. R. Dietderich, "RRP-Nb_3Sn Conductor for the LHC Upgrade Magnets," presented at the Hi-Lumi LARP collaboration meeting, Frascati, Italy, 14-Nov-2012.

[172] I. Pong, L.-R. Oberli, L. Bottura, and C. Scheuerlein, "Longitudinal and Transverse Cross-Sectional Microstructure and Critical Current Density in Superconductors," *IEEE Trans. Appl. Supercond.*, vol. 21, no. 3, pp. 2537–2540, Jun. 2011.

[173] C. Scheuerlein, M. Di Michiel, G. Arnau, R. Flukiger, F. Buta, I. Pong, et al., "Coarse Grain Formation and Phase Evolution During the Reaction of a High Sn

Content Internal Tin Strand," *IEEE Trans. Appl. Supercond.*, vol. 21, no. 3, pp. 2554–2558, Jun. 2011.

[174] C. Calzolaio, P. Bruzzone, D. Uglietti, B. Stepanov, D. Bessette, and M. Jewell, "In Situ T_c Measurements of Cable in Conduit Conductors via an Inductive Method," *IEEE Trans. Appl. Supercond.*, vol. 22, no. 3, pp. 9002604–9002604, Jun. 2012.

[175] C. Scheuerlein, M. Di Michiel, G. Arnau Izquierdo, and F. Buta, "Phase Transformations During the Reaction Heat Treatment of Internal Tin Nb_3Sn Strands With High Sn Content," *IEEE Trans. Appl. Supercond.*, vol. 18, no. 4, pp. 1754–1760, Dec. 2008.

[176] C. Tarantini, P. J. Lee, N. Craig, A. Ghosh, and D. C. Larbalestier, "Examination of the trade-off between intrinsic and extrinsic properties in the optimization of a modern internal tin Nb_3Sn conductor," *Supercond. Sci. Technol.*, vol. 27, no. 6, p. 065013, Jun. 2014.

[177] D. C. Larbalestier and P. J. Lee, "New developments in niobium titanium superconductors," in *Particle Accelerator Conference, 1995., Proceedings of the 1995*, 1995, vol. 2, pp. 1276–1281 vol.2.

[178] P. J. Lee, A. A. Polyanskii, Z.-H. Sung, D. C. Larbalestier, C. Antoine, P. C. Bauer, et al., "Flux Penetration Into Grain Boundaries Large Grain Niobium Sheet For SRF Cavities: Angular Sensitivity," in *AIP Conference Proceedings*, 2007, vol. 927, pp. 113–120.

[179] Z.-H. Sung, P. J. Lee, and D. C. Larbalestier, "Observation of the Microstructure of Grain Boundary Oxides in Superconducting RF-Quality Niobium With High-Resolution TEM (Transmission Electron Microscope)," *IEEE Trans. Appl. Supercond.*, vol. 24, no. 1, pp. 68–73, Feb. 2014.

[180] P. Li, D. Abraimov, A. Polyanskii, F. Kametani, and D. Larbalestier, "Study of grain boundary transparency in $(Yb_{x-1}Ca_x)Ba_2Cu_3O$ bicrystal thin films over a wide temperature, field, and field orientation range," *Phys. Rev. B*, vol. 91, no. 10, p. 104504, Mar. 2015.

[181] Y.-J. Kim, J. D. Weiss, E. E. Hellstrom, D. C. Larbalestier, and D. N. Seidman, "Evidence for composition variations and impurity segregation at grain boundaries in high current-density polycrystalline K- and Co-doped BaFe2As2 superconductors," *Appl. Phys. Lett.*, vol. 105, no. 16, p. 162604, Oct. 2014.

[182] M. O. Rikel and E. E. Hellstrom, "Development of 2201 intergrowths during melt processing Bi2212/Ag conductors," *Phys. C Supercond.*, vol. 357–360, Part 2, pp. 1081–1090, Aug. 2001.

[183] T. Shen, J. Jiang, F. Kametani, U. P. Trociewitz, D. C. Larbalestier, J. Schwartz, et al., "Filament to filament bridging and its influence on developing high critical current density in multifilamentary Bi2Sr2CaCu2Ox round wires," *Supercond. Sci. Technol.*, vol. 23, no. 2, p. 025009, Feb. 2010.

[184] C. A. Schneider, W. S. Rasband, and K. W. Eliceiri, "NIH Image to ImageJ: 25 years of image analysis," *Nat. Methods*, vol. 9, no. 7, pp. 671–675, Jul. 2012.

[185] J. Schindelin, I. Arganda-Carreras, E. Frise, V. Kaynig, M. Longair, T. Pietzsch, et al., "Fiji: an open-source platform for biological-image analysis," *Nat. Methods*, vol. 9, no. 7, pp. 676–682, Jul. 2012.

[186] C. Sanabria and P. Lee, "An Introduction to Digital Image Analysis of Superconductors," in *Handbook of Superconducting Materials*, Second Edition: Characterization and Applications., vol. 3. David A. Cardwell and David C. Larbalestier, Boca Raton: CRC Press / Taylor & Francis., 2017.

[187] M. Sezgin and B. Sankur, "Survey over image thresholding techniques and quantitative performance evaluation," *J. Electron. Imaging*, vol. 13, no. 1, pp. 146–168, 2004.

[188] Y. E. High, J. C. McKinnell, P. J. Lee, and D. C. Larbalestier, "Quantitative Analysis of Sausaging in Nb Barrier Clad Filaments of Nb-46.5WT% Ti as a Function of Filament Diameter and Heat Treatment," *Adv. Cryog. Eng. Mater. Ed FR Fickett RP Reed*, vol. 38, no. New York: Plenum Press, pp. 723–730, 1992.

[189] A. K. Ghosh, L. D. Cooley, J. A. Parrell, M. B. Field, Y. Zhang, and S. Hong, "Effects of Reaction Temperature and Alloying on Performance of Restack-Rod-Process Nb_3Sn," *IEEE Trans. Appl. Supercond.*, vol. 17, no. 2, pp. 2623–2626, Jun. 2007.

[190] E. Barzi, R. Bossert, S. Caspi, D. R. Dietderich, P. Ferracin, A. Ghosh, et al., "RRP Nb_3Sn Strand Studies for LARP," *IEEE Trans. Appl. Supercond.*, vol. 17, no. 2, pp. 2607–2610, 2007.

[191] C. Scheuerlein, M. D. Michiel, and A. Haibel, "On the formation of voids in internal tin Nb_3Sn superconductors," *Appl. Phys. Lett.*, vol. 90, no. 13, p. 132510, Mar. 2007.

[192] M. Naus, "Optimization of Internal-Sn Nb_3Sn Composites," University of Wisconsin-Madison, 2002.

[193] X. Xu, M. D. Sumption, and E. W. Collings, "Influence of heat treatment temperature and Ti doping on low-field flux jumping and stability in $(Nb-Ta)_3Sn$ strands," *Supercond. Sci. Technol.*, vol. 27, no. 9, p. 095009, Sep. 2014.

[194] S. Martin, A. Walnsch, G. Nolze, A. Leineweber, F. Léaux, and C. Scheuerlein, "The crystal structure of $(Nb_{0.75}Cu_{0.25})Sn_2$ in the Cu-Nb-Sn system," *Intermetallics*, vol. 80, pp. 16–21, Jan. 2017.

[195] M. D. Michiel and C. Scheuerlein, "Phase transformations during the reaction heat treatment of powder-in-tube Nb_3Sn superconductors," *Supercond. Sci. Technol.*, vol. 20, no. 10, p. L55, Oct. 2007.

[196] V. R. Nazareth, M. D. Sumption, X. Peng, E. Gregory, M. J. Tomsic, and E. W. Collings, "Effects of initial Sn/Cu ratio and heat treatment on the microstructure and microchemistry of Cu-Nb-Sn-Ta tube type composites," in *AIP Conference Proceedings*, 2008, vol. 986, pp. 260–268.

[197] W. L. Neijmeijer and B. H. Kolster, "Characteristics of a production route for filamentary Nb_3Sn superconductors based on a reaction between niobium and Nb_6Sn_5," *J. Common Met.*, vol. 160, no. 1, pp. 161–170, Apr. 1990.

[198] E. Barzi, M. Bossert, M. Field, P. Li, H. Miao, J. Parrell, et al., "Heat Treatment Optimization of Rutherford Cables for a 15-T Nb_3Sn Dipole Demonstrator," *IEEE Trans. Appl. Supercond.*, vol. 27, no. 4, pp. 1–5, Jun. 2017.

[199] N. Cheggour, "The Strain Irreversibility Cliff in Nb_3Sn RRP Wires, Its Origins, and Its Implications," presented at the MRS Spring Meeting & Exhibit, Phoenix Convention Center, Phoenix, AZ, 01-Apr-2016.

[200] V. Abacherli, D. Uglietti, P. Lezza, B. Seeber, R. Flukiger, M. Cantoni, et al., "The influence of Ti doping methods on the high field performance of $(Nb,Ta,Ti)_3Sn$ multifilamentary wires using Osprey bronze," *IEEE Trans. Appl. Supercond.*, vol. 15, no. 2, pp. 3482–3485, Jun. 2005.

[201] A. K. Ghosh, E. A. Sperry, J. D'Ambra, and L. D. Cooley, "Systematic Changes of the Nb-Sn Reaction With Time, Temperature, and Alloying in Restacked-Rod-Process (RRP) Nb_3Sn Strands," *IEEE Trans. Appl. Supercond.*, vol. 19, no. 3, pp. 2580–2583, Jun. 2009.

[202] G. Arup, "Private communication." 14-Jun-2016.

[203] E. Sidot, A. Kahn-Harari, E. Cesari, and L. Robbiola, "The lattice parameter of α-bronzes as a function of solute content: application to archaeological materials," *Mater. Sci. Eng. A*, vol. 393, no. 1–2, pp. 147–156, Feb. 2005.

[204] ASM International, *Properties and Selection: Nonferrous Alloys and Pure Metals*, vol. 2. Books on Demand, 1990.

Index

About the Author

Born as Carlos Mario Sanabria, I was soon nicknamed Charlie, Chars, Chaz, or most often just Cha... I grew up in Bogotá, Colombia, and turned out to be a borderline hyperactive kid with a great heart and a curiosity that would occasionally get me in trouble with adults. During my teenage years my parents decided to leave our native land behind—along with (pretty much) everything we owned—in an attempt to find greater opportunities elsewhere. This courageous move took us to the small (yet culturally rich) country of Panamá, and although I never felt at home, the diversity and relative calm of this peaceful country taught me a lot about taking life in stride.

We moved to Panamá having no clue about its Florida State University's satellite campus. But as soon as we found out about it, we realized it was our best chance to get the education my parents always wanted for me and my brother. So, being the hard-working Colombians our parents brought us up to be, my brother and I enrolled in FSU's Mechanical Engineering program; which started in Panamá and ended with a diploma from FSU in Tallahassee.

A few weeks after arriving in Tallahassee, I contacted every professor I could—looking for a job (any job!), and what I found would change my life forever. I was hired by the Applied Superconductivity Center and over the years I transitioned from a hardcore mechanical engineer into a true materials scientist.

I must admit that during the first few years at the ASC, it was hard for me to realize that through this job I actually had the power to influence something as important (and as big) as ITER or the LHC. But over the course of a few years my research got the attention of highly respected scientists in the field, and slowly but surely I realized that even the simplest of experiments can make a difference—when done right.

My time at the ASC taught me what it means to be a scientist, and it made me hungry for more science! Soon I wanted to know its history, its current state, and its potential future—across all fields! Today, near the end of my PhD studies in materials science, I have realized that (as scientists) we have the responsibility to keep the flame of knowledge burning brightly, expand it as much as we can, and pass it down to future generations. And that is precisely what I intend to do.